REVIEW ARTICLE

Testing the nature of dark compact objects: a status report

Vitor Cardoso[1,2] · Paolo Pani[3]

Abstract

Very compact objects probe extreme gravitational fields and may be the key to understand outstanding puzzles in fundamental physics. These include the nature of dark matter, the fate of spacetime singularities, or the loss of unitarity in Hawking evaporation. The standard astrophysical description of collapsing objects tells us that massive, dark and compact objects are black holes. Any observation suggesting otherwise would be an indication of beyond-the-standard-model physics. Null results strengthen and quantify the Kerr black hole paradigm. The advent of gravitational-wave astronomy and precise measurements with very long baseline interferometry allow one to finally probe into such foundational issues. We overview the physics of exotic dark compact objects and their observational status, including the observational evidence for black holes with current and future experiments.

Keywords Black holes · Event horizon · Gravitational waves · Quantum gravity · Singularities

Contents

✉ Vitor Cardoso
  vitor.cardoso@ist.utl.pt

Paolo Pani
paolo.pani@uniroma1.it

1   CENTRA, Departamento de Física, Instituto Superior Técnico, Universidade de Lisboa, Avenida Rovisco Pais 1, 1049 Lisbon, Portugal

2   CERN, 1 Esplanade des Particules, 1211 Geneva 23, Switzerland

3   Dipartimento di Fisica, "Sapienza" Università di Roma & Sezione INFN Roma1, Piazzale Aldo Moro 5, 00185 Rome, Italy

Ⓐ Springer

The crushing of matter to infinite density by infinite tidal gravitation forces is a phenomenon with which one cannot live comfortably. From a purely philosophical standpoint it is difficult to believe that physical singularities are a fundamental and unavoidable feature of our universe [...] one is inclined to discard or modify that theory rather than accept the suggestion that the singularity actually occurs in nature.

<div align="right">Kip Thorne, Relativistic Stellar Structure and Dynamics (1966)</div>

No testimony is sufficient to establish a miracle, unless the testimony be of such a kind, that its falsehood would be more miraculous than the fact which it endeavors to establish.

<div align="right">David Hume, An Enquiry concerning Human Understanding (1748)</div>

1 Introduction

The discovery of the electron and the known neutrality of matter led in 1904 to J. J. Thomson's "plum-pudding" atomic model. Data from new scattering experiments was soon found to be in tension with this model, which was eventually superseeded by Rutherford's, featuring an atomic nucleus. The point-like character of elementary particles opened up new questions. How to explain the apparent stability of the atom? How to handle the singular behavior of the electric field close to the source? What is the structure of elementary particles? Some of these questions were elucidated with quantum mechanics and quantum field theory. Invariably, the path to the answer led to the discovery of hitherto unknown phenomena and to a deeper understanding of the fundamental laws of Nature. The history of elementary particles is a timeline of the understanding of the electromagnetic (EM) interaction, and is pegged to its characteristic $1/r^2$ behavior (which necessarily implies that other structure *has* to exist on small scales within any sound theory).

Arguably, the elementary particle of the gravitational interaction are black holes (BHs). Within General Relativity (GR), BHs are indivisible and the simplest macroscopic objects that one can conceive. The uniqueness results—establishing that the two-parameter Kerr family of BHs describes any vacuum, stationary and asymptotically flat, regular solution to GR—have turned BHs into somewhat of a miracle elementary particle.[1]

---

[1] Quoting Subrahmanyan Chandrasekhar: "In my entire scientific life, extending over forty-five years, the most shattering experience has been the realization that an exact solution of Einstein's equations of general

Even though the first nontrivial regular, asymptotically flat, vacuum solution to the field equations describing BHs were written already in 1916 (Schwarzschild 1916; Droste 1917), several decades would elapse until such solutions became accepted and understood. The dissension between Eddington and Chandrasekhar over gravitational collapse to BHs is famous—Eddington firmly believed that nature would find its way to prevent full collapse—and it took decades for the community to overcome individual prejudices. Ironically, after that BHs quickly became the *only* acceptable solution. So much so, that currently an informal definition of a BH might well be "any dark, compact object with mass above roughly three solar masses."

1.1 Black holes: kings of the cosmos?

There are various reasons why BHs were quickly adopted as the only possible dark and compact sources triggering high-energy, violent phenomena in the Universe. The BH interior is causally disconnected from the exterior by an event horizon. Unlike the classical description of atoms, the GR description of the BH exterior is self-consistent and free of pathologies. The "inverse-square law problem"—the GR counterpart of which is the appearance of pathological curvature singularities—is swept to inside the horizon and therefore harmless for the external world. There are strong indications that classical BHs are stable against small fluctuations (Klainerman and Szeftel 2017), and attempts to produce naked singularities, starting from BH spacetimes, have failed. In addition, BHs in GR can be shown to satisfy remarkable uniqueness properties (Chruściel et al. 2012). These features promote BHs to important solutions of the field equations and ideal testbeds for new physics. But BHs are not only curious mathematical solutions to Einstein's equations: their *formation* process is sound and well understood. At the classical level, there is nothing spectacular with the presence or formation of an event horizon. The equivalence principle dictates that an infalling observer crossing this region (which, by definition, is a *global* concept) feels nothing extraordinary: in the case of macroscopic BHs all of the local physics at the horizon is rather unremarkable. Together with observations of phenomena so powerful that could only be explained via massive compact objects, the theoretical understanding of BHs turned them into undisputed kings of the cosmos.

There is, so far, no evidence for objects other than BHs that can explain all observations. Nonetheless, given the special nature of BHs, one must *question and quantify* their existence. Can BHs, as envisioned in vacuum GR, hold the same surprises that the electron and the hydrogen atom did when they started to be experimentally probed? This overview will dwell on the existence of BHs, and signatures of possible alternatives. There are a number of important reasons to do so, starting from the obvious: we *can* do it. The landmark detection of gravitational waves (GWs) showed that we are now able to analyze and understand the details of the signal produced when two compact objects merge (Abbott et al. (LIGO Scientific Collaboration and the Virgo Collaboration) 2016a, b). An increase in sensitivity of current detectors and the advent of next-generation interferometers on ground and in space will open the frontier of

---

relativity provides the absolutely exact representation of untold numbers of black holes that populate the universe." (S. Chandrasekhar, The Nora and Edward Ryerson lecture, Chicago April 22 1975).

precision GW astrophysics. GWs are produced by the coherent motion of the sources as a whole: they are ideal probes of strong gravity, and play the role that EM waves did to test the Rutherford model. In parallel, novel techniques such as radio and deep infrared interferometry (Doeleman et al. 2008; Antoniadis 2013) are now providing direct *images* of the center of ours and others galaxies, where a dark, massive and compact object is lurking (Genzel et al. 2010; Falcke and Markoff 2013; Johannsen et al. 2016; Abuter et al. (GRAVITY Collaboration) 2018b; Akiyama et al. 2019).

The wealth of data from GW and EM observations has the potential to inform us on the following outstanding issues.

1.2 Problems on the horizon

Classically, spacetime singularities seem to be always cloaked by horizons and hence inaccessible to distant observers; this is in essence the content of the weak cosmic censorship conjecture (Penrose 1969; Wald 1997). However, there is as yet no proof that the field equations always evolve regular initial data towards regular final states.

Classically, the BH exterior is pathology-free, but the interior is not. The Kerr family of BHs harbors singularities and closed timelike curves in its interior, and more generically it features a Cauchy horizon signaling the breakdown of predictability of the theory (Penrose 1978; Reall 2018; Dafermos 2005; Cardoso et al. 2018a). The geometry describing the interior of an astrophysical spinning BH is currently unknown. A resolution of this problem most likely requires accounting for quantum effects. It is conceivable that these quantum effects are of no consequence whatsoever on physics outside the horizon. Nevertheless, it is conceivable as well that the resolution of such inconsistency leads to new physics that resolves singularities and does away with horizons, at least in the way we understand them currently. Such possibility is not too dissimilar from what happened with the atomic model after the advent of quantum electrodynamics.

Black holes have a tremendously large entropy, which is hard to explain from microscopic states of the progenitor star. Classical results regarding for example the area (and therefore entropy) increase (Hawking 1971) and the number of microstates can be tested using GW measurements (Lai and Li 2018; Brustein et al. 2018), but assume classical matter. Indeed, semi-classical quantum effects around BHs are far from being under control. Quantum field theory on BH backgrounds leads to loss of unitarity, a self-consistency requirement that any predictive theory ought to fulfill. The resolution of such conundrum may involve non-local effects changing the near-horizon structure, or doing away with horizons completely (Giddings 1992, 2011, 2012, 2016, 2017a, b; Mazur and Mottola 2004; Mathur 2005, 2008, 2009; Barceló et al. 2016; Almheiri et al. 2013; Unruh and Wald 2017; Bianchi et al. 2018; Giddings et al. 2019).

As a matter of fact, there is no tested nor fully satisfactory theory of quantum gravity, in much the same way that one did not have a quantum theory of point charges at the beginning of the twentieth century.

GR is a purely classical theory. One expects quantum physics to become important beyond some energy scale. It is tacitly assumed that such "quantum gravity effects" are relevant only near the Planck scale: at lengths $\ell_P \sim \sqrt{G\hbar/c^3} \sim 10^{-35}$ m, the Schwarzschild radius is of the order of the Compton wavelength of the BH and the notion of a classical system is lost. However, it has been argued that, in the orders of magnitude standing between the Planck scale and those accessible by current experiments, new physics can hide. To give but one example, if gravity is fundamentally a higher-dimensional interaction, then the fundamental Planck length can be substantially *larger* (Arkani-Hamed et al. 1998; Randall and Sundrum 1999). In addition, some physics related to compact objects have a logarithmic dependence on the (reasonably-defined) Planck length (Cardoso and Pani 2017a) (as also discussed below). Curiously, some attempts to quantize the area of BHs predict sizable effects even at a classical level, resulting in precisely the same phenomenology as that discussed in the rest of this review (Bekenstein and Mukhanov 1995; Saravani et al. 2015; Foit and Kleban 2019; Cardoso et al. 2019a; Chakraborty and Lochan 2019). Thus, quantum-gravity effects may be within reach.

1.3 Quantifying the evidence for black holes

Horizons are not only a rather generic prediction of GR, but their existence is in fact *necessary* for the consistency of the theory at the classical level. This is the root of Penrose's (weak) Cosmic Censorship Conjecture (Penrose 1969; Wald 1997), which remains one of the most urgent open problems in fundamental physics. In this sense, the statement that there is a horizon in any spacetime harboring a singularity in its interior is such a remarkable claim, that (in an informal description of Hume's statement above) it requires similar remarkable evidence.

It is in the nature of science that paradigms have to be constantly questioned and subjected to experimental and observational scrutiny. Most specially because if the answer turns out to be that BHs do not exist, the consequences are so extreme and profound, that it is worth all the possible burden of actually testing it. As we will argue, the question is not just whether the strong-field gravity region near compact objects is consistent with the BH geometry of GR, but rather to *quantify* the limits of observations in testing event horizons. This approach is common practice in other contexts. Decades of efforts in testing the pillars of GR resulted in formalisms [such as the parametrized post-Newtonian approach (Will 2014)] which quantify the constraints of putative deviations from GR. For example, we know that the weak equivalence principle is valid to at least within one part in 10^{15} (Bergé et al. 2018). On the other hand, no such solid framework is currently available to quantify deviations from the standard BH paradigm. In fact, as we advocate in this work, the question to be asked is not whether there is a horizon in the spacetime, but how close to it do experiments or observations go. It is important to highlight that some of the most important tests of theories or paradigms—and GR and its BH solutions are no exception—arise from entertaining the existence of alternatives. It is by allowing a large space of solutions that one can begin to exclude—with observational and experimental data—some of the alternatives, thereby producing a stronger paradigm.

1.4 The dark matter connection

Known physics all but exclude BH alternatives as explanations for the dark, massive and compact objects out there. Nonetheless, the Standard Model of fundamental interactions is not sufficient to describe the cosmos—at least on the largest scales. The nature of dark matter (DM) is one of the longest-standing puzzles in physics (Bertone and Tim 2018; Barack et al. 2018). Given that the evidence for DM is—so far—purely gravitational, further clues may well be hidden in strong-gravity regions or GW signals generated by dynamical compact objects.

As an example, new fundamental fields [such as axions, axion-like particles, etc (Marsh 2016; Clifton et al. 2012)], either minimally or non-minimally coupled to gravity, are essential for cosmological models, and are able to explain all known observations concerning DM. Even the simplest possible theory of minimally coupled, massive scalar fields give rise to self-gravitating *compact* objects, which are dark if their interaction with Standard Model particles is weak. These are called boson stars or oscillatons, depending on whether the field if complex or real, respectively. Such dark objects have a maximum mass[2] which is regulated by the mass of the fundamental boson itself and by possible self-interaction terms; they form naturally through gravitational collapse and may cluster around an ultracompact configuration through "gravitational cooling" (Seidel and Suen 1994; Liebling and Palenzuela 2012; Brito et al. 2015a; Di Giovanni et al. 2018).

Furthermore, DM could be composed of entirely different fields or particles, and many of these are expect to lead to new classes of dark compact objects (Narain et al. 2006; Raidal et al. 2018; Deliyergiyev et al. 2019).

1.5 Taxonomy of compact objects: a lesson from particle physics

From a phenomenological standpoint, BHs and neutron stars could be just two "species" of a larger family of astrophysical compact objects, which might co-exist with BHs rather than replacing them. These objects are theoretically predicted in extended theories of gravity but also in other scenarios in the context of GR, such as beyond-the-Standard-Model fundamental fields minimally coupled to gravity, or of exotic states of matter.

In this context, it is tempting to draw another parallel with particle physics. After the Thomson discovery of the electron in 1897, the zoo of elementary particles remained almost unpopulated for decades: the proton was discovered only in the 1920s, the neutron and the positron only in 1932, few years before the muon (1936). Larger and more sensitive particle accelerators had been instrumental to discover dozens of new species of elementary particles during the second half of the twentieth century, and nowadays the Standard Model of particle physics accounts for hundreds of particles, either elementary or composite. Compared to the timeline of particle physics, the

---

[2] A crucial property of BHs in GR is that—owing to the scale-free nature of vacuum Einstein's equation—their mass is a free parameter. This is why the same Kerr metric can describe any type of BH in the universe, from stellar-mass (or even possibly primordial) to supermassive. It is extremely challenging to reproduce this property with a material body, since matter fields introduce a scale.

discovery of BHs, neutron stars, and binary thereof is much more recent; it is therefore natural to expect that the latest advance in GW astronomy and very long baseline interferometry can unveil new species in the zoo of astrophysical compact objects. Of course, this requires an understanding of the properties of new families of hypothetical compact objects and of their signatures.

1.6 The small ϵ-limit

In addition to the above phenomenological motivations, dark compact objects are also interesting from a mathematical point of view. For instance, given the unique properties of a BH, it is interesting to study how a dark compact object approaches the "BH limit" (if the latter exists!) as its compactness increases. Continuity arguments would suggest that any deviation from a BH should vanish in this limit, but this might occur in a highly nontrivial way, as we shall discuss. The first issue in this context is how to parametrize "how close" a self-gravitating object is to a BH in a rigorous way, by introducing a "closeness" parameter ϵ, such that $\epsilon \to 0$ corresponds to the BH limit. As we shall discuss, there are several choices for ϵ, for example the tidal deformability, the inverse of the maximum redshift in the spacetime, or a quantity related to the compactness M/R such as $\epsilon = 1 - 2M/R$, where M is the object mass in the static case and R is its radius.

In the context of DM self-gravitating objects ϵ is expected to be of order unity. However, when quantifying the evidence for horizons or in the context of quantum corrected spacetimes, one is usually interested in the $\epsilon \ll 1$ limit. The physics of such hypothetical objects is interesting on its own: these objects are by construction regular everywhere and causality arguments imply that all known BH physics must be recovered in the $\epsilon \to 0$ limit. Thus, the small ϵ-limit may prove useful in the understanding of BH themselves, or to help cast a new light in old murky aspects of objects with a teleological nature. Moreover, as we will see, such limit is amenable to many analytical simplifications and describes reasonably well even finite ϵ spacetimes. In this regard, the $\epsilon \to 0$ limit can be compared to large spacetime-dimensionality limit in Einstein field equations (Emparan et al. 2013), or even the large $\mathcal{N}$ limit in QCD ('t Hooft 1974). Here, we will focus exclusively on four-dimensional spacetimes.

2 Structure of stationary compact objects

> *Mumbo Jumbo is a noun and is the name of a grotesque idol said to have been worshipped by some tribes. In its figurative sense, Mumbo Jumbo is an object of senseless veneration or a meaningless ritual.*
>
> Concise Oxford English Dictionary

The precise understanding of the nature of dark, massive and compact objects can follow different routes,

i. a pragmatic approach of testing the spacetime close to compact, dark objects, irrespective of their nature, by devising model-independent observations that yield

unambiguous answers; this often requires consistency checks and null-hypothesis tests of the Kerr metric.

ii. a less ambitious and more theoretically-driven approach, which starts by constructing objects that are very compact, yet horizonless, within some framework. It proceeds to study their formation mechanisms and stability properties, and then discarding solutions which either do not form or are unstable on short timescales; finally, understand the observational imprints of the remaining objects, and how they differ from BHs.

In practice, when dealing with outstanding problems where our ignorance is extreme, pursuing both approaches simultaneously is preferable. Indeed, using concrete models can sometimes be a useful guide to learn about broad, model-independent signatures. As it will become clear, one can design exotic horizonless models which mimic all observational properties of a BH with arbitrary accuracy. While the statement "BHs exist in our Universe" is *fundamentally unfalsifiable*, alternatives can be ruled out with a single observation, just like Popper's black swans (Popper 1985).

Henceforth we shall refer to horizonless compact objects other than a neutron star as *Exotic Compact Objects (ECOs)*. The aim of this section is to contrast the properties of BHs with those of ECOs and to find a classification for different models.

2.1 Anatomy of compact objects

For simplicity, let us start with a four-dimensional spherically symmetric object and assume that it exterior is described by vacuum GR. Static, spherically symmetric spacetimes are described (in standard coordinates with r being the areal radius) by the line element

$$ds^2 = -f(r)dt^2 + g(r)^{-1}dr^2 + r^2 d\Omega^2. \tag{1}$$

with $d\Omega^2 = d\theta^2 + \sin^2\theta d\phi^2$. Birkhoff's theorem guarantees that any vacuum, spherically-symmetric spacetime (in particular, the exterior an isolated compact, spherically-symmetric object) is described by the Schwarzschild geometry, for which

$$f(r) = g(r) = 1 - \frac{2M}{r}, \tag{2}$$

and M is the total mass of the spacetime (we use geometrical $G = c = 1$ units, except if otherwise stated).

2.1.1 Event horizons, trapped surfaces, apparent horizons

A BH owns its name (Herdeiro and Lemos 2018) to the fact that nothing—not even light—can escape from the region enclosed by its *horizon*. Since the latter is the real defining quantity of a BH, it is important to define it rigorously. In fact, there are several inequivalent concepts of horizon (Hawking and Ellis 2011; Curiel 2019). In asymptotically-flat spacetime, a BH is the set of events from which no future-pointing

null geodesic can reach future null infinity. The *event horizon* is the (null) boundary of this region. The event horizon is a *global* property of an entire spacetime: on a given spacelike slice, the event horizon cannot be computed without knowing the entire future of the slice. Strictly speaking, an event horizon does not "form" at a certain time, but it is a nonlocal property; as such, it is of limited practical use in dynamical situations.

On the other hand, in a $3 + 1$ splitting of spacetime, a *trapped surface* is defined as a smooth closed 2-surface on the slice whose future-pointing outgoing null geodesics have negative expansion (Hawking and Ellis 2011; Thornburg 2007; Wald and Iyer 1991). Roughly speaking, on a trapped surface light rays are all directed inside the trapped surface *at that given time*. The *trapped region* is the union of all trapped surfaces, and the outer boundary of the trapped region is called the *apparent horizon*. At variance with the event horizon, the apparent horizon is defined locally in time, but it is a property that depends on the choice of the slice. Under certain hypothesis—including the assumption that matter fields satisfy the energy conditions—the existence of a trapped surface (and hence of an apparent horizon) implies that the corresponding slice contains a BH (Hawking and Ellis 2011). The converse is instead not true: an arbitrary (spacelike) slice of a BH spacetime might not contain any apparent horizon. If an apparent horizon exists, it is necessarily contained within an event horizon, or it coincides with it. In a stationary spacetime, the event and apparent horizons always coincide at a classical level (see Bardeen 1981; York 1983; Arzano and Calcagni 2016 for possible quantum effects).

In practice, we will be dealing mostly with quasi-stationary solutions, when the distinction between event and apparent horizon is negligible. For the sake of brevity, we shall often refer simply to a "horizon", having in mind the apparent horizon of a quasi-stationary solution. Notwithstanding, there is no direct observable associated to the horizon (Abramowicz et al. 2002; Cardoso and Pani 2017a; Nakao et al. 2019). There are signatures which can be directly associated to timelike surfaces, and whose presence would signal new physics. The absence of such signatures strengthens and quantifies the BH paradigm.

2.1.2 Quantifying the shades of dark objects: the closeness parameter ϵ

Alas, I abhor informality.

That Mitchell and Webb Look, Episode 2

Since we will mostly be discussing objects which look like BHs on many scales, it is useful to introduce a "closeness" parameter ϵ that indicates how close one is to a BH spacetime. There is an infinity of possible choices for such parameter (and in fact, different choices have been made in the literature, e.g., Giddings 2014, 2016). At least in the case of spherical symmetric, Birkhoff's theorem provides a natural choice for the closeness parameter: if the object has a surface at r_0, then ϵ is defined as

$$r_0 = 2M(1 + \epsilon). \tag{3}$$

We are thus guaranteed that when $\epsilon \to 0$, a BH spacetime is recovered. For spherical objects the above definition is coordinate-independent ($2\pi r_0$ is the proper equatorial circumference of the object). Furthermore, one can also define the proper distance between the surface and r_0, $\int_{2M}^{r_0} dr f^{-1/2} \sim 4M\sqrt{\epsilon}$, which is directly related to ϵ. Some of the observables discussed below show a dependence on $\log \epsilon$, making the distinction between radial and proper distance irrelevant.

We should highlight that this choice of closeness parameter is made for convenience. None of the final results depend on such an arbitrary choice. In fact, there are objects—such as boson stars—without a well defined surface, since the matter fields are smooth everywhere. In such case r_0 can be taken to be an effective radius beyond which the density drops sharply to zero. In some cases it is possible that the effective radius depends on the type of perturbations or on its frequency. It sometimes proves more useful, and of direct significance, to use instead the coordinate time τ (measurable by our detectors) that a radial-directed light signal takes to travel from the light ring to the surface of the object. For spherically symmetric spacetimes, there is a one-to-one correspondence with the ϵ parameter, $\tau = M(1 - 2\epsilon - \log(4\epsilon^2)) \sim -2M \log \epsilon$, where the last step is valid when $\epsilon \to 0$. In the rest, when convenient, we shall refer to this time scale rather than to r_0.

Overall, we shall use the magnitude of ϵ to classify different models of dark objects. A neutron star has $\epsilon \sim \mathcal{O}(1)$ and models with such value of the closeness parameter (e.g., boson stars, stars made of DM, see below) are expected to have dynamical properties which resemble those of a stellar object rather than a BH. For example, they are characterized by observables that display $\mathcal{O}(1)$ corrections relative to the BH case and are therefore easier to distinguish. On the other hand, to test the BH paradigm in an agnostic way, or for testing the effects of quantum gravity, one often has in mind $\epsilon \ll 1$. For instance, in certain models $r_0 - 2M = 2M\epsilon$ or the proper distance $\sim M\sqrt{\epsilon}$ are of the order of the Planck length ℓ_P; in such case $\epsilon \sim 10^{-40}$ or even smaller. These models are more challenging to rule out.

Finally, in dynamical situations ϵ might be effectively time dependent. Even when $\epsilon \sim \ell_P/M$ at equilibrium, off-equilibrium configurations might have significantly large ϵ (see, e.g., Brustein and Medved 2018; Brustein et al. 2017a; Wang et al. 2018a, 2019b).

2.1.3 Quantifying the softness of dark objects: the curvature parameter

In addition the closeness parameter ϵ, another important property of a dark object is its curvature scale. The horizon introduces a cut-off which limits the curvature that can be probed by an external observer. For a BH the largest curvature (as measured by the Kretschmann scalar $\mathcal{K}$) occurs at the horizon and reads

$$\mathcal{K}^{1/2} \sim \frac{1}{M^2} \approx 4.6 \times 10^{-13} \left(\frac{10 M_\odot}{M} \right)^2 \ \text{cm}^{-2}. \tag{4}$$

For astrophysical BHs the curvature at the horizon is always rather small, and it might be large only if sub-$M_\odot$ primordial BHs exist in the universe. As a reference, the curvature at the center of an ordinary neutron star is $\mathcal{K}^{1/2} \sim 10^{-14} \ \text{cm}^{-2}$.

By comparison with the BH case, one can introduce two classes of models (Raposo et al. 2019): (i) *"soft" ECOs*, for which the maximum curvature is comparable to that at the horizon of the corresponding BH; and (ii) *"hard" ECOs*, for which the curvature is much larger. In the first class, the near-surface geometry smoothly approaches that at the horizon in the BH limit (hence their "softness"), whereas in the second class the ECO can support large curvatures on its surface without collapsing, presumably because the underlying theory involves a new length scale, $\mathcal{L}$, such that $\mathcal{L} \ll M$. In these models high-energy effects drastically modify the near-surface geometry (hence their "hardness"). An example are certain classes of wormholes (see Sect. 3).

An interesting question is whether the maximum curvature $\mathcal{K}_{\mathrm{max}}$ depends on ϵ. Indeed, an ECO with a surface just above the BH limit ($\epsilon \to 0$) may always require large *internal* stresses in order to prevent its collapse, so that the curvature in the interior is very large, even if the exterior is exactly the Schwarzschild geometry. In other words, an ECO can be soft in the exterior but hard in the interior. Examples of this case are thin-shell gravastars and strongly anisotropic stars (see Sect. 3). Thus, according to this classification all ECOs might be "hard" in the $\epsilon \to 0$ limit. Likewise, the exterior of hard ECOs might be described by soft ECO solutions far from the surface, where the curvature is perturbatively close to that of a BH.

2.1.4 Geodesic motion and associated scales

The most salient geodesic features of a compact object are depicted in Fig. 1, representing the equatorial slice of a spherically-symmetric spacetime.

The geodesic motion of timelike or null particles in the geometry (1) can be described with the help of two conserved quantities, the specific energy $E = f \dot{t}$ and angular momentum $L = r^2 \dot{\varphi}$, where a dot stands for a derivative with respect to proper time (Chandrasekhar 1983). The radial motion can be computed via a normalization condition,

$$\dot{r}^2 = g \left(\frac{E^2}{f} - \frac{L^2}{r^2} - \delta_1 \right) \equiv E^2 - V_{\mathrm{geo}},\tag{5}$$

where $\delta_1 = 1, 0$ for timelike or null geodesics, respectively. The null limit can be approached letting $E, L \to \infty$ and rescaling all quantities appropriately. Circular trajectories are stable only when $r \geq 6M$, and unstable for smaller radii. The $r = 6M$ surface defines the innermost stable circular orbit (ISCO), and has an important role in controlling the inner part of the accretion flow onto compact objects. It corresponds to the orbital distance at which a geometrically thin accretion disk is typically truncated (Novikov and Thorne 1973) and it sets the highest characteristic frequency for compact emission region ("hotspots") orbiting around accreting compact objects (Broderick and Loeb 2005, 2006). Another truly relativistic feature is the existence of circular null geodesics, i.e., of circular motion for high-frequency EM waves or GWs. In the Schwarzschild geometry, a circular null geodesic is possible only at $r = 3M$ (Chandrasekhar 1983). This location defines a surface called the *photon sphere*, or, on an equatorial slice, a *light ring*. The photon sphere has a number of interesting properties, and is useful to understand certain features of compact spacetimes.
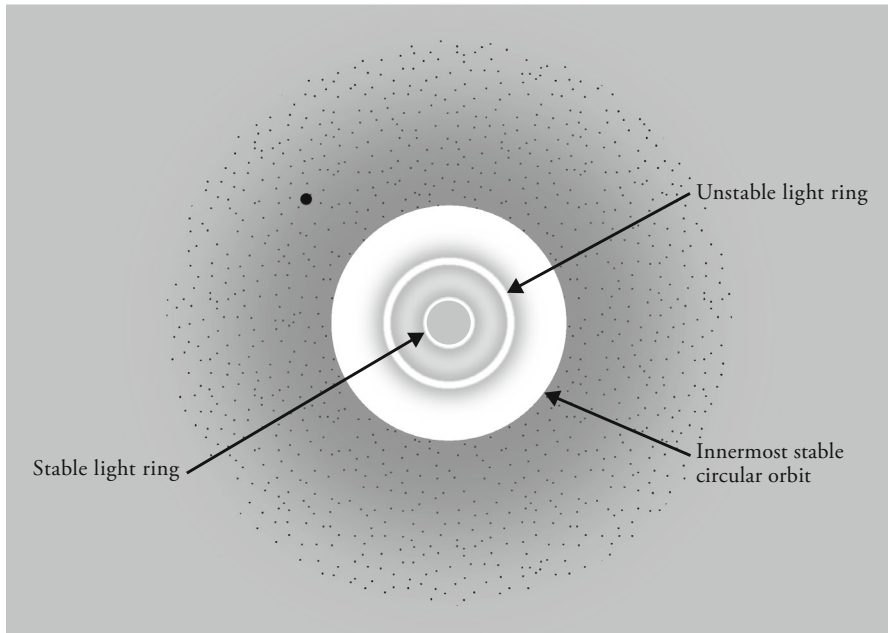
Fig. 1 An equatorial slice of a very compact object, together with the most significant (from a geodesic perspective) locations. At large distances away from the central region, physics is nearly Newtonian: planets—such as the small dot on the figure—can orbit on stable orbits. The external gray area is the entire region where stable circular motion is possible. At the innermost stable circular orbit ($r = 6M$), timelike circular motion is marginally stable, and unstable as one moves further within. High-frequency EM waves or GWs can be on circular orbit in one very special location: the light ring ($r = 3M$). Such motion is unstable, and can also be associated with the "ringdown" excited during mergers. For horizonless objects, as one approaches the geometric center another significant region may appear: a second, *stable* light ring. Once rotation is turned on, regions of negative energy ("ergoregions") are possible. The astrophysical properties of a dark compact object depends on where in this diagram its surface is located

For example, assume that an experimenter far away throws (high-frequency) photons in all directions and somewhere a compact object is sitting, as in Fig. 2. Photons that have a very large impact parameter (or large angular momentum), never get close to the object. Photons with a smaller impact parameter start feeling the gravitational pull of the object and may be slightly deflected, as the ray in the figure. Below a critical impact parameter all photons "hit" the compact object. It is a curious mathematical property that the critical impact parameter corresponds to photons that circle the light ring an infinite number of orbits, before being either absorbed or scattered. Thus, the light ring is fundamental for the description of how compact objects and BHs "look" like when illuminated by accretion disks or stars, thus defining their so-called *shadow*, see Sect. 2.2 below.

The photon sphere also has a bearing on the spacetime response to any type of high-frequency waves, and therefore describes how high-frequency GWs linger close to the horizon. At the photon sphere, $V''_{\text{geo}} = -2E^2/(3M^2) < 0$. Thus, circular null
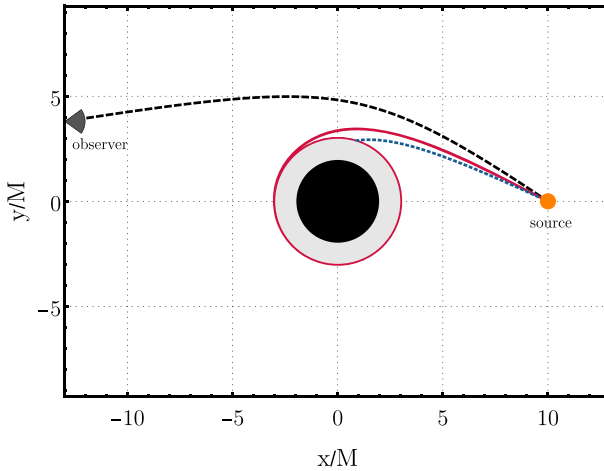
Fig. 2 A source (for example, a star) emits photons in all directions in a region of spacetime where a compact object exists (black circle). Photons with high impact parameter are weakly bent (dashed, black curve), while those with small impact parameter (short-dashed blue) are absorbed and hit the object. The separatrix corresponds to photons that travel an infinite amount of time around the light ring (solid red curve) before being scattered or absorbed. Such critical photons have an impact parameter $b = 3\sqrt{3}M$ (Chandrasekhar 1983). The gray shaded area is the photon sphere

geodesics are unstable: a displacement δ of null particles grows exponentially (Ferrari and Mashhoon 1984; Cardoso et al. 2009)

$$\delta(t) \sim \delta_0 e^{\lambda t}, \qquad \lambda = \sqrt{\frac{-f^2 V_r''}{2E^2}} = \frac{1}{3\sqrt{3}M}. \tag{6}$$

A geodesic description anticipates that light or GWs may persist at or close to the photon sphere on timescales $3\sqrt{3}M \sim 5M$. Because the geodesic calculation is local, these conclusions hold irrespectively of the spacetime being vacuum all the way to the horizon or not.

For any regular body, the metric functions f, g are well behaved at the center, never change sign and asymptote to unity at large distances. Thus, the effective potential V_{geo} is negative at large distances, vanishes with zero derivative at the light ring, and is positive close to the center of the object. This implies that there must be a second light ring in the spacetime, and that it is stable (Cardoso et al. 2014; Macedo et al. 2013a; Cunha et al. 2017a). Inside this region, there is stable timelike circular motion everywhere.[3]

2.1.5 Photon spheres

An ultracompact object with surface at $r_0 = 2M(1 + \epsilon)$, with $\epsilon \ll 1$, features exactly the same geodesics and properties close to its photon sphere as BHs. From Eq. (6), we

---

[3] Incidentally, this also means that the circular timelike geodesic at $6M$ is not really the "innermost stable circular orbit". We use this description to keep up with the tradition in BH physics.

immediately realize that after a (say) three e-fold timescale, $t \sim 15M$, the amplitude of the original signal is only 5% of its original value. On these timescales one can say that the signal died away. If on such timescales the ingoing part of the signal did not have time to bounce off the surface of the object and return to the light ring, then for an external observer the relaxation is identical to that of a BH. This amounts to requiring that $\tau \equiv \int_{2M(1+\epsilon)}^{3M} \gtrsim 15M$, or

$$\epsilon \lesssim \epsilon_{\mathrm{crit}} \sim 0.019. \tag{7}$$

Thus, the horizon plays no special role in the response of high frequency waves, nor could it: it takes an infinite (coordinate) time for a light ray to reach the horizon. The above threshold on ϵ is a natural sifter between two classes of compact, dark objects. For objects characterized by $\epsilon \gtrsim 0.019$, light or GWs can make the roundtrip from the photon sphere to the object's surface and back, before dissipation of the photon sphere modes occurs. For objects satisfying (7), the waves trapped at the photon sphere relax away by the time that the waves from the surface hit it back.

We can thus use the properties of the ISCO and photon sphere to distinguish between different classes of models:

– *Compact object*: if it features an ISCO, or in other words if its surface satisfies $r_0 < 6M$ ($\epsilon < 2$). Accretion disks around compact objects of the same mass should have similar characteristics;
– *Ultracompact object (UCO)* (Iyer et al. 1985): a compact object that features a photon sphere, $r_0 < 3M$ ($\epsilon < 1/2$). For these objects, the phenomenology related to the photon sphere might be very similar to that of a BH;
– *Clean-photon sphere object (ClePhO)*: an ultracompact object which satisfies condition (7) and therefore has a "clean" photon sphere, $r_0 < 2.038M$ ($\epsilon \lesssim 0.019$). The early-time dynamics of ClePhOs is expected to be the same as that of BHs. At late times, ClePhOs should display unique signatures of their surface.

An ECO can belong to any of the above categories. There are indications that the photon sphere is a fragile concept and that it suffers radical changes in the presence of small environmental disturbances (Shoom 2017). The impact of such result on the dynamics on compact objects is unknown.

2.2 Escape trajectories and shadows

An isolated BH would appear truly as a "hole" in the sky, since we observe objects by receiving the light they either emit or reflect. The boundary of this hole, i.e., the "silhouette" of a BH, is called the *shadow* and is actually larger than the BH horizon and intimately related with the existence of a photon sphere.

Indeed, according to Eq. (5), there exists a critical value of the angular momentum $L \equiv KME$ for a light ray to be able to escape to infinity. By requiring that a light ray emitted at a given point will not find turning points in its motion, Eq. (5) yields $K_{\mathrm{esc}} = 3\sqrt{3}$ (Chandrasekhar 1983). This corresponds to the dimensionless critical impact parameter of a photon at very large distances. Suppose now that the light ray

is emitted by a locally static observer at $r = r_0$. In the local rest frame, the velocity components of the photon are (Shapiro and Teukolsky 1983)

$$v_\varphi^{\text{local}} = \frac{MK}{r_0}\sqrt{f_0}, \qquad v_r^{\text{local}} = \sqrt{1 - K^2 M^2 \frac{f_0}{r_0^2}}, \tag{8}$$

where $f_0 \equiv f(r_0) = 1 - 2M/r_0$. With this, one can easily compute the escape angle, $\sin \psi_{\text{esc}} = 3M\sqrt{3 f_0}/r_0$. In other words, the solid angle for escape is

$$\Delta\Omega_{\text{esc}} = 2\pi \left(1 - \sqrt{1 - \frac{27M^2(r_0 - 2M)}{r_0^3}}\right) \sim 27\pi \left(\frac{r_0 - 2M}{8M}\right), \tag{9}$$

where the last step is valid for $\epsilon \ll 1$. For angles larger than these, the light ray falls back and either hits the surface of the object, if there is one, or will be absorbed by the horizon. The escape angle is depicted in Fig. 3 for different emission points r_0. The rays that are not able to escape reach a maximum coordinate distance,

$$r_{\text{max}} \sim 2M \left(1 + \frac{4 f_0 M^2}{r_0^2 \sin^2 \psi}\right). \tag{10}$$

This result is accurate away from ψ_{esc}, whereas for $\psi \to \psi_{\text{esc}}$ the photon approaches the photon sphere ($r = 3M$). The coordinate time that it takes for photons that travel initially outward, but eventually turn back and hit the surface of the object, is shown in Fig. 3 as a function of the locally measured angle ψ, and is of order $\sim M$ for most of the angles ψ, for $\epsilon \ll 1$. A closed form expression away from ψ_{crit}, which describes well the full range (see Fig. 3) reads

$$t_{\text{roundtrip}} \sim 8M \log(\cot(\psi/2)). \tag{11}$$

When averaging over ψ, the coordinate roundtrip time is then $32M \, \text{Cat}/\pi \approx 9.33M$, for any $\epsilon \ll 1$, where "Cat" is Catalan's constant. Remarkably, this result is independent of ϵ in the $\epsilon \to 0$ limit.

In other words, part of the light coming from *behind* a UCO is "trapped" by the photon sphere. If the central object is a good absorber and illuminated with a source far away from it, an observer staring at the object sees a "hole" in the sky with radius $r_0 = 3\sqrt{3}M$, which corresponds to the critical impact parameter K_{esc}. On the other hand, radiation emitted near the surface of the object (as for example due to an accretion flow) can escape to infinity, with an escape angle that vanishes as $\Delta\Omega_{\text{esc}} \sim \epsilon$ in the $\epsilon \to 0$ limit. This simple discussion anticipates that the shadow of a non-accreting UCO can be very similar to that of a BH, and that the accretion flow from ECOs with $\epsilon \to 0$ can also mimic that from an accreting BH (Vincent et al. 2016).
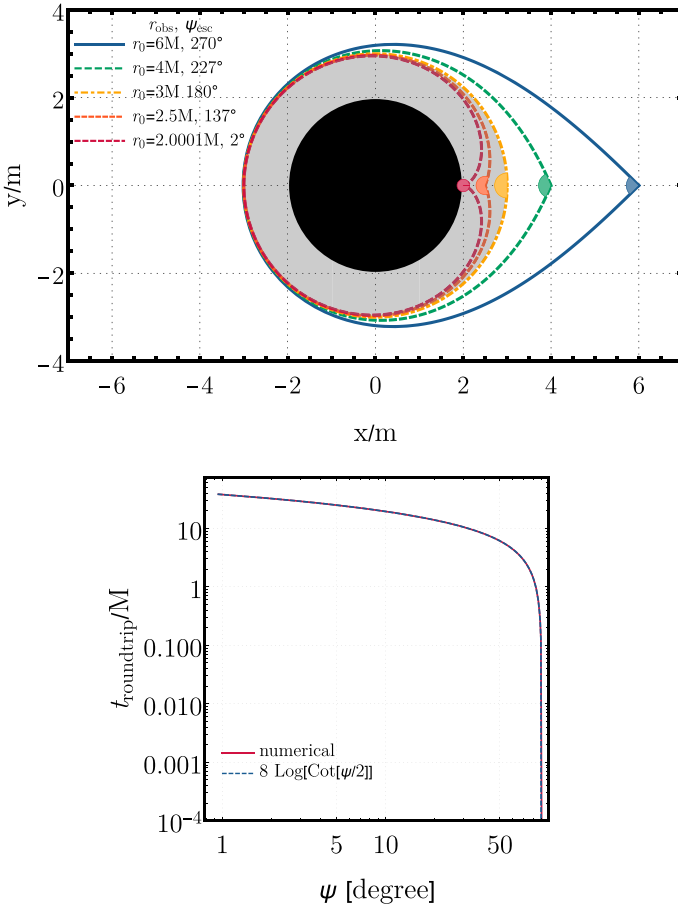
Fig. 3 Top: Critical escape trajectories of radiation in the Schwarzschild geometry. A locally static observer (located at $r = r_{\rm obs}$) emits photons isotropically, but those emitted within the colored conical sectors will not reach infinity. The gray shaded area is the photon sphere. Bottom: Coordinate roundtrip time of photons as a function of the emission angle $\psi > \psi_{\rm esc}$ and for $\epsilon \ll 1$

2.3 The role of the spin

While the overall picture drawn in the previous sections is valid also for rotating objects, angular momentum introduces qualitatively new features. Spin breaks spherical symmetry, introduces frame dragging, and breaks the degeneracy between co- and counter-rotating orbits. We focus here on two properties related to the spin which are important for the phenomenology of ECOs, namely the existence of an ergoregion and the multipolar structure of compact spinning bodies.

2.3.1 Ergoregion

An infinite-redshift surface outside a horizon is called an *ergosurface* and is the boundary of the so-called *ergoregion*. In a stationary spacetime, this boundary is defined by

the roots of $g_{tt} = 0$. Since the Killing vector $\xi^\mu = (1, 0, 0, 0)$ becomes spacelike in the ergoregion, $\xi^\mu \xi^\mu g_{\mu\nu} = g_{tt} > 0$, the ergosurface is also the static limit: an observer within the ergoregion cannot stay still with respect to distant stars; the observer is forced to co-rotate with the spacetime due to strong frame-dragging effects. Owing to this property, negative-energy (i.e., bound) states are possible within the ergoregion. This is the chief property that allows for energy and angular momentum extraction from a BH through various mechanisms, e.g., the Penrose's process, superradiant scattering, the Blandford–Znajek mechanism, etc. (Brito et al. 2015b). An ergoregion necessarily exists in the spacetime of a stationary and axisymmetric BH and the ergosurface must lay outside the horizon or coincide with it (Brito et al. 2015b). On the other hand, a spacetime with an ergoregion but without an event horizon is linearly unstable (see Sect. 4.3).

2.3.2 Multipolar structure

As a by-product of the BH uniqueness and no-hair theorems (Carter 1971; Hawking and Ellis 2011) (see also Heusler 1998; Chruściel et al. 2012; Robinson 2009), the multipole moments of any stationary BH in isolation can be written as (Hansen 1974),

$$\mathcal{M}_\ell^{\text{BH}} + i\mathcal{S}_\ell^{\text{BH}} = M^{\ell+1} (i\chi)^\ell , \qquad (12)$$

where $\mathcal{M}_\ell$ ($\mathcal{S}_\ell$) are the Geroch-Hansen mass (current) multipole moments (Geroch 1970; Hansen 1974), the suffix "BH" refers to the Kerr metric, and

$$\chi \equiv \frac{\mathcal{S}_1}{\mathcal{M}_0^2} \qquad (13)$$

is the dimensionless spin. Equation (12) implies that $\mathcal{M}_\ell^{\text{BH}}$ ($\mathcal{S}_\ell^{\text{BH}}$) vanish when ℓ is odd (even), and that all moments with $\ell \geq 2$ can be written only in terms of the mass $\mathcal{M}_0 \equiv M$ and angular momentum $\mathcal{S}_1 \equiv J$ (or, equivalently, χ) of the BH. Therefore, any independent measurement of three multipole moments (e.g., the mass, the spin and the mass quadrupole $\mathcal{M}_2$) provides a null-hypothesis test of the Kerr metric and, in turn, it might serve as a genuine strong-gravity confirmation of GR (Psaltis 2008; Gair et al. 2013; Yunes and Siemens 2013; Berti et al. 2015; Cardoso and Gualtieri 2016; Barack et al. 2018; Sathyaprakash 2019).

The vacuum region outside a spinning object is not generically described by the Kerr geometry, due to the absence of an analog to Birkhoff's theorem in axisymmetry (for no-hair results around horizonless objects see Raposo et al. 2019; Barceló et al. 2019; Quevedo and Mashhoon 1991). Thus, the multipole moments of an axisymmetric ECO will generically satisfy relations of the form

$$\mathcal{M}_\ell^{\text{ECO}} = \mathcal{M}_\ell^{\text{BH}} + \delta\mathcal{M}_\ell, \qquad (14)$$

$$\mathcal{S}_\ell^{\text{ECO}} = \mathcal{S}_\ell^{\text{BH}} + \delta\mathcal{S}_\ell, \qquad (15)$$

where $\delta\mathcal{M}_\ell$ and $\delta\mathcal{S}_\ell$ are model-dependent corrections, whose precise value can be obtained by matching the metric describing the interior of the object to that of the exterior.

For models of ECOs whose exterior is perturbatively close to Kerr, it has been conjectured that in the $\epsilon \to 0$ limit, the deviations from the Kerr multipole moments (with $\ell \geq 2$) vanish as (Raposo et al. 2019)

$$\frac{\delta\mathcal{M}_\ell}{M^{\ell+1}} \to a_\ell \frac{\chi^\ell}{\log \epsilon} + b_\ell \epsilon + \cdots, \tag{16}$$

$$\frac{\delta\mathcal{S}_\ell}{M^{\ell+1}} \to c_\ell \frac{\chi^\ell}{\log \epsilon} + d_\ell \epsilon + \cdots, \tag{17}$$

or *faster*, where a_ℓ, b_ℓ, c_ℓ, and d_ℓ are model-dependent numbers which satisfy certain selection and $\mathbb{Z}_2$ rules (Raposo et al. 2019). The coefficients a_ℓ and c_ℓ are related to the spin-induced contributions to the multipole moments and are typically of order unity or smaller, whereas the coefficients b_ℓ and d_ℓ are related to the nonspin-induced contributions. It is worth mentioning that, in all ECO models known so far, $b_\ell = d_\ell = 0$. For example, for ultracompact gravastars $b_\ell = d_\ell = 0$ for any ℓ, $a_\ell = 0$ ($c_\ell = 0$) for odd (even) values of ℓ, and the first nonvanishing terms are $a_2 = -8/45$ (Pani 2015) and $c_3 = -92/315$ (Glampedakis and Pappas 2018a).

In other words, the deviations of the multipole moments from their corresponding Kerr value must die sufficiently fast as the compactness of the object approaches that of a BH, or otherwise the curvature at the surface will grow and the perturbative regime breaks down (Raposo et al. 2019). The precise way in which the multipoles die depends on whether they are induced by spin or by other moments.

Note that the scaling rules (16) and (17) imply that in this case a quadrupole moment measurement will always be dominated by the spin-induced contribution, unless

$$\chi \ll \sqrt{\epsilon \left| \frac{b_2}{a_2} \log \epsilon \right|}. \tag{18}$$

For all models known so far, $b_\ell = 0$ so obviously only the spin-induced contribution is important. Even more in general, assuming $b_2/a_2 \sim \mathcal{O}(1)$, the above upper bound is unrealistically small when $\epsilon \to 0$, e.g., $\chi \ll 10^{-19}$ when $\epsilon \approx 10^{-40}$. This will always be the case, unless some fine-tuning of the model-dependent coefficients occurs.

3 ECO taxonomy: from DM to quantum gravity

A nonexhaustive summary of possible self-gravitating compact objects is shown in Table 1. Different objects arise in different contexts. We refer the reader to specific works (e.g., Carballo-Rubio et al. 2018a) for a more comprehensive review of the models.

Table 1 Catalogue of some proposed horizonless compact objects

Model	Formation	Stability	EM signatures	GWs
Fluid stars	✓ Shapiro and Teukolsky (1983)	✓ Iyer et al. (1985), Kokkotas and Schmidt (1999), Cardoso et al. (2014), Saida et al. (2016), Stuchlík et al. (2017), Völkel and Kokkotas (2017a,b)	✓	✓ Kokkotas and Schmidt (1999), Ferrari and Kokkotas (2000), Cardoso et al. (2014), Völkel and Kokkotas (2017a)
Anisotropic stars	✗	✓ Raposo et al. (2018), Dev and Gleiser (2003), Doneva and Yazadjiev (2012)	✓ Silva et al. (2015), Yagi and Yunes (2015a,c)	✓ Yagi and Yunes (2015a,c), Raposo et al. (2018)
Boson stars and oscillatons	✓ Seidel and Suen (1991, 1994), Okawa et al. (2014), Brito et al. (2016b), Liebling and Palenzuela (2012)	✓ Gleiser and Watkins (1989), Lee and Pang (1989), Honda and Choptuik (2002), Cardoso et al. (2008a), Brito et al. (2016a), Macedo et al. (2013a)	✓ Vincent et al. (2016), Cao et al. (2016), Shen et al. (2016)	~ Palenzuela et al. (2008), Kesden et al. (2005), Choptuik and Pretorius (2010), Macedo et al. (2013b), Cardoso et al. (2016b, 2017), Sennett et al. (2017), Maselli et al. (2018b)
Gravastars	✗	✓ Visser and Wiltshire (2004), Cardoso et al. (2008a)	✓ Sakai et al. (2014), Uchikata and Yoshida (2016), Uchikata et al. (2016)	✓ Chirenti and Rezzolla (2007), Pani et al. (2010b, c, 2009), Chirenti and Rezzolla (2016), Cardoso et al. (2016a, b, 2017), Uchikata et al. (2016), Maselli et al. (2018b), Völkel and Kokkotas (2017a, b)
AdS bubbles	✗	✓ Danielsson et al. (2017)	~ Danielsson et al. (2017)	✗

Table 1 continued

Model	Formation	Stability	EM signatures	GWs
Wornholes	✗	✓ Gonzalez et al. (2009a, b), Bromikov et al. (2012), Cuyubamba et al. (2018)	✓ Nedkova et al. (2013), Ohgami and Sakai (2015), Abdujabbarov et al. (2016), Zhou et al. (2016)	~ Cardoso et al. (2016a, 2017), Maselli et al. (2018b)
Fuzzballs	✗	✗ But see Cardoso et al. (2006), Chowdhury and Mathur (2008), Eperon et al. (2016), Eperon (2017)	✗	~ But see Cardoso et al. (2016a, b), Hertog and Hartle (2017)
Superspinars	✗	✓ Cardoso et al. (2008b), Pani et al. (2010a)	✗ But see Patil et al. (2016)	~ Cardoso et al. (2016a, b)
2–2 holes	✗	✗ But see Holdom and Ren (2017)	✗ But see Holdom and Ren (2017)	~ Cardoso et al. (2016a, b)
Collapsed polymers	✗ But see Brustein and Medved (2017), Brustein et al. (2017b)	✓ Brustein and Medved (2019)	✗ Brustein et al. (2017b)	~
Quantum bounces/dark stars	✗ But see Bambi et al. (2013), Barcelo et al. (2008)	✗	✗	~ Barceló et al. (2017)
Compact quantum objects*	✗ Dvali and Gomez (2013b, a), Giddings (2014)	✗	✗	✓ Giddings et al. (2019)
Firewalls*	✗	✗	✗	~ Barausse et al. (2014), Cardoso et al. (2016b)

A ✓ tick means that the topic was addressed. With the exception of boson stars, however, most of the properties are not fully understood yet. The symbol ~ stands for incomplete treatment. An asterisk * stands for the fact that these objects *are* BHs, but could have phenomenology similar to the other compact objects in the list
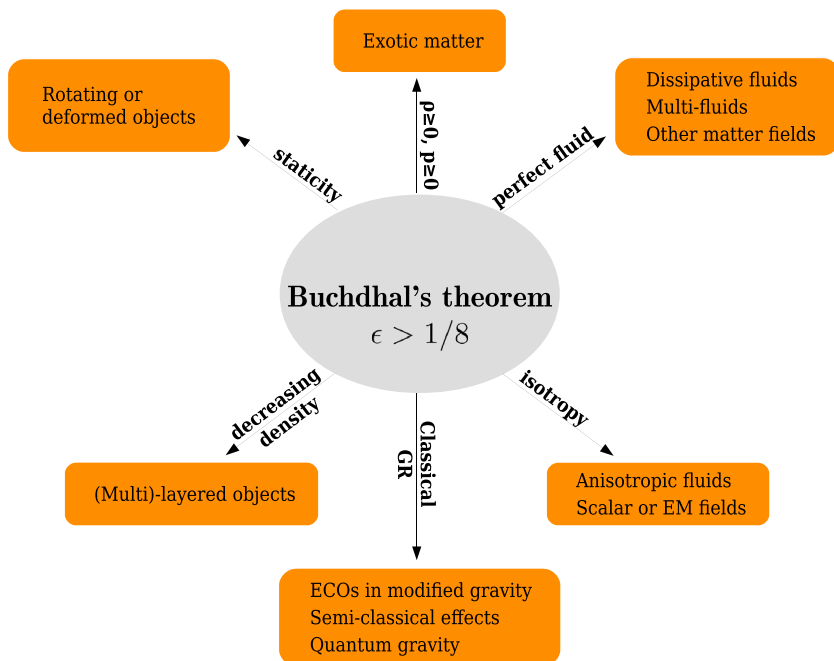
Fig. 4 Buchdahl's theorem deconstructed

3.1 A compass to navigate the ECO atlas: Buchdahl's theorem

Within GR, Buchdahl's theorem states that, under certain assumptions, the maximum compactness of a self-gravitating object is $M/r_0 = 4/9$ (i.e., $\epsilon \geq 1/8$) (Buchdahl 1959). This result prevents the existence of ECOs with compactness arbitrarily close to that of a BH. A theorem is only as good as its assumptions; one might "turn it around" and look at the assumptions of Buchdahl's theorem to find possible ways to evade it.[4] More precisely, Buchdahl's theorem assumes that (Urbano and Veermäe 2018):

1. GR is the correct theory of gravity;
2. The solution is spherically symmetric;
3. Matter is described by a single, perfect fluid;
4. The fluid is either isotropic or mildly anisotropic, in the sense that the tangential pressure is smaller than the radial one, $P_r \gtrsim P_t$;
5. The radial pressure and energy density are non-negative, $P_r \geq 0$, $\rho \geq 0$.
6. The energy density decreases as one moves outwards, $\rho'(r) < 0$.

Giving up each of these assumptions (or combinations thereof) provides a way to circumvent the theorem and suggests a route to classify ECOs based on which of the underlying assumptions of Buchdahl's theorem they violate (see Fig. 4).

---

[4] A similar approach is pursued to classify possible extensions of GR (Berti et al. 2015).

3.2 Self-gravitating fundamental fields

One of the earliest and simplest known examples of a self-gravitating compact configuration is that of a (possibly complex) minimally-coupled massive scalar field Φ, described by the action

$$S = \int d^4x \sqrt{-g} \left(\frac{R}{16\pi} - g^{\mu\nu}\bar{\Phi}_{,\mu}\Phi_{,\nu} - \frac{\mu_S^2 \bar{\Phi}\Phi}{2} \right). \tag{19}$$

The mass m_S of the scalar is related to the mass parameter as $m_S = \hbar\mu_S$, and the theory is controlled by the dimensionless coupling

$$\frac{G}{c\hbar} M\mu_S = 7.5 \times 10^9 \left(\frac{M}{M_\odot} \right) \left(\frac{m_S c^2}{\mathrm{eV}} \right), \tag{20}$$

where M is the total mass of the bosonic configuration.

Self-gravitating solutions for the theory above are broadly referred to as boson stars, and can be generalized through the inclusion of nonlinear self-interactions (Kaup 1968; Ruffini and Bonazzola 1969; Khlopov et al. 1985; Seidel and Suen 1991; Guth et al. 2015; Brito et al. 2016a; Minamitsuji 2018) (see Jetzer 1992; Schunck and Mielke 2003; Liebling and Palenzuela 2012; Macedo et al. 2013a for reviews). If the scalar is *complex*, there are *static*, spherically-symmetric geometries, while the field itself oscillates (Kaup 1968; Ruffini and Bonazzola 1969) (for reviews, see Jetzer 1992; Schunck and Mielke 2003; Liebling and Palenzuela 2012; Macedo et al. 2013a). Analogous solutions for complex massive vector fields were also shown to exist (Brito et al. 2016a). Recently, multi-oscillating boson stars which are not exactly static spacetimes were constructed, and these could represent intermediate states between static boson stars which underwent violent dynamical processes (Choptuik et al. 2019). On the other hand, *real* scalars give rise to long-term stable oscillating geometries, but with a non-trivial time-dependent stress-energy tensor, called oscillatons (Seidel and Suen 1991). Both solutions arise naturally as the end-state of gravitational collapse (Seidel and Suen 1991; Garfinkle et al. 2003; Okawa et al. 2014), and both structures share similar features.

Static boson stars form a one-parameter family of solutions governed by the value of the bosonic field at the center of the star. The mass M displays a maximum above which the configuration is unstable against radial perturbations, just like ordinary stars. The maximum mass and compactness of a boson star depend strongly on the boson self-interactions. As a rule of thumb, the stronger the self-interaction the higher the maximum compactness and mass of a stable boson stars (Schunck and Mielke 2003; Liebling and Palenzuela 2012) (see Table 2).

The simplest boson stars are moderately compact in the nonspinning case (Macedo et al. 2013a; Brito et al. 2016a; Grandclément 2017). Their mass–radius relation is shown in Fig. 5. Once spin (Grandclément 2017) or nonlinear interactions (Colpi et al. 1986; Macedo et al. 2013a; Friedberg et al. 1987) are added, boson star spacetimes can have light rings and ergoregions. The stress-energy tensor of a self-interacting bosonic

Table 2 Scalar potential and maximum mass for some scalar boson-star models. Adapted from Cardoso et al. (2017)

Model	Potential $V(|\Phi|^2)$	Maximum mass $M_{\max}/M_\odot$
Minimal (Kaup 1968; Ruffini and Bonazzola 1969)	$\mu^2|\Phi|^2$	$8\left(\frac{10^{-11}\,\text{eV}}{m_S}\right)$
Massive (Colpi et al. 1986)	$\mu^2|\Phi|^2 + \frac{\alpha}{4}|\Phi|^4$	$5\sqrt{\alpha}\hbar\left(\frac{0.1\,\text{GeV}}{m_S}\right)^2$
Solitonic (Friedberg et al. 1987)	$\mu^2|\Phi|^2\left[1 - \frac{2|\Phi|^2}{\sigma_0^2}\right]^2$	$5\left[\frac{10^{-12}}{\sigma_0}\right]^2\left(\frac{500\,\text{GeV}}{m_S}\right)$

In our units, the scalar field Φ is dimensionless and the potential V has dimensions of an inverse length squared. The bare mass of the scalar field is $m_S := \mu\hbar$. For minimal boson stars, the scaling of the maximum mass is exact. For massive boson stars and solitonic boson stars, the scaling of the maximum mass is approximate and holds only when $\alpha \gg \mu^2$ and when $\sigma_0 \ll 1$, respectively

field contains anisotropies, which in principle allow to evade naturally Buchdahl's theorem. However, there are no boson-star solutions which evade the Buchdahl's bound: in the static case, the most compact configuration has $r_0 \approx 2.869M$ ($\epsilon \approx 0.44$) (Kesden et al. 2005).

There seem to be no studies on the classification of such configurations (there are solutions known to display photon spheres, but it is unknown whether they can be as compact as ClePhOs) (Kesden et al. 2005; Grandclément 2017).

Because of their simplicity and fundamental character, boson stars are interesting on their own. A considerable interest in their properties arose with the understanding that light scalars are predicted to occur in different scenarios, and ultralight scalars can explain the DM puzzle (Hui et al. 2017). Indeed, dilute bosonic configurations provide an alternative model for DM halos.

3.3 Perfect fluids

The construction of boson stars is largely facilitated by their statistics, which allow for a large number of bosons to occupy the same level. Due to Pauli's exclusion principle, a similar construction for fermions is therefore more challenging, and approximate strategies have been devised (Ruffini and Bonazzola 1969; Shapiro and Teukolsky 1983). In most applications, such fundamental description is substituted by an effective equation of state, usually of polytropic type, which renders the corresponding Einstein equations much easier to solve (Shapiro and Teukolsky 1983).

When the stresses are assumed to be isotropic, static spheres in GR made of ordinary fluid satisfy the Buchdahl limit on their compactness, $2M/r_0 < 8/9$ (Buchdahl 1959); strictly speaking, they would not qualify as a ClePhO. However, GWs couple very weakly to ordinary matter and can travel unimpeded right down to the center of stars. Close to the Buchdahl limit, the travel time is extremely large, $\tau \sim \epsilon^{-1/2}M$, and in practice such objects would behave as ClePhOs (Pani and Ferrari 2018). In addition, polytrope stars with a light ring (sometimes referred to as ultra-compact stars) *always* have superluminal sound speed (Saida et al. 2016). Neutron stars—the only object in
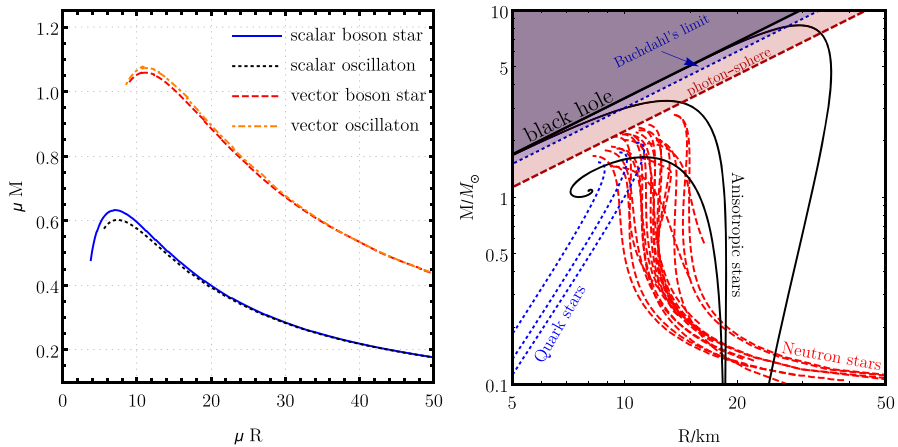
Fig. 5 Left: Comparison between the total mass of a boson star (*complex* scalar or vector fields) and an oscillaton (*real* scalar or vector fields), as a function of their radius R. R is defined as the radius containing 98% of the total mass. The procedure to find the diagram is outlined in the main text. Adapted from Brito et al. (2016b). Right: Mass–radius diagram for nonspinning fluid stars in GR. The red dashed (blue dotted) lines are ordinary NSs (quark stars) for several representative equations of state (Lattimer and Prakash 2007; Özel and Freire 2016a) [data taken from Özel and Freire (2016b)]; the black continuous lines are strongly-anisotropic stars (Raposo et al. 2018). Note that only the latter have photon spheres in their exterior and violate Buchdahl's bound

our list for which there is overwhelming evidence—are not expected to have light rings nor behave as ClePhOs for currently accepted equations of state (Iyer et al. 1985). The mass–radius relation for a standard neutron star is shown in Fig. 5.

Some fermion stars, such as neutron stars, live in DM-rich environments. Thus, DM can be captured by the star due to gravitational deflection and a non-vanishing cross-section for collision with the star material (Press and Spergel 1985; Gould et al. 1990; Goldman and Nussinov 1989; Bertone and Fairbairn 2008; Goldman and Nussinov 1989). The DM material eventually thermalizes with the star, producing a composite compact object. Compact solutions made of both a perfect fluid and a massive complex (Henriques et al. 1989, 1990; Lopes and Henriques 1992; Henriques and Mendes 2005; Sakamoto and Shiraishi 1998; Pisano and Tomazelli 1996) or real scalar or vector field (Brito et al. 2015a, 2016b) were built, and model the effect of bosonic DM accretion by compact stars. Complementary to these studies, accretion of fermionic DM has also been considered, by modeling the DM core with a perfect fluid and constructing a physically motivated equation of state (Leung et al. 2011, 2013; Tolos and Schaffner-Bielich 2015). The compactness of such stars is similar to that of the host neutron stars, and does not seem to exceed the Buchdahl limit.

3.4 Anisotropic stars

The Buchdahl limit can be circumvented when the object is subjected to large anisotropic stresses (Andreasson 2008). These might arise in a variety of contexts: at high densities (Kippenhahn et al. 2012; Ruderman 1972; Canuto and Chitre 1974),

when EM or fermionic fields play a role, or in pion condensed phase configurations in neutron stars (Sawyer and Scalapino 1973), superfluidity (Carter and Langlois 1998), solid cores (Kippenhahn et al. 2012), etc. In fact, anisotropy is common and even a simple soap bubble support anisotropic stresses (Guven and O'Murchadha 1999). Anisotropic stars were studied in GR, mostly at the level of static spherically symmetric solutions (Bowers and Liang 1974; Letelier 1980; Bayin 1982; Dev and Gleiser 2002, 2003; Mak and Harko 2003; Herrera et al. 2004; Andreasson 2008; Hillebrandt and Steinmetz 1976; Doneva and Yazadjiev 2012; Silva et al. 2015; Yagi and Yunes 2015b, c, 2016). These studies are not covariant, which precludes a full stability analysis or nonlinear evolution of such spacetimes. Progress on this front has been achieved recently (Carloni and Vernieri 2018; Isayev 2018; Raposo et al. 2018).

The compactness of very anisotropic stars may be arbitrarily close to that of a BH; compact configurations can exceed the Buchdahl limit, and some can be classified as ClePhOs. In some of these models, compact stars exist *across a wide range of masses*, evading one of the outstanding issues with BH mimickers, i.e., that most approach the BH compactness in a very limited range of masses, thus being unable to describe both stellar-mass and supermassive BH candidates across several orders of magnitude in mass (Raposo et al. 2018). Such property of BHs in GR, visible in Fig. 5, is a consequence of the scale-free character of the vacuum field equations. It is extremely challenging to reproduce once a scale is present, as expected for material bodies. Fig. 5 summarizes the mass–radius relation for fluid stars.

3.5 Quasiblack holes

An interesting class of families of BH-mimickers, the quasiblack holes, consist on extremal (charged and/or spinning) *regular* spacetimes. These objects can be thought of as stars, on the verge of becoming BHs (Lemos and Weinberg 2004; Lemos and Zaslavskii 2008).

3.6 Wormholes

Boson and fermion stars discussed above arise from a simple theory, with relatively simple equations of motion, and have clear dynamics. Their formation mechanism is embodied in the field equations and requires no special initial data. On the other hand, the objects listed below are, for the most part, generic constructions with a well-defined theoretical motivation, but for which the formation mechanisms are not well understood.

Wormholes were originally introduced by Einstein and Rosen, as an attempt to describe particles (Einstein and Rosen 1935). They were (much) later popularized as a useful tool to teach GR, its mathematical formalism and underlying geometric description of the universe (Morris and Thorne 1988; Visser 1995; Lemos et al. 2003). Wormholes connect different regions of spacetime. Within GR they are not vacuum spacetimes and require matter. The realization that wormholes can be stabilized and constructed with possibly reasonable matter has attracted a considerable attention on these objects (Visser 1995; Lemos et al. 2003; Maldacena et al. 2018) (Fig. 6).

Fig. 6 Embedding-like diagram of a wormhole connecting two different asymptotically-flat universes. The black solid line denotes the wormhole's throat. There are two light rings in the spacetime, one for which universe
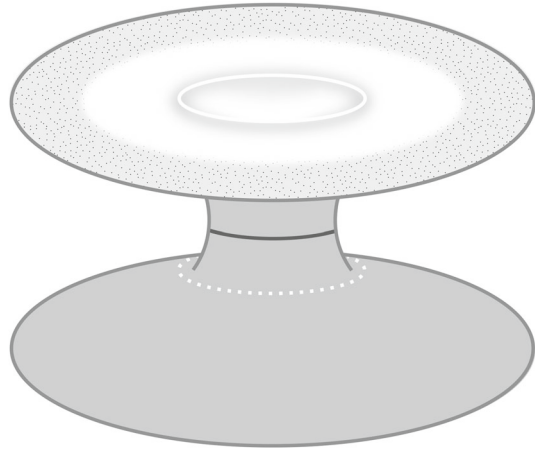
Different wormhole spacetimes can have very different properties. Since we are interested in understanding spacetimes that mimic BHs, consider the following two simple examples of a non-spinning geometries (Visser 1995; Damour and Solodukhin 2007; Cardoso et al. 2016a). In the first example, we simply take the Schwarzschild geometry describing a mass M down to a "throat" radius $r_0 > 2M$. At r_0, we "glue" such spacetime to another copy of Schwarzschild. In Schwarzschild coordinates, the two metrics are identical and described by

$$ds^2 = -\left(1 - \frac{2M}{r}\right)dt^2 + \left(1 - \frac{2M}{r}\right)^{-1}dr^2 + r^2 d\Omega^2. \tag{21}$$

Because Schwarzschild's coordinates do not extend to $r < 2M$, we use the tortoise coordinate $dr/dr_* = \pm(1 - 2M/r)$, to describe the full spacetime, where the upper and lower sign refer to the two different universes connected at the throat. Without loss of generality we assume $r_*(r_0) = 0$, so that one domain is $r_* > 0$ whereas the other domain is $r_* < 0$. The surgery at the throat requires a thin shell of matter with surface density and surface pressure (Visser 1996)

$$\sigma = -\frac{1}{2\pi r_0}\sqrt{1 - 2M/r_0}, \qquad p = \frac{1}{4\pi r_0}\frac{(1 - M/r_0)}{\sqrt{1 - 2M/r_0}}, \tag{22}$$

Although the spacetime is everywhere vacuum (except at the throat) the junction conditions force the pressure to be large when the throat is close to the Schwarzschild radius.

A similar example, this time of a non-vacuum spacetime, is the following geometry (Damour and Solodukhin 2007)

$$ds^2 = -\left(1 - \frac{2M}{r} + \lambda^2\right)dt^2 + \left(1 - \frac{2M}{r}\right)^{-1}dr^2 + r^2 d\Omega^2. \tag{23}$$

The constant λ is assumed to be extremely small, for example $\lambda \sim e^{-M^2/\ell_P^2}$ where ℓ_P is the Planck length. There is no event horizon at $r = 2M$, such location is now the spacetime throat. Note that, even though such spacetime was constructed to be arbitrarily close to the Schwarzschild spacetime, the throat at $r = 2M$ is a region of large (negative) curvature, for which the Ricci and Kretschmann invariant are, respectively,

$$R = -\frac{1}{8\lambda^2 M^2}, \quad R_{abcd}R^{abcd} = \frac{1 + 24\lambda^4}{64\lambda^4 M^4}. \tag{24}$$

Thus, such invariants diverge at the throat in the small λ-limit. A more general discussion on several wormholes models is presented in Lemos and Zaslavskii (2008).

The above constructions show that wormholes can be constructed to have any arbitrary mass and compactness. The procedure is oblivious to the formation mechanism, it is unclear if these objects can form without carefully tuned initial conditions, nor if they are stable. Wormholes in more generic gravity theories have been constructed, some of which can potentially be traversable (Shaikh and Kar 2016; Chianese et al. 2017; Hohmann et al. 2018; Shaikh 2018; Khaybullina and Tuleganova 2019). In such theories, energy conditions might be satisfied (Kanti et al. 2011). Generically however, wormholes are linearly unstable (Gonzalez et al. 2009a, b; Bronnikov et al. 2012; Cuyubamba et al. 2018).

3.7 Dark stars

Quantum field theory around BHs or around dynamic horizonless objects gives rise to phenomena such as particle creation. Hawking evaporation of astrophysical BHs, and corresponding back-reaction on the geometry is negligible (Birrell and Davies 1984). Quantum effects on collapsing *horizonless* geometries (and the possibility of halting collapse to BHs altogether) are less clear (Visser et al. 2009; Zeng 2017; Chen et al. 2018; Berthiere et al. 2018; Buoninfante and Mazumdar 2019; Terno 2019; Malafarina 2017). There are arguments that semiclassical effects might suffice to halt collapse and to produce *dark stars*, even for macroscopic configurations (Barceló et al. 2009, 2016; Kawai et al. 2013; Baccetti et al. 2017, 2018a, b; Carballo-Rubio 2018), but see Chen et al. (2018) for counter-arguments. For certain conformal fields, it was shown that a possible end-state are precisely wormholes of the form (23). Alternative proposals, made to solve the information paradox, argue that dark stars could indeed arise, but as a "massive remnant" end state of BH evaporation (Giddings 1992; Unruh and Wald 2017).

3.8 Gravastars

Similar ideas that led to the proposal of "dark stars" were also in the genesis of a slightly different object, "gravitational-vacuum stars" or *gravastars* (Mazur and Mottola 2001, 2004). These are configurations supported by a negative pressure, which might arise as an hydrodynamical description of one-loop QFT effects in curved spacetime, so

they do not necessarily require exotic new physics (Mottola and Vaulin 2006). In these models, the Buchdahl limit is evaded both because the internal effective fluid is anisotropic (Cattoen et al. 2005) and because the pressure is negative [and thus violates some of the energy conditions (Mazur and Mottola 2015)]. Gravastars have been recently generalized to include anti-de Sitter cores, in what was termed *AdS bubbles*, and which may allow for holographic descriptions (Danielsson et al. 2017; Danielsson and Giri 2018). Gravastars are a very broad class of objects, and can have arbitrary compactness, depending on how one models the supporting pressure. The original gravastar model was a five-layer construction, with an interior de Sitter core, a thin shell connecting it to a perfect-fluid region, and another thin-shell connecting it to the external Schwarzschild patch. A simpler construction that features all the main ingredients of the original gravastar proposal is the thin-shell gravastar (Visser and Wiltshire 2004), in which a de Sitter core is connected to a Schwarzschild exterior through a thin shell of perfect-fluid matter. Gravastars can also be obtained as the BH-limit of constant-density stars, past the Buchdahl limit (Mazur and Mottola 2015; Posada and Chirenti 2019). It is interesting that such stars were found to be dynamically stable in this regime (Posada and Chirenti 2019). It has been conjectured that gravastars are a natural outcome of the inflationary universe (Wang et al. 2018b), or arising naturally within the gauge-gravity duality (Danielsson et al. 2017; Danielsson and Giri 2018).

3.9 Fuzzballs and collapsed polymers

So far, quantum effects were dealt with at a semi-classical level only. A proper theory of quantum gravity needs to be able to solve some of the inherent problems in BH physics, such as the lack of unitarity in BH evaporation or the origin and nature of the huge Bekenstein–Hawking entropy $S = k_B c^3 A/(4\hbar G)$ (k_B is Boltzmann's constant and A is the BH area). In other words, what is the statistical-mechanical account of BH entropy in terms of some microscopic degrees of freedom? String theory is able to provide a partial answer to some of these questions. In particular, for certain (nearly) supersymmetric BHs, the Bekenstein–Hawking entropy, as computed in the strongly-coupled supergravity description, can be reproduced in a weakly-coupled D-brane description as the degeneracy of the relevant microstates (Strominger and Vafa 1996; Peet 1998; Das and Mathur 2000; David et al. 2002; Bena and Warner 2008).

Somewhat surprisingly, the geometric description of *individual microstates* seems to be regular and horizonless (Myers 1997; Mathur 2005; Bena and Warner 2008, 2013; Balasubramanian et al. 2008). This led to the "fuzzball" description of classical BH geometries, where a BH is dual to an ensemble of such microstates. In this picture, the BH geometry emerges in a coarse-grained description which "averages" over the large number of coherent superposition of microstates, producing an effective horizon at a radius where the individual microstates start to "differ appreciably" from one another (Lunin and Mathur 2002b, a). In this description, quantum gravity effects are not confined close to the BH singularity, rather the entire interior of the BH is "filled" by fluctuating geometries—hence this picture is often referred to as the "fuzzball" description of BHs.

Unfortunately, the construction of microstates corresponding to a fixed set of global charges has only been achieved in very special circumstances, either in higher-dimensional or in non asymptotically-flat spacetimes. Explicit regular, horizonless microstate geometries for asymptotically flat, four-dimensional spacetimes that could describe astrophysical bodies have not been constructed. Partly because of this, the properties of the geometries are generically unknown. These include the "softness" of the underlying microstates when interacting with GWs or light; the curvature radius or redshift of these geometries in their interior; the relevant lengthscale that indicates how far away from the Schwarzschild radius is the fuzziness relevant, etc.

A similar motivation led to the proposal of a very different BH interior in Brustein and Medved (2017) and Brustein et al. (2017a); the interior is described by an effective equation of state corresponding to a gas of highly excited strings close to the Hagedorn temperature. The behavior of such gas is similar to some polymers, and this was termed the "collapsed polymer" model for BH interiors. In both proposals, large macroscopic BHs are described by objects with a regular interior, and the classical horizon is absent. In these models, our parameter ϵ is naturally of the order $\sim \mathcal{O}(\ell_P/M) \in (10^{-39}, 10^{-46})$ for masses in the range $M \in (10, 10^8)M_\odot$.

3.10 "Naked singularities" and superspinars

Classical GR seems to be protected by Cosmic Censorship, in that evolutions leading to spacetime singularities also produce horizons cloaking them. Nevertheless, there is no generic proof that cosmic censorship is valid, and it is conceivable that it is a fragile, once extensions of GR are allowed. A particular impact of such violations was discussed in the context of the Kerr geometry describing spinning BHs. In GR, the angular momentum J of BHs is bounded from above by $J \leq GM^2/c$. In string theory however, such "Kerr bound" does not seem to play any fundamental role and could conceivably receive large corrections. It is thus possible that there are astrophysical objects where it is violated. Such objects were termed *superspinars* (Gimon and Hořava 2009), but it is part of a larger class of objects which would arise if singularities (in the classical theory of GR) would be visible. The full spacetime description of superspinars and other such similar objects is lacking: to avoid singularities and closed-timelike curves unknown quantum effects need to be invoked to create an effective surface somewhere in the spacetime. There are indications that strong GW bursts are an imprint of such objects (Harada et al. 2000), but a complete theory is necessary to understand any possible signature.

3.11 2–2 Holes and other geons

As we remarked already, the questioning of the BH paradigm in GR comes hand in hand with the search for an improved theory of the gravitational interaction, and of possible quantum effects. A natural correction to GR would take the form of higher-curvature terms in the Lagrangian $\mathcal{L} = R + c_1 R^2 + c_2 R_{abcd} R^{abcd} + \cdots$ with couplings c_j suppressed by some scale (Stelle 1977; Voronov and Tyutin 1984; Holdom and Ren 2016). The study of (shell-like) matter configurations in such theories revealed
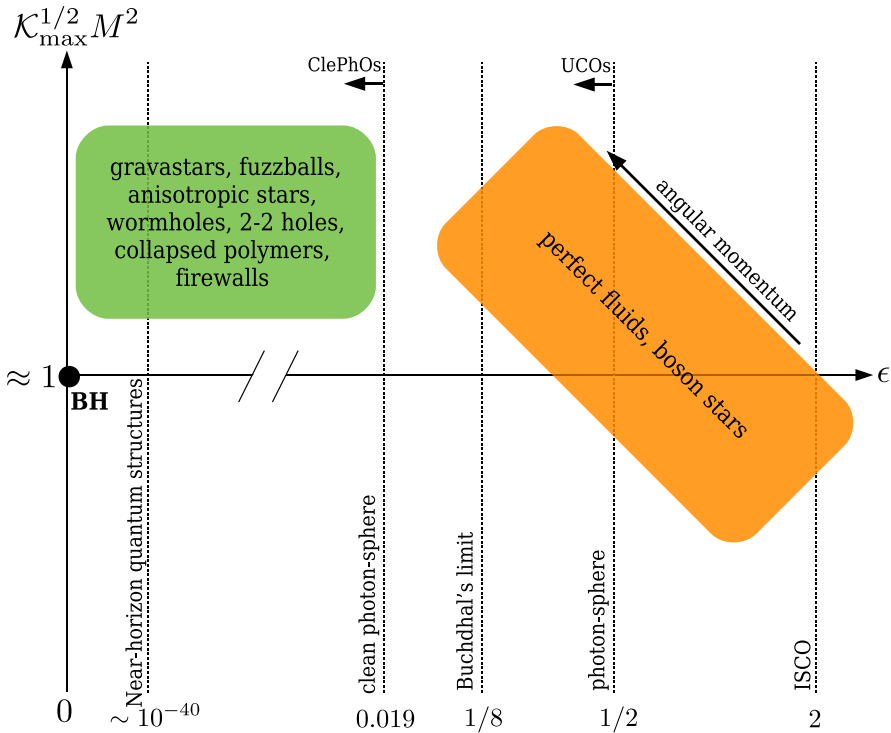
Fig. 7 Schematic representation of ECO models in a compactness-curvature diagram. The horizontal axis shows the compactness parameter ϵ associated to the object, which can be also mapped (in a model-dependent way) to a characteristic light-crossing timescale. The vertical axis shows the maximum curvature (as measured by the Kretschmann scalar $\mathcal{K}$) of the object normalized by the corresponding quantity for a BH with the same mass M. All known ECO models with $\epsilon \to 0$ have large curvature in their interior, i.e., the leftmost bottom part of the diagram is conjectured to be empty. Angular momentum tends to decrease ϵ and to increase $\mathcal{K}_{max}$

the existence novel horizonless configurations, termed "2–2-holes", which closely matches the exterior Schwarzschild solution down to about a Planck proper length of the Schwarzschild radius of the object (Holdom and Ren 2017; Ren 2019). In terms of the parameter ϵ introduced above, the theory predicts objects where $\epsilon \sim (\ell_P/M)^2 \in (10^{-78}, 10^{-92})$ (Holdom and Ren 2017; Ren 2019). The existence and stability of proper star-like configurations was not studied. More generic theories result in a richer range of solutions, many of which are solitonic in nature and can be ultracompact (see, e.g., Beltran Jimenez et al. 2018; Afonso et al. 2017, 2018; Franzin et al. 2018; Sebastiani et al. 2018). Recently, a quantum mechanical framework to describe astrophysical, horizonless objects devoid of curvature singularities was put forward in the context of nonlocal gravity (arising from infinite derivative gravity) (Koshelev and Mazumdar 2017; Buoninfante et al. 2018; Buoninfante and Mazumdar 2019). The corresponding stars can be ultracompact, although never reaching the ClePhO category.

3.12 Firewalls, compact quantum objects and dirty BHs

Many of the existing proposals to solve or circumvent the breakdown of unitarity in BH evaporation involve changes in the BH structure, without doing away with the horizon. Some of the changes could involve "soft" modifications of the near-horizon region, such that the object still looks like a regular GR BH (Giddings 2017b, 2013; Giddings et al. 2019). However, the changes could also be drastic and involve "hard" structures localized close to the horizon such as firewalls and other compact quantum objects (Almheiri et al. 2013; Kaplan and Rajendran 2019; Giddings et al. 2019). Alternatively, a classical BH with modified dispersion relations for the graviton could effectively appear as having a hard surface (Zhang and Zhou 2018; Oshita and Afshordi 2019). A BH surrounded by some hard structure—of quantum origin such as firewalls, or classical matter piled up close to the horizon—behaves for many purposes as a compact horizonless object.

The zoo of compact objects is summarized in Fig. 7. In all these cases, both quantum-gravity or microscopic corrections at the horizon scale select ClePhOs as well-motivated alternatives to BHs. Despite a number of supporting arguments—some of which urgent and well founded—it is important to highlight that there is no horizonless ClePhO for which we know sufficiently well the physics at the moment.

4 Dynamics of compact objects

> *There is a crack in everything. That's how the light gets in.*
> Leonard Cohen, Anthem (1992)

EM observations of compact bodies are typically performed in a context where spacetime fluctuations are irrelevant, either due to the long timescales involved or because the environment has a negligible backreaction on the body itself. For example, EM observations of accretion disks around a compact object can be interpreted using a stationary background geometry. Such geometry is a solution to the field equations describing the compact body while neglecting the accretion disk, the dynamics of which is governed by the gravitational pull of the central object and by internal forces. This approximation is adequate since the total amount of energy density around compact objects is but a small fraction of the object itself, and the induced changes in the geometry can be neglected (Barausse et al. 2014). In addition, the wavelength of EM waves of interest for Earth-based detectors is always much smaller that any lengthscale related to coherent motion of compact objects: light can be treated as a null particle following geodesics on a stationary background. Thus, the results of the previous sections suffice to discuss EM observations of compact objects, as done in Sect. 5 below.

For GW astronomy, however, it is the spacetime fluctuations themselves that are relevant. A stationary geometry approximation would miss GW emission entirely. In addition, GWs generated by the coherent motion of sources have a wavelength of the order of the size of the system. Therefore, the geodesic approximation becomes inadequate (although it can still be used as a guide). Compact binaries are the preferred

sources for GW detectors. Their GW signal is naturally divided in three stages, corresponding to the different cycles in the evolution driven by GW emission (Buonanno et al. 2007; Berti et al. 2007; Sperhake et al. 2013a): the inspiral stage, corresponding to large separations and well approximated by post-Newtonian theory; the merger phase when the two objects coalesce and which can only be described accurately through numerical simulations; and finally, the ringdown phase when the merger end-product relaxes to a stationary, equilibrium solution of the field equations (Sperhake et al. 2013a; Berti et al. 2009; Blanchet 2014). All three stages provide independent, unique tests of gravity and of compact GW sources. Overall, GWs are almost by definition attached to highly dynamical spacetimes, such as the coalescence and merger of compact objects. We turn now to that problem.

4.1 Quasinormal modes

Consider first an isolated compact object described by a stationary spacetime. Again, we start with the spherically-symmetric case and for simplicity. Birkhoff's theorem then implies that the exterior geometry is Schwarzschild. Focus on a small disturbance to such static spacetime, which could describe a small moving mass (a planet, a star, etc), or the late-stage in the life of a coalescing binary (in which case the disturbed "isolated compact object" is to be understood as the final state of the coalescence).

In the linearized regime, the geometry can be written as $g_{\mu\nu} = g^{(0)}_{\mu\nu} + h_{\mu\nu}$, where $g^{(0)}_{\mu\nu}$ is the geometry corresponding to the stationary object, and $h_{\mu\nu}$ are the small deviations induced on it by whatever is causing the dynamics. The metric fluctuations can be combined in a single master function Ψ which in vacuum is governed by a master partial differential equation of the form (Zerilli 1970; Berti et al. 2009)

$$\frac{\partial^2 \Psi(t,z)}{\partial z^2} - \frac{\partial^2 \Psi(t,z)}{\partial t^2} - V(r)\Psi(t,z) = S(t,z). \tag{25}$$

where z is a suitable coordinate. The source term $S(t,z)$ contains information about the cause of the disturbance $\Psi(t,z)$. The information about the angular dependence of the wave is encoded in the way the separation was achieved, and involves an expansion in tensor harmonics. One can generalize this procedure and consider also scalar or vector (i.e., EM) waves. These can also be reduced to a master function of the type (25), and separation is achieved with spin-s harmonics for different spins s of field. These angular functions are labeled by an integer $l \geq |s|$. For a Schwarzschild spacetime, the effective potential is

$$V = f\left(\frac{l(l+1)}{r^2} + (1-s^2)\frac{2M}{r^3}\right), \tag{26}$$

with $s = 0, \pm 1, \pm 2$ for scalar, vector or (axial) tensor modes. The $s = \pm 2$ equation does not describe completely all of the gravitational degrees of freedom. There is an another (polar) gravitational mode (in GR, there are two polarizations for GWs), also described by Eq. (25) with a slightly more complicated potential (Chandrasekhar and

Detweiler 1975; Kokkotas and Schmidt 1999; Berti et al. 2009). Note that such results apply only when there are no further degrees of freedom that couple to the GR modes (Blázquez-Salcedo et al. 2016; Cardoso and Gualtieri 2009; Tattersall et al. 2018; Cardoso et al. 2018b; Molina et al. 2010).

The solutions to Eq. (25) depend on the source term and initial conditions, just like for any other physical system. We can gain some insight on the general properties of the system by studying the source-free equation in Fourier space. This corresponds to studying the "free" compact object when the driving force died off. As such, it gives us information on the late-time behavior of any compact object. By defining the Fourier transform through $\Psi(t, r) = \frac{1}{\sqrt{2\pi}} \int e^{-i\omega t} \psi(\omega, r) d\omega$, one gets the following ODE

$$\frac{d^2\psi}{dz^2} + \left(\omega^2 - V\right)\psi = 0. \tag{27}$$

For a Schwarzschild spacetime, the "tortoise" coordinate z is related to the original r by $dr/dz = f$, i.e.,

$$z = r + 2M \log\left(\frac{r}{2M} - 1\right), \tag{28}$$

such that $z(r)$ diverges logarithmically near the horizon. In terms of z, Eq. (27) is equivalent to the time-independent Schrödinger equation in one dimension and it reduces to the wave equation governing a string when $M = l = 0$. For a string of length L with fixed ends, one imposes Dirichlet boundary conditions and gets an eigenvalue problem for ω. The boundary conditions can only be satisfied for a discrete set of *normal* frequencies, $\omega = n\pi/L$ ($n = 1, 2, \ldots$). The corresponding wavefunctions are called normal modes and form a basis onto which one can expand any configuration of the system. The frequency is purely real because the associated problem is conservative.

If one is dealing with a BH spacetime, the appropriate conditions (required by causality) correspond to having waves traveling outward to spatial infinity ($\Psi \sim e^{i\omega(z-t)}$ as $z \to \infty$) and inwards to the horizon ($\Psi \sim e^{-i\omega(z+t)}$ as $z \to -\infty$) [see Fig. 8]. The effective potential displays a maximum approximately at the photon sphere, $r \approx 3M$, the exact value depending on the type of perturbation and on the value of l ($r \to 3M$ in the $l \to \infty$ limit). Due to backscattering off the effective potential (26), the eigenvalues ω are not known in closed form, but they can be computed numerically (Chandrasekhar and Detweiler 1975; Kokkotas and Schmidt 1999; Berti et al. 2009). The fundamental $l = 2$ mode (the lowest dynamical multipole in GR) of gravitational perturbations reads (CENTRA 2019)

$$M\omega_{\mathrm{BH}} \equiv M(\omega_R + i\omega_I) \approx 0.373672 - i0.0889623. \tag{29}$$

Remarkably, the entire spectrum is the same for both the axial or the polar gravitational sector; this property is ofter referred to as *isospectrality* (Chandrasekhar and Detweiler 1975). The frequencies are complex and are therefore called *quasinormal mode* (QNM) frequencies. Their imaginary component describes the decay in time of fluctuations
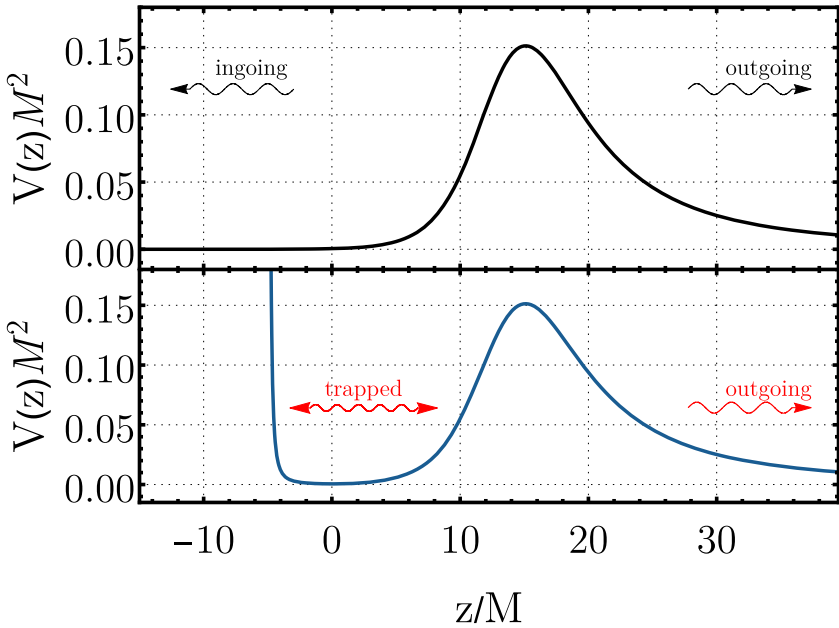
Fig. 8 Typical effective potential for perturbations of a Schwarzschild BH (top panel) and of an horizonless compact object (bottom panel). The effective potential is peaked at approximately the photon sphere, $r \approx 3M$. For BHs, QNMs are waves which are outgoing at infinity ($z \to +\infty$) and ingoing at the horizon ($z \to -\infty$), whereas the presence of a potential well (provided either by a partly reflective surface, a centrifugal barrier at the center, or by the geometry) supports quasi-trapped, long-lived modes

on a timescale $\tau \equiv 1/|\omega_I|$, and hints at the stability of the geometry. Unlike the case of a string with fixed end, we are now dealing with an open system: waves can travel to infinity or down the horizon and therefore it is physically sensible that any fluctuation damps down. The corresponding modes are QNMs, which in general do *not* form a complete set (Kokkotas and Schmidt 1999).

Boundary conditions play a crucial role in the structure of the QNM spectrum. If a reflective surface is placed at $r_0 = 2M(1 + \epsilon) \gtrsim 2M$, where (say) Dirichlet or Neumann boundary conditions have to be imposed, the spectrum changes considerably. The QNMs in the $\epsilon \to 0$, low-frequency limit read (Vilenkin 1978; Maggio et al. 2017, 2019)

$$M\omega_R \simeq -\frac{M\pi}{2|z_0|} \left(q + \frac{s(s+1)}{2} \right) \sim |\log \epsilon|^{-1}, \tag{30}$$

$$M\omega_I \simeq -\beta_{ls} \frac{M}{|z_0|} (2M\omega_R)^{2l+2} \sim -|\log \epsilon|^{-(2l+3)}, \tag{31}$$

where $z_0 \equiv z(r_0) \sim 2M \log \epsilon$, q is a positive odd (even) integer for polar (axial) modes (or equivalently for Dirichlet (Neumann) boundary conditions), and $\beta_{ls} = \left[\frac{(l-s)!(l+s)!}{(2l)!(2l+1)!!} \right]^2$ (Starobinskij and Churilov 1973; Brito et al. 2015b; Maggio et al. 2019).

Note that the two gravitational sectors are no longer isospectral. More importantly, the perturbations have smaller frequency and are much longer lived, since a decay channel (the horizon) has disappeared. For example, for $\epsilon = 10^{-6}$ we find numerically the fundamental scalar modes

$$M\omega_{\text{polar}} \approx 0.13377 - i\, 2.8385 \times 10^{-7}, \tag{32}$$

$$M\omega_{\text{axial}} \approx 0.13109 - i\, 2.3758 \times 10^{-7}. \tag{33}$$

These QNMs were computed by solving the exact linearized equations numerically but agree well with Eqs. (30) and (31).

The above scaling with ϵ can be understood in terms of modes trapped between the peak of the potential (26) at $r \sim 3M$ and the "hard surface" at $r = r_0$ (Cardoso et al. 2016a, b; Völkel and Kokkotas 2017a; Mark et al. 2017; Maggio et al. 2019) [see Fig. 8]. Low-frequency waves are almost trapped by the potential, so their wavelength scales as the size of the cavity (in tortoise coordinates), $\omega_R \sim 1/z_0$, just like the normal modes of a string. The (small) imaginary part is given by waves which tunnel through the potential and reach infinity. The tunneling probability can be computed analytically in the small-frequency regime and scales as $|\mathcal{A}|^2 \sim (M\omega_R)^{2l+2} \ll 1$ (Starobinskij and Churilov 1973). After a time t, a wave trapped inside a box of size z_0 is reflected $N = t/z_0$ times, and its amplitude reduces to $A(t) = A_0 \left(1 - |\mathcal{A}|^2\right)^N \sim A_0 \left(1 - t|\mathcal{A}|^2/z_0\right)$. Since, $A(t) \sim A_0 e^{-|\omega_I|t} \sim A_0(1 - |\omega_I|t)$ in this limit, we immediately obtain

$$\omega_R \sim 1/z_0, \qquad \omega_I \sim |\mathcal{A}|^2/z_0 \sim \omega_R^{2l+3}. \tag{34}$$

This scaling agrees with exact numerical results and is valid for any l and any type of perturbation.

The reverse-engineering of the process, i.e., a reconstruction of the scattering potential V from a mode measurement was proposed in Völkel and Kokkotas (2017b, 2018), Völkel (2018). The impact of measurement error on such reconstruction is yet to be assessed.

Clearly, a perfectly reflecting surface is an idealization. In certain models, only low-frequency waves are reflected, whereas higher-frequency waves probe the internal structure of the specific object (Saravani et al. 2015; Mathur and Turton 2014). In general, the location of the effective surface and its properties (e.g., its reflectivity) can depend on the energy scale of the process under consideration. Partial absorption is particularly important in the case of spinning objects, as discussed in Sect. 4.3.

4.2 Gravitational-wave echoes

4.2.1 Quasinormal modes, photon spheres, and echoes

The effective potential V for wave propagation reduces to that for geodesic motion (V_{geo}) in the high-frequency, high-angular momentum (i.e., eikonal) regime. Thus, some properties of geodesic motion have a wave counterpart (Ferrari and Mashhoon 1984; Cardoso et al. 2009). The instability of light rays along the null circular geodesic

translates into some properties of waves around objects compact enough to feature a photon sphere. A wave description needs to satisfy "quantization conditions", which can be worked out in a WKB approximation. Since GWs are quadrupolar in nature, the lowest mode of vibration should satisfy

$$M\omega_R^{\text{geo}} = 2\frac{\dot{\varphi}}{\dot{t}} = \frac{2}{3\sqrt{3}} \sim 0.3849. \tag{35}$$

In addition the mode is damped, as we showed, on timescales $3\sqrt{3}M$. Overall then, the geodesic analysis predicts

$$M\omega^{\text{geo}} \sim 0.3849 - i\,0.19245. \tag{36}$$

This crude estimate, valid in principle only for high-frequency waves, matches well even the fundamental mode of a Schwarzschild BH, Eq. (29).

Nevertheless, QNM frequencies can be defined for any dissipative system, not only for compact objects or BHs. Thus, the association with photon spheres has limits, for instance it neglects possible coupling terms (Blázquez-Salcedo et al. 2016), nonminimal kinetic terms (Konoplya and Stuchlík 2017), etc. Such an analogy is nonetheless enlightening in the context of objects so compact that they have photon spheres and resemble Schwarzschild deep into the geometry, in a way that condition (7) is satisfied (Cardoso et al. 2016a, b; Price and Khanna 2017; Ghersi et al. 2019).

For a BH, the excitation of the spacetime modes happens at the photon sphere (Davis et al. 1971, 1972; Ferrari and Mashhoon 1984). Such waves travel outwards to possible observers or down the event horizon. The structure of GW signals at late times is therefore expected to be relatively simple. This is shown in Fig. 9, for the scattering of a Gaussian pulse of axial quadrupolar modes off a BH. The pulse crosses the photon sphere, and excites its modes. The ringdown signal, a fraction of which travels to outside observers, is to a very good level described by the lowest QNMs. The other fraction of the signal generated at the photon sphere travels downwards and into the horizon. It dies off and has no effect on observables at large distances.

Contrast the previous description with the dynamical response of ultracompact objects for which condition (7) is satisfied (i.e., a ClePhO) [cf. Fig. 9]. The initial description of the photon sphere modes still holds, by causality. Thus, up to timescales of the order $|z_0| \sim -M \log \epsilon$ (the roundtrip time of radiation between the photon sphere and the surface) the signal is *identical* to that of BHs (Cardoso et al. 2016a, b). At later times, however, the pulse traveling inwards is bound to see the object and be reflected either at its surface or at its center. In fact, this pulse is semi-trapped between the object and the light ring. Upon each interaction with the light ring, a fraction exits to outside observers, giving rise to a series of *echoes* of ever-decreasing amplitude. From Eqs. (30)–(31), repeated reflections occur in a characteristic echo delay time (Cardoso et al. 2016a, b; Ghersi et al. 2019) [see Fig. 10]
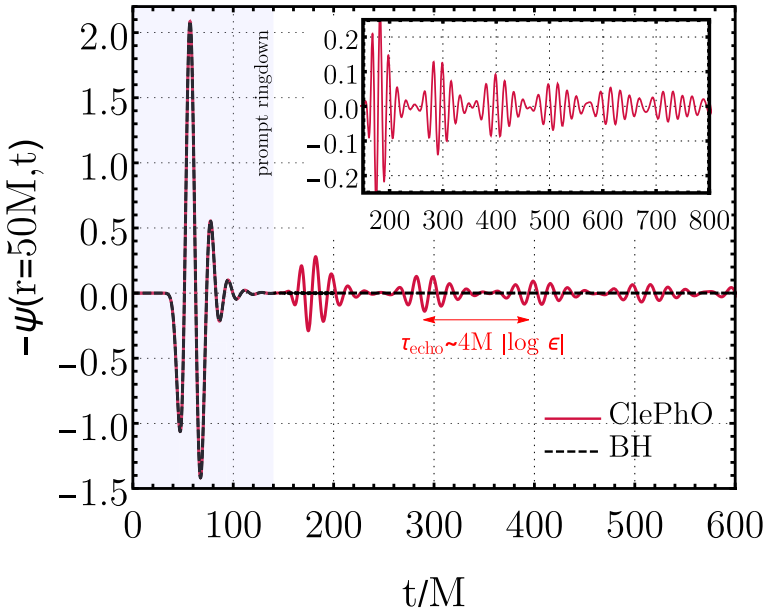
Fig. 9 Ringdown waveform for a BH (dashed black curve) compared to a ClePhO (solid red curve) with a reflective surface at $r_0 = 2M(1+\epsilon)$ with $\epsilon = 10^{-11}$. We considered $l = 2$ axial gravitational perturbations and a Gaussian wavepacket $\psi(r, 0) = 0$, $\dot{\psi}(r, 0) = e^{-(z-z_m)^2/\sigma^2}$ (with $z_m = 9M$ and $\sigma = 6M$) as initial condition. Note that each subsequent echo has a smaller frequency content and that the damping of subsequent echoes is much larger than the late-time QNM prediction ($e^{-\omega_I t}$ with $\omega_I M \sim 4 \times 10^{-10}$ for these parameters). Data available online (CENTRA 2019)

$$\tau_{\text{echo}} \sim 4M |\log \epsilon|. \tag{37}$$

However, the main burst is typically generated at the photon sphere and has therefore a *frequency content* of the same order as the BH QNMs (29). The initial signal is of high frequency and a substantial component is able to cross the potential barrier. Thus, asymptotic observers see a series of echoes whose amplitude is getting smaller and whose frequency content is also going down. It is crucial to understand that echoes occur in a *transient* regime; at *very late times*, the signal is dominated by the lowest-damped QNMs, described by Eqs. (30)–(31).

We end this discussion by highlighting that GW echoes are a feature of very compact ECOs, but also arise in many other contexts: classical BHs surrounded by a "hard-structure" close to the horizon (Barausse et al. 2014; Kaplan and Rajendran 2019; Ramos and Barausse 2019), or far from it (Barausse et al. 2014; Konoplya et al. 2019; Lin et al. 2019), or embedded in a theory that effectively makes the graviton see a hard wall there (Zhang and Zhou 2018; Oshita and Afshordi 2019) will respond to incoming GWs producing echoes. Finally, as we described earlier, even classical but very compact neutron or strange quark stars may be prone to exciting echoes (Ferrari and Kokkotas 2000; Raposo et al. 2018; Pani and Ferrari 2018; Mannarelli and Tonelli 2018). A simple picture of how echoes arise in a simple two-barrier system is provided in Mirbabayi (2018).
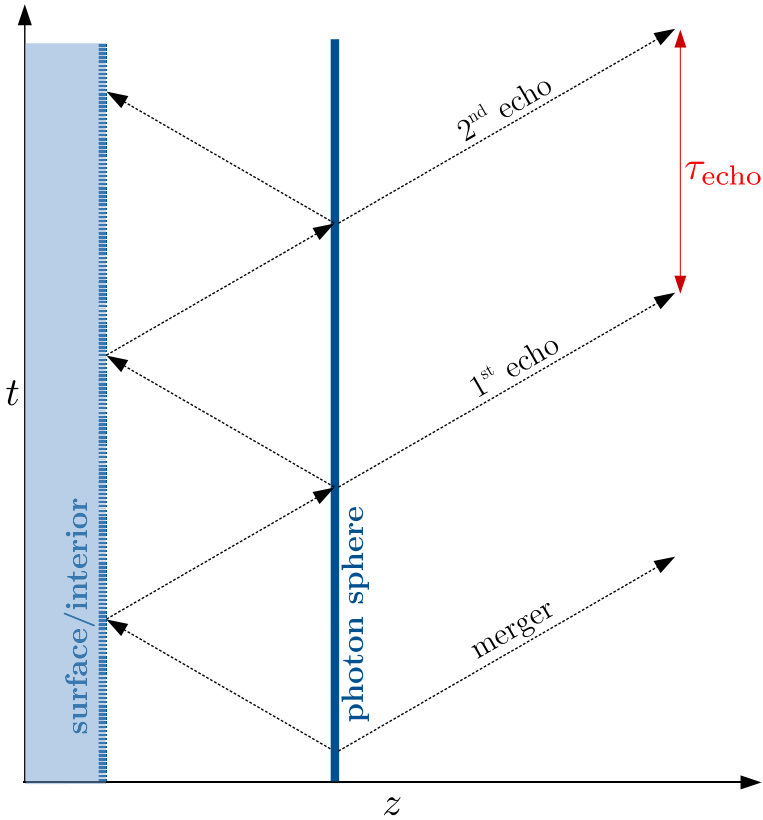
Fig. 10 Schematic Penrose diagram of GW echoes from an ECO. Adapted from Abedi et al. (2017a) [similar versions of this plot appeared in other contexts in Vilenkin (1978) and Mark et al. (2017)]

4.2.2 A black-hole representation and the transfer function

The QNMs of a spacetime were defined as the eigenvalues of the homogeneous ordinary differential equation (27). Their role in the full solution to the homogeneous problem becomes clear once we re-write Eq. (25) in Fourier space,

$$\frac{d^2\psi}{dz^2} + \left(\omega^2 - V\right)\psi = \mathcal{S}, \tag{38}$$

where $\mathcal{S}$ is the Fourier transformed source term S. Since the potential is zero at the boundaries, two independent homogeneous solutions are

$$\psi_- = \begin{cases} e^{-i\omega z} & z \to -\infty \\ A_{\text{in}}e^{-i\omega z} + A_{\text{out}}e^{i\omega z} & z \to +\infty \end{cases}, \tag{39}$$

and

$$\psi_+ = \begin{cases} B_{\text{in}}e^{-i\omega z} + B_{\text{out}}e^{i\omega z} & z \to -\infty \\ e^{i\omega z} & z \to +\infty \end{cases}, \tag{40}$$

Note that ψ_+ was chosen to satisfy outgoing conditions at large distances; this is the behavior we want to impose on a system which is assumed to be isolated. On the other hand, ψ_- satisfies the correct near-horizon boundary condition *in the case of a BH*. Define reflection and transmission coefficients,

$$\mathcal{R}_{\text{BH}} = \frac{B_{\text{in}}}{B_{\text{out}}}, \qquad \mathcal{T}_{\text{BH}} = \frac{1}{B_{\text{out}}}. \tag{41}$$

Given the form of the ODE, the Wronskian $W \equiv \psi_-\psi'_+ - \psi'_-\psi_+$ is a constant (here $' \equiv d/dz$), which can be evaluated at infinity to yield $W = 2i\omega A_{\text{in}}$. The general solution to our problem can be written as (Bender and Orszag 1999)

$$\psi = \psi_+ \int^z \frac{\mathcal{S}\psi_-}{W}dz + \psi_- \int^z \frac{\mathcal{S}\psi_+}{W}dz + A_1\psi_- + A_2\psi_+, \tag{42}$$

where A_1, A_2 constants. If we impose the boundary conditions appropriate for BHs, we find

$$\psi_{\text{BH}} = \psi_+ \int_{-\infty}^z \frac{\mathcal{S}\psi_-}{W}dz + \psi_- \int_z^\infty \frac{\mathcal{S}\psi_+}{W}dz. \tag{43}$$

This is thus the response of a BH spacetime to some source. Notice that close to the horizon the first term drops and $\psi_{\text{BH}}(r \sim r_+) \sim e^{-i\omega z} \int_z^\infty \frac{\mathcal{S}\psi_+}{W}dz$. For detectors located far away from the source, on the other hand $\psi_{\text{BH}}(r \to \infty) \sim e^{i\omega z} \int_{-\infty}^\infty \frac{\mathcal{S}\psi_-}{W}dz$. It is easy to see now that QNMs correspond to poles of the propagator (Berti et al. 2009), and hence they do indeed have a significant contribution to the signal, both at infinity and near the horizon.

Consider now that instead of a BH, there is an ultracompact object. Such object has a surface at r_0, corresponding to large negative tortoise z_0. Then, the boundary condition (39) on the left needs to be changed to

$$\psi_{\text{ECO}} \sim e^{-i\omega z} + \mathcal{R}e^{i\omega z}, \quad z \to z_0, \tag{44}$$

where we assume the compact object surface to have a (possible frequency-dependent) reflectivity $\mathcal{R}$. We will now show that the spacetime response to an ultracompact object can be expressed in terms of the BH response and a transfer function (Mark et al. 2017) (for a previous attempt along these lines see Nakano et al. 2017). First, notice that the ODE to be solved is exactly the same, with different conditions on one of the boundaries. We can thus still pick the two independent homogeneous solutions (39) and (40), but choose different integration constants in (42) so that the boundary condition is satisfied. Adding a homogeneous solution $\mathcal{K}\psi_+ \int_{-\infty}^\infty \frac{\mathcal{S}\psi_+}{W}dz$ to (43) is

allowed since it still satisfies outgoing conditions at large spatial distances. We then find at large negative z

$$\psi_{\text{ECO}} = \left(e^{-i\omega z} + \mathcal{K}(B_{\text{in}}e^{-i\omega z} + B_{\text{out}}e^{i\omega z})\right)\int_{z_0}^{\infty} \frac{\mathcal{S}\psi_+}{W}dz. \tag{45}$$

where $\mathcal{K}$ is a constant. On the other hand, to obey the boundary condition (44), one must impose $\psi_{\text{ECO}} = k_0\left(e^{-i\omega z} + \mathcal{R}e^{i\omega z}\right)$ with an unknown constant k_0. Matching outgoing and ingoing coefficients, we find

$$\mathcal{K} = \frac{\mathcal{T}_{\text{BH}}\mathcal{R}}{1 - \mathcal{R}_{\text{BH}}\mathcal{R}}. \tag{46}$$

Thus, a detector at large distances sees now a signal

$$\psi_{\text{ECO}}(r \to \infty) = \psi_{\text{BH}}(r \to \infty) + \mathcal{K}e^{2i\omega z}\psi_{\text{BH}}(r \sim r_+). \tag{47}$$

In other words, the signal seen by detectors is the same as the one from a BH, modified by a piece that is controlled by the reflectivity of the compact object.

Following Mark et al. (2017), the extra term can be expanded as a geometric series

$$\mathcal{K} = \mathcal{T}_{\text{BH}}\mathcal{R}\sum_{n=1}^{\infty}(\mathcal{R}_{\text{BH}}\mathcal{R})^{n-1}. \tag{48}$$

A natural interpretation emerges: a main burst of radiation is generated for example when an object crosses the light ring (where the peak of the effective potential is located). A fraction of this main burst is outward traveling and gives rise to the "prompt" response $\psi_{\text{BH}}(r \to \infty)$, which is equivalent to the response of a BH. However, another fraction is traveling inwards. The first term is the result of the primary reflection of ψ_{BH} at z_0. Note the time delay factor $2(z-z_0)$ between the first pulse and the main burst due the pulse's extra round trip journey between the boundary the peak of the scattering potential, close to the light ring at $z \sim 0$. When the pulse reaches the potential barrier, it is partially transmitted and emerges as a contribution to the signal. The successive terms are "echoes" of this first reflection which bounces an integer number of times between the potential barrier and the compact object surface. Thus, a mathematically elegant formulation gives formal support to what was a physically intuitive picture.

The derivation above assumes a static ECO spacetime, and a potential which vanishes at its surface. An extension of the procedure above to include both a more general potential and spin is worked out in Conklin et al. (2018). Such a "transfer-function" representation of echoes was embedded into an effective-field-theory scheme (Burgess et al. 2018), showing that linear "Robin" boundary conditions at $r = r_0$ dominate at low energies. In this method the (frequency dependent) reflection coefficient and the surface location can be obtained in terms of a single low-energy effective coupling. Recently, another model for the frequency-dependent reflectivity of quantum BHs has been proposed in Oshita et al. (2019).

The previous description of echoes and of the full signal is reasonable and describes all the known numerical results. At the technical level, more sophisticated tools are required to understand the signal: the intermediate-time response is dominated by the BH QNMs, which are *not* part of the QNM spectrum of an ECO (Cardoso et al. 2016a; Barausse et al. 2014; Khanna and Price 2017). While this fact is easy to understand in the time domain due to causality [in terms of time needed for the perturbation to probe the boundaries (Cardoso et al. 2016a)], it is not at all obvious in the frequency domain. Indeed, the poles of the ECO Green's functions in the complex frequency plane are different from the BH QNMs. The late-time signal is dominated by the dominant ECO poles, whereas the prompt ringdown is governed by the by the dominant QNMs of the corresponding BH spacetime.

4.2.3 A Dyson-series representation

The previous analysis showed two important aspects of the late-time behavior of very compact objects: (i) that it can be expressed in terms of the corresponding BH response if one uses a transfer function $\mathcal{K}$; (ii) that the signal after the main burst and precursor are a sequence of echoes, trapped between the object and the (exterior) peak of the potential.

The response of any system with a non-trivial scattering potential and nontrivial boundary conditions includes echo-like components. To see that, let us use a very different approach to solve (38), namely the Lippman–Schwinger integral solution used in quantum mechanics (Correia and Cardoso 2018). In this approach, the setup is that of flat spacetime, and the scattering potential is treated as a *perturbation*. In particular, the field is written as

$$\psi = \psi_0 + \int_{z_0}^{\infty} g(z, z')\, V(z') \psi(z')\, dz', \tag{49}$$

where

$$g(z, z') = \frac{e^{i\omega|z-z'|} + \mathcal{R}\, e^{i\omega(z+z')}}{2i\omega}, \tag{50}$$

is the Green's function of the free wave operator $d^2/dx^2 + \omega^2$ with boundary condition (44), and $\psi_0 = \int_{z_0}^{\infty} g(z, z')\mathcal{S}(z')dz'$ is the free-wave amplitude. The formal solution of Eq. (49) is the Dyson series (sometimes also called Born or Picard series)

$$\psi = \sum_{k=1}^{\infty} \int_{z_0}^{\infty} g(z, z_1) \cdots g(z_{k-1}, z_k) V(z_1) \cdots V(z_{k-1}) \mathcal{S}(z_k) dz_1 \cdots dz_k, \tag{51}$$

which effectively works as an expansion in powers of V/ω^2, so we expect it to converge rapidly for high frequencies and to be a reasonable approximation also for fundamental modes. It is possible to reorganize (51) and express it as a series in powers of $\mathcal{R}$. We start by separating the Green's function (50) into $g = g_o + \mathcal{R}g_r$, with

$$g_o(z, z') = \frac{e^{i\omega|z-z'|}}{2i\omega} \, , \tag{52}$$

the open system Green's function, and

$$g_r(z, z') = \frac{e^{i\omega(z+z')}}{2i\omega} \, , \tag{53}$$

the "reflection" Green's function. We can then write (49) as

$$\psi = \int_{z_0}^{\infty} g_o(z, z')\mathcal{S}(z')dz' + \mathcal{R}\int_{z_0}^{\infty} g_r(z, z')\mathcal{S}(z')dz' + \int_{z_0}^{\infty} g(z, z')V(z')\psi(z')dz'. \tag{54}$$

Now, in the same way as a Dyson series is obtained, we replace the $\psi(\omega, x')$ in the third integral with the entirety of the rhs of Eq. (54) evaluated at x'. Collecting powers of $\mathcal{R}$ yields

$$\psi = \int g_o\mathcal{S} + \iint g_o V g_o\mathcal{S} + \mathcal{R}\left[\int g_r\mathcal{S} + \iint (g_r V g_o + g_o V g_r)\mathcal{S}\right]$$
$$+ \mathcal{R}^2\iint g_r V g_r\mathcal{S} + \iint g \, V g \, V\psi. \tag{55}$$

If we continue this process we end up with a geometric-like series in powers of R,

$$\psi = \psi_o + \sum_{n=1}^{\infty} \psi_n \, , \tag{56}$$

with each term a Dyson series itself:

$$\psi_o = \sum_{k=1}^{\infty} \int_{z_0}^{\infty} g_o(z, z_1) \cdots g_o(z_{k-1}, z_k)V(z_1) \cdots V(z_{k-1})\mathcal{S}(z_k)dz_1 \cdots dz_k. \tag{57}$$

The reflectivity terms can be re-arranged as:

$$\psi_n = \sum_{k=n}^{\infty} \frac{\mathcal{R}^n}{n!(k-n)!} \sum_{\sigma \in P_k} \int_{z_0}^{+\infty} g_r(z_{\sigma(1)-1}, z_{\sigma(1)})$$
$$\cdots g_r(z_{\sigma(n)-1}, z_{\sigma(n)})g_o(z_{\sigma(n+1)-1}, z_{\sigma(n+1)})$$
$$\cdots g_o(z_{\sigma(k)-1}, z_{\sigma(k)}) \times V(x_1) \cdots V(z_{k-1})\,\mathcal{S}(z_k)\,dz_1 \cdots dz_k, \tag{58}$$

where $x_0 := x$, P_k is the permutation group of degree k and $\frac{1}{n!(k-n)!}\sum_{\sigma \in P_k}$ represents the sum on all possible distinct ways of ordering n g_r's and $k - n$ g_o's, resulting in a total of $\frac{|P_k|}{n!(k-n)!} = \binom{k}{n}$ terms (Correia and Cardoso 2018).

Although complex-looking, Eq. (58) has a special significance, giving the amplitude of the (Fourier-transformed) n-th *echo* of the initial burst (Correia and Cardoso 2018). When $\mathcal{R} = 0$ then $\psi = \psi_o$, the open system waveform. There are no echoes as expected. When $\mathcal{R} \neq 0$ there are additional (infinite) Dyson-series terms. The series is expected to converge, (i.e., the contribution of ψ_n becomes smaller for large n), because of two features of Eq. (58): first, if $|\mathcal{R}| < 1$, $\mathcal{R}^n$ contributes to damp the contribution of large-n terms. Moreover, the Dyson series starts at $k = n$. Since g_o and g_r are of the same order of magnitude, it is natural to expect that the series starting ahead (with less terms) has a smaller magnitude and contributes less to ψ than the ones preceding them. This can be verified numerically.

Finally, an important outcome of this analysis is that echoes that arise later have a smaller frequency component than the first ones: the Dyson series is basically an expansion on powers of V/ω^2; thus by starting at $k = n$, ψ_n skips the high frequency contribution to the series until that term. This is easily explained on physical grounds: high frequency components "leak" easily from the cavity (the cavity being formed by the ultracompact object and the potential barrier). Lower frequency components are harder to tunnel out. Thus, at late times only low frequencies are present.

Recently, this approach was extended to ECOs modeled with a multiple-barrier filter near the surface, showing that the late-time ringdown exhibits mixing of echoes (Li and Piao 2019).

4.2.4 Echo modeling

The GW signal composed of echoes is a *transient* signal, which captures the transition between the photosphere ringdown. GW echoes are not well described by the QNMs of the ECO, which dominate the response only at very late times. Thus, a proper understanding of the signal in the "echoing stage" requires the full understanding of the theory and ensuing dynamics of the object. Unfortunately, as we discussed, there is a plethora of proposed candidate theories and objects, with unknown properties. Thus, the GW signal is known accurately for only a handful of special setups, and under very specific assumptions on the matter content (Cardoso et al. 2016b; Price and Khanna 2017). For this reason the echo signal is very rich, and different approaches have been recently developed to model it.

Templates for matched-filters   The first phenomenological time-domain echo template was proposed in Abedi et al. (2017a). It is based on a standard GR inspiral-merger-ringdown template $\mathcal{M}(t)$ and five extra free parameters,

$$h(t) \equiv A \sum_{n=0}^{\infty} (-1)^{n+1} \eta^n \mathcal{M}(t + t_{\mathrm{merger}} - t_{\mathrm{echo}} - n \Delta t_{\mathrm{echo}}, t_0), \qquad (59)$$

with $\mathcal{M}(t, t_0) \equiv \Theta(t, t_0) \mathcal{M}(t)$ and where

$$\Theta(t, t_0) \equiv \frac{1}{2} \left\{ 1 + \tanh \left[\frac{1}{2} \omega(t)(t - t_{\mathrm{merger}} - t_0) \right] \right\}, \qquad (60)$$

is a smooth cut-off function. The parameters are the following: $\Delta t_{\text{echo}} = 2\tau_{\text{echo}}$ is the time-interval in between successive echoes, see Eq. (37) for nonspinning objects and Eq. (74) below when rotation is included; t_{echo} is the time of arrival of the first echo, which can be affected by nonlinear dynamics near merger and does not necessarily coincide with Δt_{echo}; t_0 is a cutoff time which dictates the part of the GR merger template used to produce the subsequent echoes; $\eta \in [0, 1]$ is the (frequency-dependent) damping factor of successive echoes; A is the overall amplitude of the echo template with respect to the main burst at the merger (at $t = t_{\text{merger}}$). Finally, $\omega(t)$ is a phenomenological time-dependent mode frequency that is used in standard inspiral-merger-ringdown phenomenological models (Abbott et al. (LIGO Scientific Collaboration and the Virgo Collaboration) 2016b). For a given model, the above parameters are not necessarily independent, as discussed below. The $(-1)^{n+1}$ term in Eq. (59) is due to the phase inversion of the truncated model in each reflection. This implies that Dirichlet boundary conditions are assumed on the surface [or, more generally, that the reflection coefficient is real and negative, see discussion in Testa and Pani (2018)]. The phase inversion does not hold for Neumann-like boundary conditions or for wormholes (Testa and Pani 2018). This template was used in actual searches for echoes in the post-merger phases of LIGO/Virgo BH events, with conflicting claims discussed in Sect. 5.12. Extensions of the original template (Abedi et al. 2017a) have been developed and analyzed in Wang and Afshordi (2018) and in Uchikata et al. (2019).

A more phenomenological time-domain template, less anchored to the physics of echoes was proposed in Maselli et al. (2017b), using a superposition of sine-Gaussians with several free parameters. This template is very generic, but on the other hand suffers from a proliferation of parameters, which should not be in fact independent.

Note that the above two templates were directly modelled for spinning ECOs, since their underlying ingredients are very similar to the nonspinning case.

A frequency-domain template for nonspinning ECOs was built in Testa and Pani (2018) by approximating the BH potential with a Pöschl–Teller potential (Poschl and Teller 1933; Ferrari and Mashhoon 1984), thus finding an analytical approximation to the transfer function defined in Eq. (48). The template construction assumes that the source is localized in space, which allows to solve for the Green's function analytically. The final form of the ECO response in the frequency domain reads

$$h(\omega) = h_{\text{BH}}^{\text{ringdown}}(\omega) \left[1 + \mathcal{R}' \frac{\pi - e^{2i\omega d} \Upsilon \cosh\left(\frac{\pi \omega_R}{\alpha}\right)}{\pi + e^{2i\omega d} \mathcal{R}' \Upsilon \cosh\left(\frac{\pi \omega_R}{\alpha}\right)} \right], \tag{61}$$

where d is the width of the cavity of the potential (i.e., the distance between the surface and the potential barrier),

$$\mathcal{R}' \equiv \mathcal{R} e^{2i\omega z_0}, \tag{62}$$

is the ECO reflection coefficient defined as in Mark et al. (2017), Testa and Pani (2018) [notice the phase difference relative to that of Eq. (44)], $h_{\text{BH}}^{\text{ringdown}}$ is the standard BH ringdown template, ω_R is the real part of the QNMs of the corre-

sponding BH, α is a parameter of the Pöschl-Teller potential, defined by $\omega_R = \sqrt{V_0 - \alpha^2/4}$, $V_{\max}$ being the value of the exact potential at the maximum, and $\Upsilon = \Gamma\left(\frac{1}{2} - i\frac{\omega+\omega_R}{\alpha}\right)\Gamma\left(\frac{1}{2} - i\frac{\omega-\omega_R}{\alpha}\right)\frac{\Gamma\left(1+\frac{i\omega}{\alpha}\right)}{\Gamma\left(1-\frac{i\omega}{\alpha}\right)}$. The above expression assumes that the source is localized near the surface, a more general expression is provided in Testa and Pani (2018). Notice that the quantity $\mathcal{R}'$ has a more direct physical meaning than $\mathcal{R}$. For example, Dirichlet and Neumann boundary conditions on ψ correspond to $\mathcal{R}' = -1$ and $\mathcal{R}' = 1$, respectively [see Eq. (44)].

The above template depends only on two physical inputs: the reflection coefficient $\mathcal{R}$ (or $\mathcal{R}'$)—which can be in general a complex function of the frequency—and the width of the cavity d, which is directly related to the compactness of the object. For a given model of given compactness, $\mathcal{R}(\omega)$ and d are fixed and the mode does not contain other free parameters. For example, the damping factor introduced in the previous template can be written in terms of $\mathcal{R}$ and the reflection coefficient of the BH potential, $\mathcal{R}_{\mathrm{BH}}$ [see Eq. (41)] as $\eta = |\mathcal{R}\mathcal{R}_{\mathrm{BH}}|$ (Testa and Pani 2018). Since $\mathcal{R}_{\mathrm{BH}}$ is frequency dependent so must be η, even in the case of perfect reflectivity ($|\mathcal{R}| = 1$). The time-domain waveform contains all the features previously discussed for the echo signal, in particular amplitude and frequency modulation and phase inversion of each echo relative to the previous one for certain boundary conditions (Testa and Pani 2018).

Note that practically all generic modeling of echoes which do not start from a first-principles calculation of the GW signal assume equal-spacing for the echoes. This seems certainly a good approximation for stationary geometries, but will fail for collapsing objects for example (Wang et al. 2018a, 2019b). Furthermore, if the ECO reflective properties are modeled as a multiple-barrier filter—as in certain scenarios motivated by BH area quantization (Bekenstein and Mukhanov 1995; Cardoso et al. 2019a)—mixing of echoes occurs (Li and Piao 2019).

Wavelets for burst searches   Heuristic expressions for the echoing signal are useful, but the performance of template-based search techniques is highly dependent on the (unknown, in general) "faithfulness" of such templates. Based on the excellent performance of wavelet analysis for glitch signals, Tsang et al. (2018) proposed a "morphology-independent" echo-search. The analysis is based on generalized wavelets which are "combs" of sine-Gaussians, characterized by a time separation between the individual sine-Gaussians as well as a fixed phase shift between them, an amplitude damping factor, and a widening factor. Even though actual echo signals are unlikely to resemble any single generalized wavelet and may not even have well-defined values for any of the aforementioned quantities, superpositions of generalized wavelets are expected to capture a wide variety of physical echo waveforms. The comb is composed of a number N_G of sine-Gaussians,

$$h = \sum_{n=0}^{N_G} A\eta^n \exp\left(-(t - t_n)^2/(w^{2n}\tau^2)\right)\cos\left(2\pi f_0(t - t_n) + \phi_0 + n\Delta\phi\right), \quad (63)$$

with f_0 a central frequency, τ is a damping time, Δt the time between successive sine-Gaussians, $\Delta\phi$ is a phase difference between them, η is a damping factor between

one sine-Gaussian and the next, and w is a widening factor. Here, A is an overall amplitude, t_0 the central time of the first echo and ϕ_0 a reference phase.

Searches with Fourier windows.   A similar but independent search technique was devised in Conklin et al. (2018), and uses the fact that echoes should pile up power at very specific frequencies (those implied by the cavity delay time) which are nearly equally spaced [cf. Eq. (30)] (but see Wang et al. 2018a, 2019b). Thus, the technique consists on producing a "combing" window in Fourier space, able to match (maximizing over extrinsic parameters) the frequencies of the cavity. The specific shape of the tooth-comb was found not to be determinant, as long as it is able to capture the power in the resonant mode. An extension of this strategy is discussed in Conklin and Holdom (2019).

4.2.5 Echoes: a historical perspective

There exist in the literature examples of works where the main gist of the idea behind echoes is present, albeit only for specific examples and without the full appreciation of the role of the light ring. Already in 1978, the study of the instability of spinning horizonless compact objects (see Sect. 4.4.1) led to the understanding that the driving mechanism were the recurrent reflections of quasi-bound states within the ergoregion (Vilenkin 1978). *Mutatis mutandis*, these modes produce the echoes discussed above. Indeed, a Penrose diagram similar to that of Fig. 10 was already shown in Vilenkin (1978) (without a discussion of the GW emission slowly leaking from the potential barrier).

Probably the first example of echoes dates back to 1995, with the study of axial GWs emitted by perturbed (through Gaussian wavepackets) constant-density compact stars (Kokkotas and Schmidt 1999; Kokkotas 1995). This was later extended in the following years to include the scattering of point particles (Tominaga et al. 1999, 2001; Andrade and Price 1999; Ferrari and Kokkotas 2000; Andrade 2001). In all these studies the GW signal shows a series of clear echoes after the main burst of radiation, which were identified as the excitation of quasi-trapped modes of ultracompact stars (Chandrasekhar and Ferrari 1991). As we explained in Sect. 4.2.1, the true trapped-mode behavior only sets in at much later times, and the correct description is that of echoes. The original references did not attempt to explain the pattern in the signal, but in hindsight these results fit perfectly in the description we provided above: axial modes do not couple to the fluid [nor polar modes, which couple only very weakly (Andersson et al. 1996)] and travel free to the geometrical center of the star, which is therefore the effective surface in this particular case. The time delay of the echoes in Fig. 1 of Ferrari and Kokkotas (2000) is very well described by the GW's roundtrip time to the center, $\tau_{\mathrm{echo}} \sim \frac{27\pi}{8}\epsilon^{-1/2}M$, where $r_0 = \frac{9}{4}M(1+\epsilon)$ is the radius of the star (Pani and Ferrari 2018) and $r_0 = \frac{9}{4}M$ is the Buchdahl's limit (Buchdahl 1959).

Shortly after, but in a very different context, the overall picture of echoes would emerge in the fuzzball program. In Lunin and Mathur (2002a) and Giusto et al. (2005), the authors express the reflection coefficient of low-energy scalars as a sum over the number of bounces at the "throat" of these geometries. The idea behind is similar

to the expansion (48), and results in a series of "echoes" (Giusto et al. 2005). A quantitative calculation of the response, as well as the role of the light ring, were left undone.

In the context of wormhole physics [particularly the geometry (23)], the main features of the response of ClePhOs were identified in Damour and Solodukhin (2007). The postmerger train of echoes of the main burst was not addressed quantitatively.

Finally, in yet a different context, Barausse et al. (2014) discussed the late-time response of "dirty" BHs, modeling environmental effects (such as stars, gas etc) and showed that there are "secondary pulses" of radiation in the late-time response. These secondary pulses are just the echoes of a "mirrored" version of our original problem, where now it is the far region responsible for extra features in the effective potential, and hence the cavity is composed of the photosphere and the far region where matter is located.

4.3 The role of the spin

The previous sections dealt with static background spacetimes. Rotation intro-duces qualitatively new effects. For a Kerr BH, spinning with horizon angular velocity Ω along the azimuthal angle ϕ, perturbations are well understood using the Newman–Penrose formalism and a decomposition in so-called spin-weighted spheroidal harmonics (Teukolsky 1972, 1973; Chandrasekhar 1983). It is still pos-sible to reduce the problem to a PDE similar to Eq. (25), but the effective potential is frequency-dependent; breaks explicitly the azimuthal symmetry, i.e., it depends also on the azimuthal number m (fluctuations depend on the azimuthal angle as $\sim e^{im\phi}$); is generically complex, although there exist transformations of the perturba-tion variables that make it real (Detweiler 1977; Maggio et al. 2019); In particular, the explicit dependence on m gives rise to a Zeeman splitting of the QNMs as func-tions of the spin, whereas the frequency dependence gives rise to the interesting phenomenon of *superradiance* whereby modes with frequency ω are amplified when $\omega(\omega - m\Omega) < 0$. In particular, the potential is such that $V(r \to \infty) = \omega^2$, whereas $V(r \to r_+) = k^2$, with $k = \omega - m\Omega$. The relation between null geodesics and BH QNMs in the eikonal limit is more involved but conceptually similar to the static case (Yang et al. 2012).

Further features arise if the object under consideration is not a Kerr BH. In general, the vacuum region outside a spinning object is not described by the Kerr geometry. However, when $\epsilon \to 0$ any deviation from the multipolar structure of a Kerr BH must die off sufficiently fast (Raposo et al. 2019; Glampedakis and Pappas 2018a) (see Sect. 2.3.2). Explicit examples are given in Pani (2015), Uchikata and Yoshida (2016), Uchikata et al. (2016), Yagi and Yunes (2015b, c) and Posada (2017). Therefore, if one is interested in the very small ϵ limit, one can study a *Kerr-like ECO* (Cardoso et al. 2008b; Abedi et al. 2017a; Maggio et al. 2017; Nakano et al. 2017), i.e., a geometry described by the Kerr metric when $r > r_0 = r_+(1 + \epsilon)$ and with some membrane with model-dependent reflective properties at $r = r_0$. Beyond the $\epsilon \to 0$ limit, ECOs may have arbitrary multipole moments and even break equatorial symmetry (Raposo et al. 2019; Papadopoulos and Kokkotas 2018). In such cases, it may not be possible

to separate variables (Glampedakis and Pappas 2018a, b; Allahyari et al. 2019; Pappas and Glampedakis 2018) and the results below may not hold.

4.3.1 QNMs of spinning Kerr-like ECOs

Scalar, EM and gravitational perturbations in the exterior Kerr geometry are described in terms of Teukolsky's master equations (Teukolsky 1972, 1973; Teukolsky and Press 1974)

$$
\Delta^{-s} \frac{d}{dr} \left(\Delta^{s+1} \frac{d_s R_{lm}}{dr} \right) + \left[\frac{K^2 - 2is(r-M)K}{\Delta} + 4is\omega r - \lambda \right] {}_s R_{lm}
$$
$$
= 0, \tag{64}
$$
$$
\left[\left(1 - x^2 \right) {}_s S_{lm,x} \right]_{,x} + \left[(a\omega x)^2 - 2a\omega sx + s + {}_s A_{lm} - \frac{(m+sx)^2}{1-x^2} \right] {}_s S_{lm}
$$
$$
= 0, \tag{65}
$$

where $a = \chi M$, ${}_s S_{lm}(\theta)e^{im\phi}$ are spin-weighted spheroidal harmonics, $x \equiv \cos\theta$, $K = (r^2 + a^2)\omega - am$, and the separation constants λ and ${}_s A_{lm}$ are related by $\lambda \equiv {}_s A_{lm} + a^2\omega^2 - 2am\omega$. When $\chi = 0$, the angular eigenvalues are $\lambda = (l-s)(l+s+1)$, whereas for $\chi \neq 0$ they can be computed numerically or with approximated analytical expansions (Berti et al. 2006a).

It is convenient to make a change of variables by introducing the function (Detweiler 1977)

$$
{}_s X_{lm} = \Delta^{s/2} \left(r^2 + a^2 \right)^{1/2} \left[\alpha \, {}_s R_{lm} + \beta \Delta^{s+1} \frac{d_s R_{lm}}{dr} \right], \tag{66}
$$

where α and β are certain radial functions. Introducing the tortoise coordinate r_*, defined such that $dr_*/dr = (r^2 + a^2)/\Delta$, the master equation (64) becomes

$$
\frac{d_s^2 X_{lm}}{dr_*^2} - V(r,\omega) \, {}_s X_{lm} = 0, \tag{67}
$$

where the effective potential is

$$
V(r,\omega) = \frac{U\Delta}{(r^2 + a^2)^2} + G^2 + \frac{dG}{dr_*}, \tag{68}
$$

and

$$
G = \frac{s(r-M)}{r^2 + a^2} + \frac{r\Delta}{(r^2 + a^2)^2}, \tag{69}
$$
$$
U = \frac{2\alpha' + (\beta'\Delta^{s+1})'}{\beta\Delta^s} - \frac{1}{\Delta} \left[K^2 - is\Delta'K + \Delta(2isK' - \lambda) \right]. \tag{70}
$$
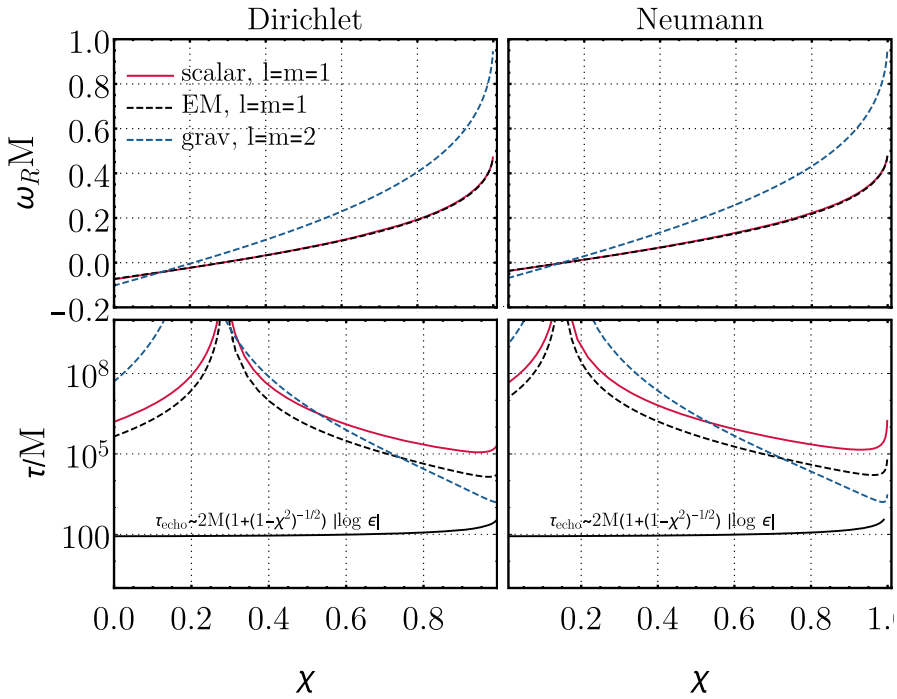
Fig. 11 Frequency (top panels) and damping/growing time (bottom panels) of scalar, EM, and gravitational QNMs of a Kerr-like ECO with a perfectly reflective surface for either Dirichlet (left panels) or Neumann (right panels) boundary conditions. We choose $\epsilon = 10^{-10}$ [data adapted from Maggio et al. (2019)]. Modes are stable (i.e., they decay in time) for $\omega_R < 0$, whereas they turn unstable (i.e., they grow in time) when $\omega_R > 0$. The damping/growing time diverges for marginally stable modes, when $\omega_R = 0$. In the bottom panels, the continuous black curve represents the characteristic echo delay time, much shorter than the instability time scale

The prime denotes a derivative with respect to r and the functions α and β can be chosen such that the resulting potential is *purely real* [definitions of α and β can be found in Detweiler (1977) and Maggio et al. (2019) for EM and gravitational perturbations respectively]. It is natural to define the generalization of Eq. (44) as (Maggio et al. 2019)

$$X_{\mathrm{ECO}} \sim e^{-ikz} + \mathcal{R}e^{ikz}, \quad z \to z_0, \tag{71}$$

where now $\mathcal{R}$ generically depends on the frequency and on the spin and z is the Kerr tortoise coordinate defined by $dz/dr = (r^2 + a^2)/\Delta$.

To search for the characteristic or QNMs of the system, Eq. (67) is to be solved with boundary condition (71) at $z \sim z_0$ and (outgoing) $X \sim e^{i\omega z}$ at infinity (Maggio et al. 2019). A small frequency approximation yields (Starobinskij and Churilov 1973; Maggio et al. 2017, 2019)

$$M\omega_R \simeq m\Omega - \frac{M\pi}{2|z_0|}\left(q + \frac{s(s+1)}{2}\right), \tag{72}$$

$$M\omega_I \simeq -\frac{\beta_{ls}}{|z_0|}\left(\frac{2M^2 r_+}{r_+ - r_-}\right)\left[\omega_R(r_+ - r_-)\right]^{2l+1}(\omega_R - m\Omega), \tag{73}$$

where now $z_0 \sim M[1+(1-\chi^2)^{-1/2}]\log\epsilon$. This result shows how angular momentum can bring about substantial qualitative changes. The spacetime is unstable for $\omega_R(\omega_R - m\Omega) < 0$ [i.e., in the superradiant regime (Brito et al. 2015b; Vicente et al. 2018)], on a timescale $\tau_{\rm inst} \equiv 1/\omega_I$. This phenomenon is called *ergoregion instability* (Friedman 1978b; Brito et al. 2015b; Moschidis 2016; Vicente et al. 2018) (see Sect. 4.4.1 below). In the $\epsilon \to 0$ limit and for sufficiently large spin, $\omega_R \sim m\Omega$ and $\omega_I \sim |\log\epsilon|^{-2}$. Note that, owing to the $\omega_R - m\Omega$ term in Eq. (73), polar and axial modes are not isospectral in the spinning case, even when $\epsilon \to 0$: indeed, they have the same frequency but a slightly different time scale. Numerical results, shown in Fig. 11, are in excellent agreement with the above analytical approximations whenever $\omega M \ll 1$, which also implies small rotation rates (Maggio et al. 2019). For very large spins there exists a more complex analytical approximation (Hod 2017). Note that in the superradiant regime the "damping" factor, $\omega_I/\omega_R > 0$, so that, at very late times (when the pulse frequency content is indeed described by these formulas), the amplitude of the QNMs *increases* due to the instability. This effect is small—for example, $\omega_I/\omega_R \approx 4 \times 10^{-6}$ when $\epsilon = 0.001, l = 2$ and $\chi = 0.7$—and, more importantly, it does not affect the first several echoes, since the latter appear on a timescale much shorter than the instability time scale (see Fig. 11).

4.3.2 Echoes from spinning ECOs

GW echoes from spinning ECOs have been investigated actively (Abedi et al. 2017a; Nakano et al. 2017; Bueno et al. 2018; Conklin et al. 2018; Vicente et al. 2018). The overall picture is similar to the static case, with two notable differences. The echo delay time (37) now reads (Abedi et al. 2017a)

$$\tau_{\rm echo} \sim 2M[1+(1-\chi^2)^{-1/2}]|\log\epsilon|, \tag{74}$$

in the $\epsilon \to 0$ limit. This time scale corresponds to the period of the *corotating* mode, $\tau_{\rm echo} \sim (\omega_R - m\Omega)^{-1}$. In addition, as we discussed above the spacetime is unstable over a time scale $\tau = 1/|\omega_I|$. Such timescale is parametrically longer than $\tau_{\rm echo}$ (see Fig. 11) and does not affect the first $N \approx \tau/\tau_{\rm echo} \sim |\log\epsilon|$ echoes. As we explained earlier, the signal can only be considered as a series of well-defined pulses at early stages, when the pulse still contains a substantial amount of high-frequency components. Thus, amplification occurs only at late times; the early-time evolution of the pulse generated at the photon sphere is more complex.

The transfer function of Eq. (46) can be generalized to spinning "Kerr-like" ECO subjected to boundary condition (71) near the surface. The final result reads formally the same, although $\mathcal{T}_{\rm BH}$ and $\mathcal{R}_{\rm BH}$ are defined in terms of the amplitudes of the waves scattered off the Kerr effective potential (Conklin et al. 2018; Testa et al. 2019). Echoes from Kerr-like wormholes [i.e., a spinning extension of the Damour–Solodukhin solution (Damour and Solodukhin 2007)] have been studied in Bueno et al. (2018). Phenomenological templates for echoes from Kerr-like objects were

constructed in Abedi et al. (2017a), Nakano et al. (2017), Maselli et al. (2017b), Wang and Afshordi (2018) and are discussed in Sect. 4.2.4.

4.4 The stability problem

There is nothing stable in the world; uproar's your only music.
John Keats, Letter to George and Thomas Keats, Jan 13 (1818)

Appealing solutions are only realistic if they form and remain as long-term stable solutions of the theory. In other words, solutions have to be stable when slightly perturbed or they would not be observed (or they would not even form in the first place). There are strong indications that the exterior Kerr spacetime is stable, although a rigorous proof is still missing (Dafermos and Rodnianski 2013). On the other hand, some—and possibly most of—horizonless compact solutions are linearly or nonlinearly unstable.

Some studies of linearized fluctuations of ultracompact objects are given in Table 1. We will not discuss specific models, but we would like to highlight some general results.

4.4.1 The ergoregion instability

Several models of UCOs and ClePhOs are stable under *radial* perturbations (Iyer et al. 1985; Visser and Wiltshire 2004) (see Table 1). However, UCOs (and especially ClePhOs) can develop negative-energy regions once spinning. In such a case, they develop a *linear* instability under *non-radial* perturbations, which is dubbed as ergoregion instability. Such instability affects any horizonless geometry with an ergoregion (Friedman 1978b; Kokkotas et al. 2004; Moschidis 2016; Cardoso et al. 2008a; Oliveira et al. 2014; Maggio et al. 2017; Vicente et al. 2018) and is deeply connected to superradiance (Brito et al. 2015b). The underlying mechanism is simple: a negative-energy fluctuation in the ergoregion is forced to travel outwards; at large distances only positive-energy states exist, and energy conservation implies that the initial disturbance gives rise to a positive fluctuation at infinity plus a larger (negative-energy) fluctuation in the ergoregion. Repetition of the process leads to a cascading instability. The only way to prevent such cascade from occurring is by absorbing the negative energy states, which BHs do efficiently (and hence Kerr BHs are stable against massless fields), but perfectly-reflecting horizonless objects must then be unstable.

This instability was discovered by Friedman for ultracompact slowly-rotating stars with an ergoregion (Friedman 1978a), and later extended in Comins and Schutz (1978), Yoshida and Eriguchi (1996), Kokkotas et al. (2004). Application to Kerr-like horizonless objects started in Vilenkin (1978), whereas an analysis for gravastars, boson stars, and other objects was done in Cardoso et al. (2006, 2008a, b), Chirenti and Rezzolla (2008). More recently, Maggio et al. (2017, 2019) gave a detailed analysis of scalar, electromagnetic, and gravitational perturbations of a partially-reflective Kerr-like ECO in the $\epsilon \to 0$ limit.

The overall summary of these studies is that the instability time scale depends strongly on the spin and on the compactness of the objects. The ergoregion-instability

timescale can very long (Friedman 1978b; Cardoso et al. 2008a; Maggio et al. 2017). For concreteness, for gravastars with $\epsilon \sim 0.1 - 1$ the ergoregion is absent even for moderately high spin (Chirenti and Rezzolla 2008). However, at least for perfectly-reflecting Kerr-like ECOs in the $\epsilon \to 0$ limit, the critical spin above which the object is unstable is very low (Maggio et al. 2019) [see Eq. (73)]

$$\chi_{\text{crit}} \sim \frac{\pi}{m|\log \epsilon|}\left(q + \frac{s(s+1)}{2}\right).$$ (75)

For example, a totally reflecting surface a Planck length outside the horizon of a $10M_\odot$ ECO ($\epsilon = l_P/r_+ \approx 5 \times 10^{-40}$) will generate an ergoregion instability if $\chi \gtrsim 0.07$ for $q = 1$, $m = 1$, and $s = -2$. Note that the instability time scale can be very large near the instability threshold. From Eq. (73), we can estimate the timescale of the instability of a spinning ClePhO,

$$\tau_{\text{inst}} \equiv \frac{1}{\omega_I} \sim -|\log \epsilon|\frac{1 + (1 - \chi^2)^{-1/2}}{2\beta_{ls}}\left(\frac{r_+ - r_-}{r_+}\right)\frac{\left[\omega_R(r_+ - r_-)\right]^{-(2l+1)}}{\omega_R - m\Omega}.$$ (76)

As previously discussed, a spinning ClePhO is (superradiantly) unstable only above a critical value of the spin. For example, for $l = m = s = 2$ and $\chi = 0.7$, the above formula yields

$$\tau \in (5, 1)\left(\frac{M}{10^6 M_\odot}\right)\text{ yr}\quad\text{when}\ \epsilon \in (10^{-45}, 10^{-22}).$$ (77)

Generically, the ergoregion instability acts on timescales which are parametrically longer than the dynamical timescale, $\sim M$, of the object, but still short enough to be relevant in astrophysical scenarios. Although the evolution of this instability remains an open problem, it is likely that it will remove angular momentum from the object, spinning it down until the threshold condition, $\chi = \chi_{\text{crit}}$, is reached (Barausse et al. 2018). The phenomenological consequences of this phenomenon will be discussed in Sect. 5.

A possible way to quench the instability is by absorbing the negative-energy modes trapped within the ergoregion. Kerr BHs can absorb such modes efficiently and are indeed expected to be stable even if they have an ergoregion. Given its long timescales, it is possible that the instability can be efficiently quenched by some dissipation mechanism of nongravitational nature, although this effect would be model-dependent (Maggio et al. 2017, 2019). Unfortunately, the effect of viscosity in ECOs is practically unknown (Cardoso et al. 2014; Guo et al. 2018), and so are the timescales involved in putative dissipation mechanisms that might quench this instability. It is also possible that, when spinning, a partially-absorbing object can support quasi-trapped superradiant modes with $\omega_R < m\Omega$, which might lead to an instability similar to that of massive bosonic fields around Kerr BHs (Brito et al. 2015b).

Finally, there are indications that instabilities of UCOs are merely the equivalent of Hawking radiation for these geometries, and that therefore there might be a smooth

transition in the emission properties when approaching the BH limit (Chowdhury and Mathur 2008; Damour and Solodukhin 2007).

4.4.2 Nonlinear instabilities I: long-lived modes and their backreaction

Linearized gravitational fluctuations of any nonspinning UCO are extremely long-lived and decay no faster than logarithmically (Keir 2016; Cardoso et al. 2014; Eperon et al. 2016; Eperon 2017). Indeed, such perturbations can be again understood in terms of modes quasi-trapped within the potential barrier shown in Fig. 8: they require a photon sphere but are absent in the BH case [hence the photon sphere is sometimes referred to as "loosely trapped" or "transversely trapping" surface (Shiromizu et al. 2017; Yoshino et al. 2017)]. For a ClePhO, these modes are very well approximated by Eqs. (30)–(31) in the static case and by their aforementioned extension in the spinning case. The long damping time of these modes has led to the conjecture that any UCO is *nonlinearly* unstable and may evolve through a Dyson–Chandrasekhar–Fermi type of mechanism (Keir 2016; Cardoso et al. 2014). The endstate is unknown, and most likely depends on the equation of the state of the particular UCO: some objects may fragment and evolve past the UCO region into less compact configurations, via mass ejection, whereas other UCOs may be forced into gravitational collapse to BHs.

The above mechanism is supposed to be active for any spherically symmetric UCO, and also on spinning solutions. However, it is nonlinear in nature and not well understood so far. For example, there are indications that a putative nonlinear instability would occur on very long timescales only; a model problem predicts an exponential dependence on the size of the initial perturbation (John 1981).

4.4.3 Nonlinear instabilities II: causality, hoop conjecture, and BH formation

The teleological nature of horizons leads to possible spacelike behavior in the way they evolve. In turn, this has led to constraints on the possible compactness of horizonless objects. Carballo-Rubio et al. (2018b) finds the conceptual bound

$$\epsilon \leq 4\dot{M}, \tag{78}$$

based on a special accreting geometry (so-called Vaidya spacetime) and on the requirement that the surface of the accreting ECO grows in a timelike or null way. The assumptions behind such result are relatively strong: the accreting matter is a very particular null dust, eternally accreting at a constant rate and without pressure. In addition, superluminal motion for the ECO *surface* is not forbidden, and may well be a rule for such compact geometries.

A different, but related, argument makes use of the hoop conjecture (Chen et al. 2019) (see also Addazi et al. 2019 for similar work). In broad terms, the hoop conjecture states that if a body is within its Schwarzschild radius, then it must be a BH (Thorne 1972; Choptuik and Pretorius 2010). Take two ECOs of mass $m_2 \ll m_1$, inspiralling to produce a single ECO. The burst of energy emitted in ringdown modes is of order (Berti et al. 2007)

$$\frac{E_{\text{ringdown}}}{m_1 + m_2} \sim 0.44 \left(\frac{m_1 m_2}{(m_1 + m_2)^2} \right)^2 , \tag{79}$$

This estimate holds for BHs, and it seems plausible that it would approximately holds also for ECOs. A similar amount of energy goes *inwards*. Then, when the small body crosses the photon sphere of the large ECO, an amount of mass (79) is emitted inwards and is swallowed by the large ECO increasing its mass to $m_1 + E_{\text{ringdown}}$. The hoop conjecture implies that $2(m_1 + E_{\text{ringdown}}) \leq 2m_1(1 + \epsilon)$, or

$$\epsilon \gtrsim 0.44 \frac{m_2^2}{m_1^2}, \tag{80}$$

to avoid BH formation. Thus, ϵ of Planckian order are not allowed. There are issues with this type of arguments: The GWs are not spherical and not localized (their wavelength is of the order or larger than the ECO itself), thus localizing it on a sphere of radius $2m_1(1 + \epsilon)$ is impossible. Furthermore, the argument assumes that all energy reaching the surface is accreted, whereas it might be efficiently absorbed by other channels.

The above argument can be made more powerful, making full use of the hoop conjecture: take two ECOs and boost them to large enough energies. Since all energy gravitates and is part of the hoop, the final object must be inside its Schwarzschild radius, hence it must be a BH [indeed, at large enough center of mass energies, the structure of the colliding objects is irrelevant (Eardley and Giddings 2002; Choptuik and Pretorius 2010; Sperhake et al. 2013b)]. It is very challenging to bypass this argument *at the classical level*. Nevertheless, it is important to highlight a few points: (i) Most of the arguments for ECO formation (and existence) rely directly or indirectly on unknown *quantum* effects associated with horizon or singularity formation (Giddings 1992, 2011, 2012, 2017b; Mazur and Mottola 2004; Mathur 2005, 2008, 2009; Barceló et al. 2016, 2017). Thus, it is very likely that horizons may form classically but that such picture is blurred by quantum effects (on unknown timescales and due to unknown dynamics);[5] (ii) even classically, the argument does not forbid the existence of ECOs, it merely forces their interaction at high energy to result in BH formation (indeed, the same argument can be applied if the two objects are neutron stars).

4.5 Binary systems

Consider a compact binary of masses m_i ($i = 1, 2$), total mass $m = m_1 + m_2$, mass ratio $q = m_1/m_2 \geq 1$, and dimensionless spins χ_i. In a post-Newtonian (PN) approximation (i.e., a weak-field/slow-velocity expansion of Einstein's equations), dynamics is driven by energy and angular momentum loss, and particles are endowed

---

[5] In this respect, a parallel can drawn with neutron stars, which can be well described within GR by a simple self-gravitating perfect fluid, but whose formation process is significantly more complex than the gravitational collapse of a perfect fluid. Incidentally, such processes involve complex microphysics and quantum effects such as those occurring in a supernova collapse. In other words, the fact that an equilibrium solution can be well described by simple matter fields does not necessarily mean that its formation is equally simple nor does it exclude more complex formation processes.

with a series of multipole moments and with finite-size tidal corrections (Blanchet 2006). Up to 1.5PN order, the GW phase depends only on m_i and χ_i and is oblivious to the compactness of the binary components. Starting from 2PN order, the nature of the inspiralling objects is encoded in:

(i) the way they respond to their own gravitational field—i.e., on their own multipolar structure (Krishnendu et al. 2017, 2019; Kastha et al. 2018);
(ii) the way they respond when acted upon by the external gravitational field of their companion—through their tidal Love numbers (TLNs) (Poisson and Will 1953);
(iii) on the amount of radiation that they possibly absorb, i.e., on tidal heating (Hartle 1973; Hughes 2001).

These effects are all included in the waveform produced during the inspiral, and can be incorporated in the Fourier-transformed GW signal as

$$\tilde{h}(f) = \mathcal{A}(f)e^{i(\psi_{PP}+\psi_{TH}+\psi_{TD})} \tag{81}$$

where f and $\mathcal{A}(f)$ are the GW frequency and amplitude, $\psi_{PP}(f)$ is the "pointlike" phase (Blanchet 2006), whereas $\psi_{TH}(f)$, $\psi_{TD}(f)$ are the contributions of the tidal heating and the tidal deformability, respectively.

4.5.1 Multipolar structure

Spin–orbit and spin–spin interactions are included in ψ_{PP}, the latter also depending on all higher-order multipole moments. The dominant effect is that of the spin-induced quadrupole moment, M_2, which yields a 2PN contribution to the phase (Krishnendu et al. 2017)

$$\psi_{\text{quadrupole}} = \frac{75}{64} \frac{\left(m_2 M_2^{(1)} + m_1 M_2^{(2)}\right)}{(m_1 m_2)^2} \frac{1}{v}, \tag{82}$$

where the expansion parameter $v = (\pi m f)^{1/3}$ is the orbital velocity. By introducing the dimensionless spin-induced, quadrupole moment, $\bar{M}_2^{(i)} = M_2^{(1)}/(\chi_i^2 m_i^3)$, it is clear that the above correction is quadratic in the spin. For a Kerr BH, $\bar{M}_2^{(i)} = -1$, whereas for an ECO there will be generic corrections that anyway are bound to vanish as $\epsilon \to 0$ (Raposo et al. 2019) (Sect. 2.3.2).

4.5.2 Tidal heating

A spinning BH absorbs radiation of frequency $\omega > m\Omega$, but amplifies radiation of smaller frequency (Brito et al. 2015b). In this respect, BHs are dissipative systems which behave just like a Newtonian viscous fluid (Damour 1982; Poisson 2009; Cardoso and Pani 2013). Dissipation gives rise to various interesting effects in a binary system—such as tidal heating (Hartle 1973; Hughes 2001), tidal acceleration, and tidal locking, as in the Earth–Moon system, where dissipation is provided by the friction of the oceans with the crust.

For low-frequency circular binaries, the energy flux associated to tidal heating at the horizon, $\dot{E}_H$, corresponds to the rate of change of the BH mass (Alvi 2001; Poisson 2004),

$$\dot{M} = \dot{E}_H \propto \frac{\Omega_K^5}{M^2}(\Omega_K - \Omega), \tag{83}$$

where $\Omega_K \ll 1/M$ is the orbital angular velocity and the (positive) prefactor depends on the masses and spins of the two bodies. Thus, tidal heating is stronger for highly spinning bodies relative to the nonspinning by a factor $\sim \Omega/\Omega_K \gg 1$.

The energy flux (83) leads to a potentially observable phase shift of GWs emitted during the inspiral. The GW phase ψ is governed by $d^2\psi/df^2 = 2\pi(dE/df)/\dot{E}$, where $E \sim v^2$ is the binding energy of the binary. To the leading order, this yields (for circular orbits and spins aligned with the orbital angular momentum) (Maselli et al. 2018b)

$$\psi_{\mathrm{TH}}^{\mathrm{BH}} = \psi_{\mathrm{N}} \left(F(\chi_i, q) v^5 \log v + G(q) v^8 [1 - 3 \log v] \right), \tag{84}$$

where $\psi_{\mathrm{N}} \sim v^{-5}$ is the leading-order contribution to the point-particle phase (corresponding to the flux $\dot{E}_{\mathrm{GW}}$), and

$$F(\chi_i, q) = -\frac{10 \left(q^3 \left(3\chi_1^3 + \chi_1 \right) + 3\chi_2^3 + \chi_2 \right)}{3(q + 1)^3}, \tag{85}$$

$$G(\chi_i, q) = \frac{10}{27(q + 1)^5} \left[q^5 A_1 + A_2 + q^4 B_1 + q B_2 + q^3 C_1 + q^2 C_2 \right], \tag{86}$$

with

$$A_i = 2 \left(3\chi_i^2 + 1 \right) \left(3 - 10\chi_i^2 + 3\Delta_i \right), \tag{87}$$

$$B_i = 3 \left(3\chi_i^2 + 1 \right) \left(2 - 5\chi_i^2 + 2\Delta_j - 5\chi_i \chi_j \right), \tag{88}$$

$$C_i = -20 \left(3\chi_i^2 + 1 \right) \chi_i \chi_j, \tag{89}$$

$\Delta_i \equiv \sqrt{1 - \chi_i^2}$ and $j \neq i$. Therefore, absorption at the horizon introduces a 2.5PN(4PN) $\times \log v$ correction to the GW phase of spinning (nonspinning) binaries, relative to the leading term.

Thus, it might be argued that an ECO binary can be distinguished from a BH binary, because $\dot{E}_H = 0$ for the former. However, the trapping of radiation in ClePhOs can efficiently mimic the effect of a horizon (Maselli et al. 2018b). In order for absorption to affect the orbital motion, it is necessary that the time radiation takes to reach the companion, T_{rad}, be much longer than the radiation-reaction time scale due to heating, $T_{\mathrm{RR}} \simeq E/\dot{E}_H$, where $E \simeq -\frac{1}{2}M(M\Omega_K)^{2/3}$ is the binding energy of the binary (assuming equal masses). For BHs, $T_{\mathrm{rad}} \to \infty$ because of time dilation, so that the condition $T_{\mathrm{rad}} \gg T_{\mathrm{RR}}$ is always satisfied. For ClePhOs, T_{rad} is of the order of the

GW echo delay time, Eq. (74), and therefore increases logarithmically as $\epsilon \to 0$. Thus, an effective tidal heating might occur even in the absence of a horizon if the object is sufficient compact. The critical value of ϵ increases strongly as a function of the spin. For orbital radii larger than the ISCO, the condition $T_{\rm rad} \gg T_{\rm RR}$ requires $\epsilon \ll 10^{-88}$ for $\chi \lesssim 0.8$, and therefore even Planck corrections at the horizon scale are not sufficient to mimic tidal heating. This is not necessarily true for highly spinning objects, for example $T_{\rm rad} \gg T_{\rm RR}$ at the ISCO requires $\epsilon \ll 10^{-16}$ for $\chi \approx 0.9$.

4.5.3 Tidal deformability and Love numbers

Finally, the nature of the inspiralling objects is also encoded in the way they respond when acted upon by the external gravitational field of their companion—through their tidal Love numbers (TLNs) (Poisson and Will 1953). An intriguing result in classical GR is that the TLNs of BHs are zero. This result holds: (i) in the nonspinning case for weak tidal fields (Damour 1983; Binnington and Poisson 2009; Damour and Nagar 2009) and also for tidal fields of arbitrary amplitude (Gürlebeck 2015); (ii) in the spinning case (Poisson 2015; Pani et al. 2015b; Landry and Poisson 2015) for weak tidal fields, at least in the axisymmetric case to second order in the spin (Pani et al. 2015b) and generically to first order in the spin (Landry and Poisson 2015). On the other hand, the TLNs of ECOs are small but finite (Pani 2015; Uchikata et al. 2016; Porto 2016; Cardoso et al. 2017; Wade et al. 2013; Giddings et al. 2019).

In spherical symmetry, the TLNs can be defined as the proportionality factor between the induced mass quadrupole moment, M_2, and the (quadrupolar) external tidal field, E_2. Let us consider the mutual tides induced on the two bodies of a binary system at orbital distance r due to the presence of a companion. In this case

$$M_2^{(1)} = \lambda_1 E_2^{(2)} \qquad M_2^{(2)} = \lambda_2 E_2^{(1)}, \tag{90}$$

where λ_i is the tidal deformability parameter of the i-th body. At Newtonian order, the external tidal field produced by the i-th object on its companion is simply

$$E_2^{(i)} \sim \frac{m_i}{r^3} \propto v^6. \tag{91}$$

The above results can be used to compute the contributions of the tidal deformability to the binding energy of the binary, $E(f)$, and to the energy flux dissipated in GWs, $\dot{E}$. The leading-order corrections read (Vines et al. 2011)

$$E(f) = -\frac{mq}{2(1+q)^2} v^2 \left(1 - \frac{6q(k_1 q^3 + k_2)}{(1+q)^5} v^{10} \right), \tag{92}$$

$$\dot{E}(f) = -\frac{32}{5} \frac{q^2}{(1+q)^4} v^{10} \left(1 + \frac{4 \left(q^4(3+q)k_1 + (1+3q)k_2 \right)}{(1+q)^5} v^{10} \right), \tag{93}$$

where k_i is the (dimensionless) TLN of the i-th object, defined as $\lambda_i = \frac{2}{3} k_i m_i^5$. By plugging the above equations in $\frac{d^2\psi(f)}{df^2} = \frac{2\pi}{\dot{E}} \frac{dE}{df}$, we can solve for the tidal phase to leading order,

$$\psi_{\text{TD}}(f) = -\psi_{\text{N}} \frac{624\Lambda}{m^5} v^{10}, \tag{94}$$

where $39\Lambda = (1 + 12/q) m_1^5 k_1 + (1 + 12q) m_2^5 k_2$ is the weighted tidal deformability. Thus, the tidal deformability of the binary components introduces a 5PN correction (absent in the BH case) to the GW phase relative to the leading-order GW term. This can be understood by noticing that the v^6 term in Eqs. (90) and (91) multiplies the $1/v$ term in Eq. (82), giving an overall factor v^5 which is a 5PN correction relative to $\psi_{\text{N}} \sim v^{-5}$. This derivation is valid for nonspinning objects, the effect of spin is suppressed by a further 1.5PN order and introduces new classes of *rotational TLNs* Poisson (2015), Pani et al. (2015a), Landry and Poisson (2015), Abdelsalhin et al. (2018) and Jiménez Forteza et al. (2018).

The TLNs of a nonspinning ultracompact object of mass M and radius $r_0 = 2M(1 + \epsilon)$ (with $\epsilon \ll 1$) in Schwarzschild coordinates vanish logarithmically in the BH limit (Cardoso et al. 2017), $k \sim 1/|\log \epsilon|$, opening the way to probe horizon scales. This scaling holds for any ECO whose exterior is governed (approximately) by vacuum-GR equations, and with generic Robin-type boundary conditions on the Zerilli function Ψ at the surface, $a\Psi + b\frac{d\Psi}{dz} = c$ (Maselli et al. 2018a). In this case, in the $\epsilon \to 0$ limit one gets

$$k \sim \frac{2(4a - 3c)}{15a \log \epsilon}. \tag{95}$$

Particular cases of the above scaling are given in Table I of Cardoso et al. (2017). Thus, the only exception to the logarithmic behavior concerns the zero-measure case $a = \frac{3}{4} c$, for which $k \sim \epsilon/\log \epsilon$. No ECO models described by these boundary conditions are known.

Such generic logarithmic behavior acts as a *magnifying glass* to probe near-horizon quantum structures (Cardoso et al. 2017; Maselli et al. 2018b). Since $k \sim \mathcal{O}(10^{-3}-10^{-2})$ when $\epsilon \sim \ell_P/M$. As a comparison, for a typical neutron star $k_{\text{NS}} \approx 200$, and probing quantum structures near the horizon will require a precision about 4 orders of magnitude better than current LIGO constraints (Abbott et al. (LIGO Scientific Collaboration and the Virgo Collaboration) 2018a). Prospects to detect this effect are discussed in Sect. 5.8. The logarithmic mapping between k and ϵ makes it challenging constraint ϵ from measurements of the TLNs, because measurements errors propagate exponentially (Maselli et al. 2018b; Addazi et al. 2018). Nevertheless, this does not prevent to distinguish ECOs from BHs using TLNs, nor to perform model selection between different ECO models all with new microphysics at the Planck scale (Maselli et al. 2018a).

This is shown in Fig. 12—inspired by standard analysis to discriminate among neutron-star equations of state (Hinderer et al. 2010; Maselli et al. 2013). The figure shows the tidal deformability $\lambda = \frac{2}{3} M^5 |k|$ as a function of the object mass for three
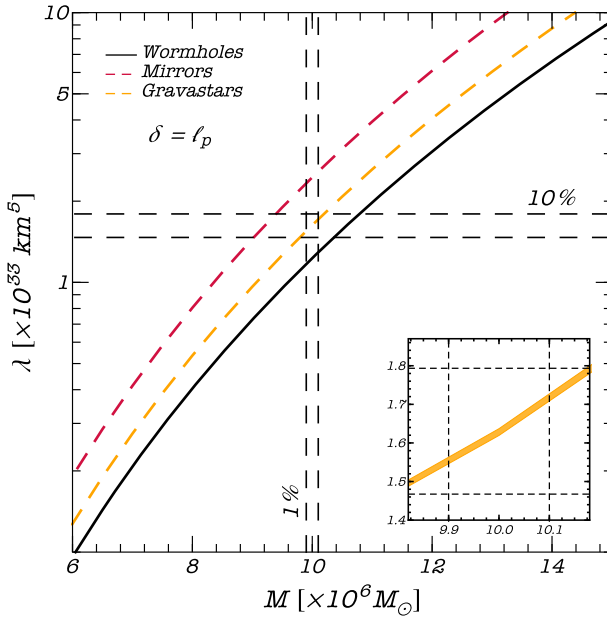
Fig. 12 Tidal deformability λ as a function of the mass for three toy models of ECOs. For all models the surface is at Planckian distance from the Schwarzschild radius, $r_0 - 2M = \ell_P$. The dashed lines refer to a putative measurement of the TLN at the level of 10% for an object with $M = 10^7 M_\odot$, which would allow to distinguish among different models at more than 90% confidence level. The zoomed inset resolves the thickness of each curve, with a width given by the intrinsic error due to the quantum uncertainty principle (Addazi et al. 2018). Adapted from Maselli et al. (2018a)

different toy models (gravastars, wormholes, and perfectly-reflecting Schwarzschild-like ECOs) characterized by the same Planckian scale of the correction, $\delta \equiv r_0 - 2M = \ell_P \approx 1.6 \times 10^{-33}$ cm.

To summarize, finite-size effects in the inspiral waveform provide three different null-hypothesis tests of BHs. BHs have vanishing TLNs but introduce a nonzero tidal heating ($\psi_{TD} = 0$, $\psi_{TH} \neq 0$), while ECOs have (logarithmically small) TLNs but zero tidal heating ($\psi_{TD} \neq 0$, $\psi_{TH} = 0$). In addition BHs have a very well defined set of multipole moments which depend on only two parameters (mass and angular momentum), whereas ECOs have in principle limitless possibilities. In addition, it is possible that the inspiral excites the characteristic modes of each of the objects, i.e., their QNMs. The extent to which this happens, and its impact on the inspiral stage are still to be understood (Cardoso et al. 2019b).

The TLNs were computed for boson stars (Mendes and Yang 2017; Cardoso et al. 2017; Sennett et al. 2017), very compact anisotropic fluid stars (Raposo et al. 2018), and gravastars (Uchikata et al. 2016; Cardoso et al. 2017). The TLNs of simple-minded ultracompact Schwarzschild-exterior spacetimes with a stiff equation of state at the surface were computed in Cardoso et al. (2017). The TLNs of spacetimes mimicking "compact quantum objects" were recently investigated (Giddings et al. 2019).

4.5.4 Accretion and drag in inspirals around and inside DM objects

When an object moves through any medium, it will be subject to (at least) two types of drag. One is direct and caused by accretion: the accreting object grows in mass and slows down. In addition, the moving body exerts a gravitational pull on all the medium, the backreaction of which produces dynamical friction (known also as "gravitational drag"), slowing the object down. To quantify these effects, it is important to know how the medium behaves. Collisionless media cause, generically, a gravitational drag different from that of normal fluids (Macedo et al. 2013a, b). The gravitational drag caused by media which is coherent on large scales may be suppressed (Hui et al. 2017), but further work is necessary to understand this quantitatively.

Consider now a binary of two compact objects, in which one is made of DM. At large separations inspiral will be driven mostly by GW emission. However, at small distances, the dynamics will generically be dominated by accretion and gravitational drag. The phase evolution of a binary, taking gravitational radiation, accretion and drag was studied when a small BH or neutron star inspirals around *and inside* a massive boson star (Macedo et al. 2013a, b). These results can also be directly translated to inspirals within a DM environment (Barausse et al. 2014; Macedo et al. 2013a, b; Eda et al. 2015; Yue and Han 2018; Hannuksela et al. 2019). Full nonlinear simulations of the inspiral and merger of boson stars, oscillatons and axion stars include GW emission, drag and accretion and tidal deformations. Although considerably more difficult to systematize and perform, such studies have been undertaken recently (Bezares et al. 2017; Palenzuela et al. 2017; Bezares and Palenzuela 2018; Helfer et al. 2019; Dietrich et al. 2019; Clough et al. 2018).

4.5.5 GW emission from ECOs orbiting or within neutron stars

It is conceivable that ECOs play also a role in GW (as well as EM) emission when orbiting close to neutron stars or white dwarfs. This might arise via two different possible ways. ECOs can form via gravitational collapse of DM or unknown quantum effects, and cluster around compact stars through tidal dissipation mechanisms. Alternatively, compact stars evolving in DM-rich environments may accrete a significant amount of DM in their interior: DM is captured by the star due to gravitational deflection and a non-vanishing cross-section for collision with the star material (Press and Spergel 1985; Gould et al. 1990; Goldman and Nussinov 1989; Bertone and Fairbairn 2008; Brito et al. 2015a). The DM material eventually thermalizes with the star, and accumulates inside a finite-size core (Brito et al. 2015a, 2016b; Gould et al. 1990; Goldman and Nussinov 1989).

Interaction of the core with the surrounding star may lead to characteristic EM signatures (Brito et al. 2015a, 2016b). Alternatively, a more generic imprint of such ECOs is GW emission, either via standard inspiralling processes (Maselli et al. 2017a; Horowitz and Reddy 2019) or by small oscillations of such ECOs *inside* neutron stars or white dwarfs (Horowitz and Reddy 2019; Ellis et al. 2018).

4.6 Formation and evolution

In the context of DM physics, the formation and existence of ECOs is very reasonable (Giudice et al. 2016). We know that DM exists, that it interacts gravitationally and that its coupling to Standard Model fields is very weak. Therefore, gravitationally bound structures made of DM particles are dark (by definition) and can potentially be compact. Examples which are well understood include boson stars, made of scalars or vectors, which constitute one notable exception to our ignorance on the formation of ECOs. These configurations can arise out of the gravitational collapse of massive scalars (or vectors). Their interaction and mergers can be studied by evolving the Einstein–Klein–Gordon (–Maxwell) system, and there is evidence that accretion of less massive boson stars makes them grow and cluster around the configuration of maximum mass. In fact, boson stars have efficient *gravitational cooling* mechanisms that allow them to avoid collapse to BHs and remain very compact after interactions (Seidel and Suen 1991, 1994; Brito et al. 2016b; Di Giovanni et al. 2018). Similar studies and similar conclusions hold for axion stars, where the coupling to the Maxwell field is taken into account (Widdicombe et al. 2018). The cosmological formation of such dark compact solitons, their gravitational clustering and strong interactions such as scattering and mergers was recently investigated (Amin and Mocz 2019). If DM is built out of dark fermions, then formation should parallel that of standard neutron stars, and is also a well understood process. Collisions and merger of compact boson stars (Liebling and Palenzuela 2012; Bezares et al. 2017), boson-fermion stars (Bezares and Palenzuela 2018; Bezares et al. 2019), and axion stars (Helfer et al. 2017; Clough et al. 2018) have been studied in detail.

On the other hand, although supported by sound arguments, the vast majority of the alternatives to BHs are, at best, incompletely described. Precise calculations (and often even a rigorous framework) incorporating the necessary physics are missing. Most models listed in Table 1 were built in a phenomenological way or they arise as solutions of Einstein equations coupled to exotic matter fields. For example, models of quantum-corrected objects do not include all the (supposedly large) local or non-local quantum effects that could prevent collapse from occurring. In the absence of a complete knowledge of the missing physics, it is unlikely that a ClePhO forms out of the merger of two ClePhOs. These objects are so compact that at merger they will be probably engulfed by a common apparent horizon. The end product is, most likely a BH as argued in Sect. 4.4.3. On the other hand, if large quantum effects do occur, they would probably act on short timescales to prevent apparent horizon formation possibly in all situations. Thus, for example quantum backreaction has been argued to lead to wormhole solutions rather than BHs (Berthiere et al. 2018). In some models, Planck-scale dynamics naturally leads to abrupt changes close to the would-be horizon, without fine tuning (Holdom and Ren 2017). Likewise, in the presence of (exotic) matter or if GR is classically modified at the horizon scale, Birkhoff's theorem no longer holds, and a star-like object might be a more natural outcome than a BH. However, some studies suggest that compact horizonless bodies may form naturally as the result of gravitational collapse (Beltracchi and Gondolo 2019). The generality of such result is unknown.

An important property of the vacuum field equations is their scale-invariance, inherited by BH solutions. Thus, the scaling properties of BHs are simple: their size scales with their mass, and if a non-spinning BH of mass M_1 is stable, then a BH of mass M_2 is stable as well, the timescales being proportional to the mass. Such characteristic is summarized in Fig. 5. Once matter is added, this unique property is lost. Thus, it is challenging to find theories able to explain, with horizonless objects, all the observations of dark compact objects with masses ranging over more than seven orders of magnitude, although some ECO models can account for that (Raposo et al. 2018). Such "short blanket" problem is only an issue if one tries to explain away *all* the dark compact objects with horizonless alternatives. If particle physics is a guidance, it is well possible that nature offers us a much more diverse universe content.

5 Observational evidence for horizons

It is well known that the Kerr solution provides the unique solution for stationary BHs in the universe. But a confirmation of the metric of the Kerr spacetime (or some aspect of it) cannot even be contemplated in the foreseeable future.
　　　　　　　　　　　S. Chandrasekhar, The Karl Schwarzschild Lecture,
　　　　　　　　　　Astronomische Gesellschaft, Hamburg (September 18, 1986)

Horizons act as perfect sinks for matter and radiation. The existence of a hard or smooth surface will lead in general to clear imprints. Classically, EM waves are the traditional tool to investigate astrophysical objects. There are a handful of interesting constraints on the location of the surface of ECOs using light (Narayan et al. 1997; Narayan and Heyl 2002; McClintock et al. 2004; Broderick and Narayan 2006, 2007; Narayan and McClintock 2008; Broderick et al. 2009; Lu et al. 2017). However, testing the nature of dark, compact objects with EM observations is challenging. Some of these challenges, as we will discuss now, are tied to the incoherent nature of the EM radiation in astrophysics, and the amount of modeling and uncertainties associated to such emission. Other problems are connected to the absorption by the interstellar medium. As discussed in the previous section, testing quantum or microscopic corrections at the horizon scale with EM probes is nearly impossible. Even at the semiclassical level, Hawking radiation is extremely weak to detect and not exclusive of BH spacetimes (Paranjape and Padmanabhan 2009; Barcelo et al. 2011; Harada et al. 2019).

The historical detection of GWs (Abbott et al. (LIGO Scientific Collaboration and the Virgo Collaboration) 2016a) opens up the exciting possibility of testing gravity in extreme regimes with unprecedented accuracy (Abbott et al. (LIGO Scientific Collaboration and the Virgo Collaboration) 2016b; Yunes and Siemens 2013; Barausse et al. 2014; Berti et al. 2015; Giddings 2016; Yunes et al. 2016; Maselli et al. 2018b). GWs are generated by coherent motion of massive sources, and are therefore subjected to less modeling uncertainties (they depend on far fewer parameters) relative to EM probes. The most luminous GWs come from very dense sources, but they also interact very feebly with matter, thus providing the cleanest picture of the cosmos, complementary to that given by telescopes and particle detectors.

Henceforth we will continue using the parameter ϵ defined by Eq. (3) to quantify the constraints that can be put on the presence/absence of a horizon. The current and projected bounds discussed below are summarized in Table 3 at the end of this section.

5.1 Tidal disruption events and EM counterparts

Main-sequence stars can be driven towards ECOs through different mechanisms, including two-body or resonant relaxation or other processes (Alexander 2005; Binney and Tremaine 2011). At sufficiently short orbital distances, stars are either tidally disrupted (if they are within the Roche limit of the central ECO), or swallowed whole. In both cases, strong EM emission is expected for ECOs with a hard surface relative to the case of a BH (Abramowicz et al. 2016; Malafarina and Joshi 2016; Zhang et al. 2016; Benavides-Gallego et al. 2019). If the ECO mass is above $\sim 10^{7.5} \, M_\odot$, such emission should be seen in broad surveys and produce bright optical and UV transients. Such an emission has been ruled out by Pan-STARRS 3π survey (Chambers 2016) at 99.7% confidence level, if the central massive objects have a hard surface at radius larger than $2M(1 + \epsilon)$ with (Lu et al. 2017)

$$\epsilon \approx 10^{-4.4}. \tag{96}$$

The limit above was derived under the assumption of spherical symmetry, isotropic equation of state, and dropping some terms in the relevant equation. It assumes in addition that the infalling matter clusters at the surface (thereby excluding from the analysis those ECO models made of weakly interacting matter (e.g., boson stars) for which ordinary matter does not interact with the surface and accumulates in the interior).

5.2 Equilibrium between ECOs and their environment: Sgr A*

The previous results used a large number of objects and—in addition to the caveats just pointed—assume that all are horizonless. The compact radio source Sgr A* at the center of galaxy is—due to its proximity—a good candidate to improve on the above. Sgr A* has an estimated mass $M \sim 4 \times 10^6 \, M_\odot$, and is currently accreting at an extremely low level, with (accretion disk) luminosity $L_{\text{disk}} \sim 10^{36} \, \text{erg s}^{-1}$ (peaking at wavelength ~ 0.1 mm), about 10^{-9} times the Eddington luminosity for the central mass (Johannsen 2016a; Eckart et al. 2017). The efficiency of the accretion disk at converting gravitational energy to radiation is less than 100%, which suggests a lower bound on the accretion rate $\dot{M} \geq L_{\text{disk}} \sim 10^{15} \, \text{g s}^{-1}$ (10^{-24} in geometric units).

Assume now that the system is in steady state, and that there is a hard surface at $r_0 = 2M(1+\epsilon)$. In such a case, the emission from the surface has a blackbody spectrum with temperature $T^4 = \dot{M}/(4\pi\sigma r_0^2) \sim 3.5 \times 10^3$ K and bright in the infrared (wavelength $\sim 1 \, \mu\text{m}$) (Carballo-Rubio et al. 2018b). However, measured infrared fluxes at 1–10 μm from Sgr A* are one to two orders of magnitude below this prediction. Initial studies used this to place an extreme constraint, $\epsilon \lesssim 10^{-35}$ (Broderick and Narayan 2006, 2007). However, the argument has several flaws (Cardoso and Pani 2017a, b):

i. It assumes that a thermodynamic and dynamic equilibrium must be established between the accretion disk and the central object, on relatively short timescales. However, strong lensing prevents this from happening; consider accretion disk matter, releasing isotropically (for simplicity) scattered radiation on the surface of the object. As discussed in Sect. 2.2, only a fraction $\sim \epsilon$ is able to escape during the first interaction with the star, cf. Eq. (9). The majority of the radiation will fall back onto the surface after a time $t_{\text{roundtrip}} \sim 9.3M$ given by the average of Eq. (11).[6] Suppose one injects, instantaneously, an energy δM onto the object. Then, after a time T_a, the energy emitted to infinity during $N = T_a/t_{\text{roundtrip}}$ interactions reads

$$\Delta E \sim \left[1 - (1 - \epsilon)^N\right] \delta M \approx \epsilon \left(\frac{T_a}{t_{\text{roundtrip}}}\right) \delta M. \qquad (97)$$

where the last step is valid for $\epsilon N \ll 1$.

We can assume $T_a = \tau_{\text{Salpeter}} \approx 4.5 \times 10^7$ yr and $\dot{M} = f_{\text{Edd}} \dot{M}_{\text{Edd}}$, where $\dot{M}_{\text{Edd}} \approx 1.3 \times 10^{39} (M/M_\odot)$ erg/s is the Eddington mass accretion rate onto a BH. Then, from Eq. (97) we get

$$\dot{E} \sim 10^{-25} \left(\frac{\epsilon}{10^{-15}}\right) \left(\frac{f_{\text{Edd}}}{10^{-9}}\right). \qquad (98)$$

where we have normalized the fraction of the Eddington mass accretion rate, f_{Edd}, to its typical value for Sgr A*. Requiring this flux to be compatible with the lack of observed flux from the central spot ($\dot{E} \lesssim 10^{-25}$), one finds $\epsilon \lesssim 10^{-15}$. Assuming $L \sim \dot{E}$ and using the Stefan-Boltzmann law, Eq. (98) yields an estimate for the effective surface temperature of Sgr A* if the latter had a hard surface,

$$T \sim 7.8 \times 10^3 \left(\frac{4 \times 10^6 M_\odot}{M}\right)^{1/2} \left(\frac{\epsilon}{10^{-15}}\right)^{1/4} \left(\frac{\delta M}{10^{-7}M}\right)^{1/4} \text{ K.} \qquad (99)$$

ii. It assumes that the central object is returning in EM radiation most of the energy that it is taking in from the disk. However, even if the object were returning all of the incoming radiation on a sufficiently short timescale, a sizable fraction of this energy could be in channels other than EM. For freely-falling matter on a radial trajectory, its four-velocity $v^\mu_{(1)} = (E/f, -\sqrt{E^2 - f}, 0, 0)$. Particles at the surface of the object have $v^\mu_{(2)} = (\sqrt{f}, 0, 0, 0)$. When these two collide, their CM energy reads (Banados et al. 2009),

$$E_{\text{CM}} = m_0 \sqrt{2} \sqrt{1 - g_{\mu\nu} v^\mu_{(1)} v^\mu_{(2)}} \sim \frac{m_0 \sqrt{2E}}{\epsilon^{1/4}}, \qquad (100)$$

---

[6] One might wonder if the trapped radiation bouncing back and forth the surface of the object might not interact with the accretion disk. As we showed in Sect. 2.2, this does not happen, as the motion of trapped photons is confined to within the photosphere.

Thus, even for only moderately small ϵ, the particles are already relativistic. At these CM energies, all known particles (photons, neutrinos, gravitons, etc) should be emitted "democratically," and in the context of DM physics, new degrees freedom can also be excited. Even without advocating new physics beyond the 10 TeV scale, extrapolation of known hadronic interactions to large energies suggests that about 20% of the collision energy goes into neutrinos, whose total energy is a sizable fraction of that of the photons emitted in the process (Kelner et al. 2006). To account for these effects, we take

$$\epsilon \lesssim 10^{-14}, \tag{101}$$

as a reasonable conservative bound coming from this equilibrium argument.

If only a fraction of the falling material interacts with the object (for example, if it is made of DM with a small interaction cross-section), then the above constraint would deteriorate even further.

iii. The estimate (101) was reached without a proper handling of the interaction between the putative outgoing radiation and the disk itself, and assumes spherical symmetry. Thus, there might be large systematic uncertainties associated (and which occur for any astrophysical process where incoherent motion of the radiating charges play a key role).

5.3 Bounds with shadows: Sgr A* and M87

Recent progress in very long baseline interferometry allows for direct imaging of the region close to the horizon, with the potential to provide also constraints on putative surfaces. These images are also referred to as "shadows" since they map sky luminosity to the source (typically an accretion disk), see Sect. 2.2. Two supermassive BHs have been studied, namely the Sgr A* source and the BH at the center of M87, whose imaging requires the lowest angular resolution (Doeleman et al. 2008; Doeleman 2012; Broderick et al. 2014; Goddi et al. 2016; Abuter et al. (GRAVITY Collaboration) 2018b; Amorim et al. (GRAVITY Collaboration) 2019; Johannsen et al. 2016; Akiyama et al. 2019).

In particular, the Event Horizon Telescope Collaboration has very recently obtained a radio image of the supermassive BH candidate in M87 (Akiyama et al. 2019) and similar results for Sgr A* are expected soon. The Event Horizon Telescope images of Sgr A* and M87* in the millimeter wavelength so far are consistent with a point source of radius $r_0 = (2-4)\,M$ (Doeleman et al. 2008; Doeleman 2012; Johannsen et al. 2016; Akiyama et al. 2019), or

$$\epsilon \sim 1. \tag{102}$$

This corresponds to the size of the photon sphere, which as we described in Sect. 2 will be the dominant relevant strong-field region for these observations. The absence of an horizon will influence the observed shadows, since some photons are now able to directly cross the object, or be reflected by it. There are substantial differences

between the shadows of BHs and some horizonless objects [most notably boson stars (Cunha et al. 2015, 2017b; Cunha and Herdeiro 2018)]. Nevertheless, because of large astrophysical uncertainties and the focusing effect for photons when $\epsilon \to 0$ [Eq. (9)], all studies done so far indicate that it is extremely challenging to use such an effect to place a constraint much stronger than Eq. (102) (Vincent et al. 2016; Cunha et al. 2018; Cardenas-Avendano et al. 2019).

In principle, the accretion flow can be very different in the absence of a horizon, when accreted matter can accumulate in the interior, possibly producing a bright spot within the object's shadow (Olivares et al. 2018). However, in practice this bright source may be too small to be resolved. Assuming matter is accreted at a fraction f_{Edd} of the Eddington rate, the relative angular size of the matter accumulated at the center relative to the size of central object is

$$\frac{\Delta m_{\mathrm{accr}}}{M} \sim f_{\mathrm{Edd}} \frac{T_{\mathrm{age}}}{\tau_{\mathrm{Salpeter}}} \approx 3 \times 10^{-2} \left(\frac{f_{\mathrm{Edd}}}{10^{-4}} \right), \tag{103}$$

where in the last step we conservatively assumed that the central object is accreting at constant rate for $T_{\mathrm{age}} = T_{\mathrm{Hubble}} \approx 300\tau_{\mathrm{Salpeter}}$ and have normalized f_{Edd} to the current value predicted for Sgr A* (Quataert et al. 1999). Similar mass accretion rates are predicted for M87* (Di Matteo et al. 2003). Therefore, a resolution at least ≈ 100 times better than current one is needed to possibly resolve the effect of matter accumulated in the interior of these sources. This is beyond what VLBI on Earth can achieve.

In a similar spirit, tests based on strong-lensing events (Nandi et al. 2018; Shaikh et al. 2019) (in fact, a variant of shadows) or quantum versions of it (Sabín 2017) have been proposed. Adding to the list of possible discriminators, Gracia-Linares and Guzman (2016) studied the impact of supersonic winds blowing through BHs and boson stars. The conclusion is that, while qualitatively the stationary regime of downstream wind distribution is similar, the density may defer by almost an order of magnitude depending on the boson star configuration. At an observational level, these differences would show up presumably as friction on the compact object. However, quantitative tests based on observations are challenging to devise.

Finally, "hotspots" orbiting around supermassive objects can also provide information about near-horizon signatures (Broderick and Loeb 2005, 2006). Recently, the first detection of these orbiting features at the ISCO of Sgr A* was reported (Abuter et al. (GRAVITY Collaboration) 2018a), implying a bound of the same order as Eq. (102).

5.4 Tests with accretion disks

Tests on the spacetime geometry can also be performed by monitoring how *matter* moves and radiates as it approaches the compact object. Matter close to compact objects can form an accretion disk (Lynden-Bell 1969; Novikov and Thorne 1973; Page and Thorne 1974), in which each element approximately moves in circular, Keplerian orbits. The disk is typically "truncated" at the ISCO (cf. Fig. 1), which represents a transition point in the physics of the accretion disk. It is in principle possible to extract

the ISCO location and angular velocity—and hence infer properties of the central object such as the mass, spin, and quadrupole moment—from the EM signal emitted (mostly in the X-ray band) by the accreting matter, either for a stellar-mass BH or for a supermassive BH (Bambi 2017). In practice, the physics of accretion disks is very complex and extracting such properties with a good accuracy is challenging.

A promising approach is the analysis of the *iron $K\alpha$ line* (Fabian et al. 1989), one of the brightest components of the X-ray emission from accreting BH candidates. This line is broadened and skewed due to Doppler and (special and general) relativistic effects, which determine its characteristic shape. An analysis of this shape (assuming that the spacetime is described by the Kerr metric) provides a measurement of the BH spin and the inclination of the accretion disk (Reynolds 2014). Although limited by systematic effects (Bambi 2017), this technique has been used also to test the spacetime metric (Johannsen and Psaltis 2010, 2013; Bambi 2013; Jiang et al. 2015; Johannsen 2014; Moore and Gair 2015; Hoormann et al. 2016) and to distinguish boson stars from BHs (Cao et al. 2016; Shen et al. 2016). Another approach is the study of the thermal component of the spectrum from stellar-mass BHs using the so-called *continuum-fitting method* (Li et al. 2005; McClintock et al. 2014; Reynolds 2014), which can provide information about the ISCO location and hence the BH spin (McClintock et al. 2014). The method can be also used to test the spacetime geometry (Johannsen and Psaltis 2010; Bambi and Barausse 2011; Bambi 2012, 2014; Kong et al. 2014; Johannsen 2014; Moore and Gair 2015; Hoormann et al. 2016) but is limited by the fact that deviations from the Kerr geometry are typically degenerate with the ISCO properties, e.g., with the spin of the object (Bambi 2017; Johannsen 2016b). Finally, an independent approach is the study of the *quasi-periodic oscillations* observed in the X-ray flux emitted by accreting compact objects (Stella and Vietri 1999; Stella et al. 1999; Abramowicz and Kluzniak 2001). The underlying mechanism is not well understood yet, but these frequencies are believed to originate in the innermost region of the accretion flow (van der Klis 2000), and they might carry information about the spacetime near compact objects. Some of the proposed models try to explain such phenomena with combinations of the orbital and epicyclic frequencies of geodesics around the object. Based on these models, constraints on boson stars have been discussed in Franchini et al. (2017).

These approaches are helpful in providing indirect tests for the nature of the accreting central object, but are by construction unable to probe directly the existence of a surface. A possible alternative is the study of the time lag ("*reverberation*") between variability in the light curves in energy bands, corresponding to directly observed continuum emission from the corona around the BH and to X-rays reflected from the accretion disc (Wilkins and Fabian 2013). Such technique was explored assuming the central object to be a BH; the impact of a different central object or of a putative hard surface is unknown.

5.5 Signatures in the mass-spin distribution of dark compact objects

The previous tests were based exclusively on EM measurements. There are tests which can be done either via EM or GW signals. An exciting example concerns

Fig. 13 Exclusion plot in the $\chi - \epsilon$ plane due to the ergoregion instability of ECOs, assumed to be described by the Kerr geometry in their exterior. Shaded areas represent regions where a perfectly-reflecting ECO is unstable against gravitational perturbations with $l = m = 2$, as described by Eqs. (76) and (75)
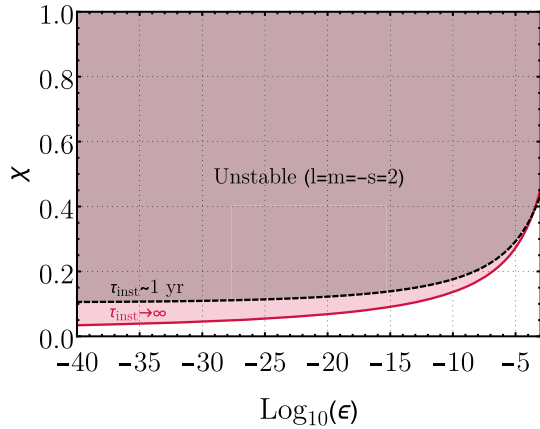
the measurement of the spin of compact objects, which can be performed either via the aforementioned EM tests or from GW detections of binary inspirals and mergers (Abbott et al. (LIGO Scientific Collaboration and the Virgo Collaboration) 2018b). This requires a large population of massive objects to have been detected and their spins estimated to some accuracy. EM or GW observations indicating statistical prevalence of slowly-spinning compact objects, across the entire mass range, indicate either a special formation channel for BHs, or could signal that such objects are in fact horizonless: the development of the ergoregion instability is expected to deplete angular momentum from spinning ClePhOs, independently of their mass, as we discussed in Sect. 4.4.1. Thus, the spin-mass distribution of horizonless compact objects skews towards low spin. Although the effectiveness of such process is not fully understood, it would lead to slowly-spinning objects as a final state, see Fig. 13. On the other hand, observations of highly-spinning BH candidates can be used to constrain ECO models.

Spin measurements in X-ray binaries suggest that some BH candidates are highly spinning (Middleton 2016). However, such measurements are likely affected by unknown systematics; in several cases different techniques yield different results, cf. Table 1 in Middleton (2016). Furthermore, the very existence of the ergoregion instability in ECOs surrounded by gas has never been investigated in detail, and the backreaction of the disk mass and angular momentum on the geometry, as well as the viscosity of the gas, may change the character and timescale of the instability. Finally, as discussed at the end of Sect. 4.4.1, dissipation within the object might also quench the instability completely (Maggio et al. 2017, 2019).

5.6 Multipole moments and tests of the no-hair theorem

5.6.1 Constraints with comparable-mass binaries

An estimate of the bounds on the spin-induced quadrupole moment from GW detection of compact-binary inspirals was performed in Krishnendu et al. (2017, 2019) (see Fig. 14). As we discussed, this correction enters at 2PN order in the GW inspiral
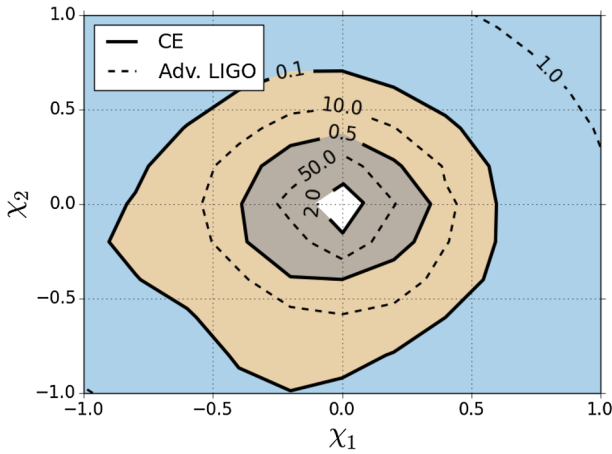
Fig. 14 Errors on the spin induced quadrupole moment ($\kappa_s = (\kappa_1 + \kappa_2)/2$) of a binary system with a total mass of $(10 + 9)M_\odot$ in the dimensionless spin parameters plane ($\chi_1 - \chi_2$), assuming the binary components are BHs, i.e., $\kappa_s = 1$. Here κ_i are the spin induced quadrupole moment parameters of the binary constituents, i.e., $M_2^{(i)} = -\kappa_i \chi_i^2 m_i^3$. The binary is assumed to be optimally oriented at a luminosity distance of 100 Mpc. (Extended from Krishnendu et al. 2017, 2019)

phase and is quadratic in the spin. Therefore, it requires relatively low-mass binaries (which perform many cycles in band before merger) and high spins. The quadrupole moment of the binary was parametrized as $\mathcal{M}_2^{(i)} = -\kappa_i \chi_i^2 m_i^3$ ($i = 1, 2$), where $\kappa_i = 1$ for a Kerr BH.

For moderately large values of the spin ($\chi_i \approx 0.5$) and a binary at 500 Mpc, the projected bounds with Advanced LIGO are roughly $\kappa_s \equiv (\kappa_1 + \kappa_2)/2 \approx 50$. This constraint will become approximately 50 times more stringent with third-generation (3G) GW detectors [such as the Einstein Telescope (Punturo et al. 2010) and Cosmic Explorer (Dwyer et al. 2015)]. Similar constraints could be placed by the space detector LISA (Amaro-Seoane et al. 2017) for spinning supermassive binaries at luminosity distance of 3 Gpc (Krishnendu et al. 2017). Assuming an ECO model, a bound on κ_i can be mapped into a constraint on ϵ. The correction to the spin-induced quadrupole relative to the Kerr value for a generic class of ECO models (whose exterior is perturbatively close to Kerr) is given by the first term in Eq. (16). This yields $\kappa = 1 + a_2/\log \epsilon$, where $a_2 \sim \mathcal{O}(1)$ is a model-dependent parameter. Therefore, based on a constraint on $\Delta\kappa \equiv |\kappa - 1|$, we can derive the upper bound

$$\epsilon \lesssim e^{-\frac{|a_2|}{\Delta\kappa}}, \tag{104}$$

which (assuming $a_2 \sim \mathcal{O}(1)$) gives $\epsilon \lesssim 1$ with Advanced LIGO and a factor 3 more stringent with 3G and LISA. For a gravastar, $a_2 = -8/45$ (Pani 2015) and we obtain approximately $\epsilon \lesssim 1$ with all detectors. These constraints require highly-spinning binaries and the analysis of (Krishnendu et al. 2017, 2019; Kastha et al. 2018) assumes that the quadrupole moment is purely quadratic in the spin. This property is true for Kerr BHs, but not generically; for example, the quadrupole moment of highly-spinning

boson stars contains $O(\chi^4)$ and higher corrections (Ryan 1997), which are relevant for highly-spinning binaries.

In addition to projected bounds, observational bounds on parametrized corrections to the 2PN coefficient of the inspiral waveform from binary BH coalescences can be directly translated—using Eq. (82)—into a bound on (a symmetric combination of) the spin-induced quadrupole moments of the binary components.[7] This parametrized PN analysis has been recently done for various BH merger events, the combined constraint on the deviation of the 2PN coefficient reads $\delta\varphi_2 \lesssim 0.3$ at 90% confidence level (Abbott et al. (LIGO Scientific Collaboration and the Virgo Collaboration) 2019). However, the component spins of these sources are compatible with zero so these constraints cannot be translated into an upper bound on the spin-induced quadrupole moment in Eq. (16). They might be translated into an upper bound on the non-spin induced quadrupole moment, which is however zero in all ECO models proposed so far.

5.6.2 Projected constraints with EMRIs

Extreme-mass ratio inspirals (EMRIs) detectable by the future space mission LISA will probe the spacetime around the central supermassive object with exquisite precision (Gair et al. 2013; Berti et al. 2015; Barack et al. 2018). These binaries perform $\sim m_1/m_2$ orbits before the plunge, the majority of which are very close to the ISCO. The emitted signal can be used to constrain the multipole moments of the central object. In particular, preliminary analysis (using kludge waveforms and a simplified parameter estimation) have placed the projected constrain $\delta\mathcal{M}_2/M^3 < 10^{-4}$ (Babak et al. 2017; Barack and Cutler 2007). In order to translate this into a bound on ϵ, we need to assume a model for ECOs. Assuming the exterior to be described by vacuum GR and that $\delta\mathcal{M}_2$ is spin induced, from Eq. (16) we can derive the following bound on ϵ

$$\epsilon \lesssim \exp\left(-\frac{10^4}{\zeta}\right), \tag{105}$$

where we defined $\zeta \equiv \frac{\delta\mathcal{M}_2/M^3}{10^{-4}}$. Note that this is the best-case scenario, since we assumed saturation of Eq. (16) (with an order-unity coefficient). Other models can exist in which $\delta\mathcal{M}_2 \sim \epsilon^n$, which would lead to much less impressive constraints. On the other hand, Eq. (105) applies to certain models, e.g., gravastars. Notice how stringent the above bound is for those models (Raposo et al. 2019). For this reason, it is

---

[7] Unfortunately, for the majority of binary BH events detected so far (Abbott et al. (LIGO Scientific Collaboration and the Virgo Collaboration) 2018b), either the spin of the binary component is compatible to zero, or the event had a low signal-to-noise ratio (SNR) in the early inspiral, where the PN approximation is valid. The most promising candidate for this test would be GW170729, for which the measured effective binary spin parameter is $\chi_{\mathrm{eff}} \approx 0.36^{+0.21}_{-0.25}$ (Abbott et al. (LIGO Scientific Collaboration and the Virgo Collaboration) 2018b; Chatziioannou et al. 2019). However, for such event no parametrized-inspiral test has been performed so far (Abbott et al. (LIGO Scientific Collaboration and the Virgo Collaboration) 2019). If confirmed, the recent claimed detection (Zackay et al. 2019) of a highly-spinning BH binary would be ideal to perform tests of the spin-induced quadrupole moment.

important to extend current analysis with more accurate waveforms [kludge waveforms are based on a PN expansion of the field equations (Barack and Cutler 2007) but the PN series converges very slowly in the extreme mass ratio limit (Fujita 2012), so results based on these waveforms are only indicative when $m_1/m_2 > 10^3$].

Model dependent studies on the ability of EMRIs to constrain quadrupolar deviations from Kerr have been presented in Ryan (1997), Vigeland and Hughes (2010) and Moore et al. (2017).

5.7 Tidal heating

Horizons absorb incoming high frequency radiation, and serve as sinks or amplifiers for low-frequency radiation able to tunnel in, see Sect. 4.5.2. UCOs and ClePhOs, on the other hand, are not expected to absorb any significant amount of GWs. Thus, a "null-hypothesis" test consists on using the phase of GWs to measure absorption or amplification at the surface of the objects (Maselli et al. 2018b).

Because horizon absorption is related to superradiance and the BH area theorem (Brito et al. 2015b), testing this effect is an indirect proof of the second law of BH thermodynamics. While this effect is too small to be detectable from a single event with second-generation detectors, a large number ($\approx 10^4$) of LIGO-Virgo detections might support Hawking's area theorem at 90% confidence level (Lai and Li 2018).

On the other hand, highly-spinning supermassive binaries detectable with a LISA-type GW interferometer will have a large SNR and will place stringent constraints on this effect, potentially reaching Planck scales near the horizon (Maselli et al. 2018b). This is shown in the left panel of Fig. 15, which presents the bounds on parameter γ defined by adding the tidal-heating term in the PN phase as $\gamma \psi_{\text{TH}}^{\text{BH}}$ [see Eq. (84)]. For a BH $\gamma = 1$, whereas $\gamma = 0$ for a perfectly reflecting ECO. Notice that the
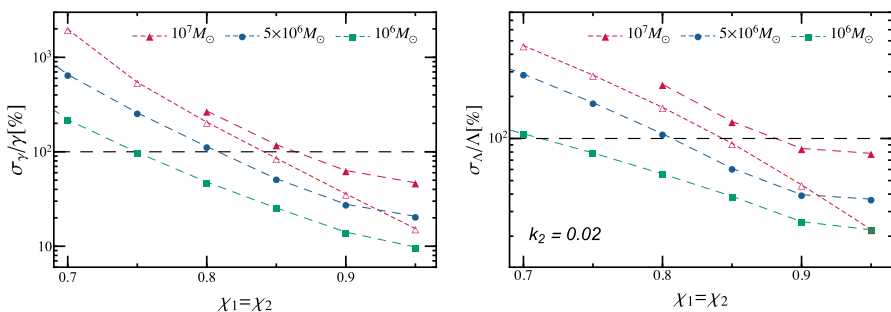
Fig. 15 Percentage relative projected errors on the tidal-heating parameter γ (left panel) and on the average tidal deformability Λ (right panel) as a function of the spin parameter $\chi_1 = \chi_2$, for different values of the central mass $m_1 = (10^6, 5 \times 10^6, 10^7)M_\odot$ assuming a future detection with LISA. In the left and right panel we considered negligible tidal deformability ($\Lambda = 0$) and negligible tidal heating ($\gamma = 0$), respectively. Full (empty) markers refer to mass ratio $m_1/m_2 = 1.1$ ($m_1/m_2 = 2$). Points below the horizontal line correspond to detections that can distinguish between a BH and an ECO at better than 1σ level. We assume binaries at luminosity distance 2 Gpc; σ_a scales with the inverse luminosity distance, and σ_Λ scales with $1/\Lambda$ when $k \ll 1$. Image reproduced with permission from Maselli et al. (2018b), copyright by APS
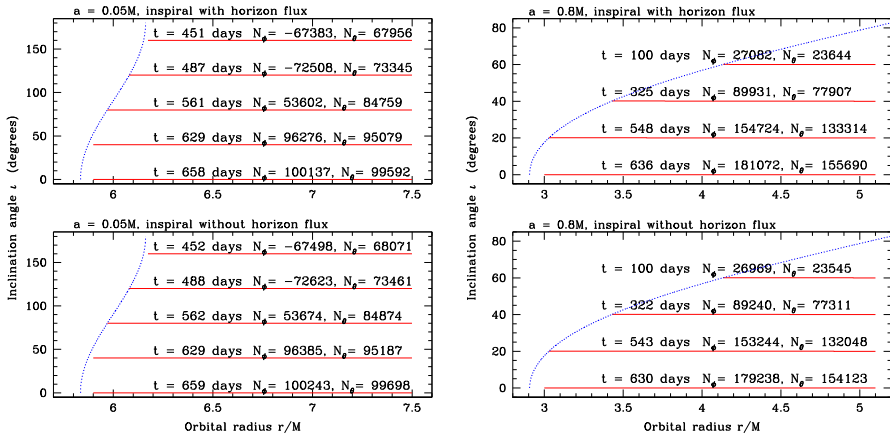
Fig. 16 Inspiral trajectories in the strong field of a Kerr BH with $\chi = 0.05$ (left) and $\chi = 0.8$ (right) in the inclination-orbital radius plane for circular orbits. The top (bottom) panel includes (exclude) the effect of tidal heating, i.e., energy absorption at the horizon. Notice that tidal heating depends strongly on the spin and on the orbit. Adapted from Hughes (2001), courtesy of Scott Hughes

effect is linear in the spin and it would be suppressed by two further PN orders in the nonspinning case.

Absence of tidal heating leaves also a detectable imprint in EMRIs (Hughes 2001; Datta and Bose 2019). In that case the point-particle motion is almost geodesic, with orbital parameters evolving adiabatically because the system loses energy and angular momentum in GWs both at infinity and at the horizon. Energy loss at the horizon is subleading but its putative absence impact the phase of the orbits (and hence the GW signal) in a detectable way, especially if the central object is highly spinning (Hughes 2001). In Fig. 16 we show a comparison between the inspiral trajectories with and without the tidal-heating term.

The effect is clearly important, but the known multiple systematics involved (e.g., due to waveform modeling and to parameter estimation in a signal-driven detector like LISA) still need to be quantified. Finally, the ability of tidal heating in constraining the closeness parameter ϵ (or the blueshift of photons in Table 3 below) for EMRIs is yet to be understood, both because of the above systematics and also because the absence of tidal heating might be directly mapped into a bound on ϵ, since it depends mostly on the object interior rather than on the location of the surface (see, however, discussion at the end of Sect. 4.5.2).

5.8 Tidal deformability

As discussed in Sect. 4.5.3, the TLNs of a BH are identically zero, whereas those of an ECO are not. Although this correction enters at 5PN order in the waveform, the tidal deformability of an object with radius r_0 is proportional to $(r_0/M)^5$, so its effect in the GW phase is magnified for less compact objects. This effect has been recently explored for boson-star binaries, by investigating the distinguishability of

binary boson stars from both binary BHs (Cardoso et al. 2017; Sennett et al. 2017; Wade et al. 2013; Johnson-Mcdaniel et al. 2018) and binary neutron stars (Sennett et al. 2017). Second-generation GW detectors at design sensitivity should be able to distinguish boson-stars models with no self-potential and with a quartic self-potential (cf. Table 2) from BHs, whereas 3G (resp., LISA) is necessary to distinguish the most compact solitonic boson stars from stellar-mass (resp., supermassive) BHs (Cardoso et al. 2017). As a rule of thumb, the stronger the boson self-interaction the more compact are stable boson-star equilibrium configurations, and hence the smaller the tidal deformability and the chances of detectability. Fits for the TLNs of various boson-star models are provided in Sennett et al. (2017); codes to compute these quantities are publicly available (CENTRA 2019).

For ECOs inspired by Planckian corrections at the horizon scale, the TLNs scale as $k \sim 1/|\log \epsilon|$ for a variety of models [see Sect. 4.5.3 and Table I in Cardoso et al. (2017)]. Due to this scaling, in these models the TLNs are only roughly 4 orders of magnitude smaller than for an ordinary neutron star. Nonetheless, measuring such small TLN is probably out of reach even with 3G and would require LISA golden binaries (Maselli et al. 2018b) (see right panel of Fig. 15). Due to the logarithmic scaling, in these models the statistical errors on ϵ would depend exponentially on the TLNs and reaching a Planckian requires a very accurate measurement of k (Addazi et al. 2018). Nonetheless, this does not prevent to perform ECO model selection (see Fig. 12).

Finally, in the extreme mass-ratio limit the GW phase (94) *grows linearly* with the mass ratio $q = m_1/m_2 \gg 1$ and is proportional to the TLN of the central object, $\psi_{\rm TD}(f) \approx -0.004 k_1 q$ (Pani and Maselli 2019). In this case the relative measurements errors on k_1 scale as $1/\sqrt{q}$ at large SNR. Provided one can overcome the systematics on EMRI modeling, this effect might allow to measure TLNs as small as $k_1 \approx 10^{-4}$ for EMRI with $q = 10^6$ detectable by LISA (Pani and Maselli 2019). Assuming models for which $k_1 \sim 1/\log \epsilon$ [see Eq. (95)], we can derive the impressive bound

$$\epsilon \lesssim \exp\left(-\frac{10^4}{\zeta}\right), \tag{106}$$

where now we defined $\zeta \equiv \frac{k_1}{10^{-4}}$. Note that the above bound is roughly as stringent as that in Eq. (105) for $k_1 \approx \delta \mathcal{M}_2/M^3$. In both cases the dependence on the departures from the BH case is exponential, so the final bound is particularly sensitive also to the prefactors in Eqs. (95) and (16). Also in this case, for models in which $k_2 \sim \epsilon^n$ the bound on ϵ would be much less stringent.

5.9 Resonance excitation

The contribution of the multipolar structure, tidal heating, and tidal deformability on the gravitational waveform is perturbative and produces small corrections relative to the idealized point-particle waveform. However, there are nonperturbative effects that can be triggered during inspiral, namely the excitation of the vibration modes of the inspiralling objects. In particular, if the QNMs are of sufficiently low frequency, they can be excited during inspiral (Pani et al. 2010c; Macedo et al. 2013a, b, 2018; Cardoso

et al. 2019b). This case is realized for certain models of ECOs (e.g., ultracompact gravastars and boson stars) and generically for Kerr-like ECOs in the $\epsilon \to 0$, see Eq. (72). In addition to spacetime modes, also model-dependent fluid modes might also be excited (Yunes et al. 2016). Due to redshift effects, these will presumably play a subdominant role in the GW signal.

5.10 QNM tests

One of the simplest and most elegant tools to test the BH nature of central objects, and GR itself, is to use the uniqueness properties of the Kerr family of BHs: vacuum BHs in GR are fully specified by mass and angular momentum, and so are their vibration frequencies (Berti et al. 2006b, 2009). Thus, detection of one mode (i.e., ringing frequency and damping time) allows for an estimate of the mass and angular momentum of the object (assumed to be a GR BH). The detection of two or more modes allows to test GR and/or the BH nature of the object (Dreyer et al. 2004; Berti et al. 2006b, 2016; Berti and Cardoso 2006; Meidam et al. 2014).

Current detectors can only extract one mode for massive BH mergers, and hence one can estimate the mass and spin of the final object, assumed to be a BH (Abbott et al. (LIGO Scientific Collaboration and the Virgo Collaboration) 2016b). Future detectors will be able to detect more than one mode and perform "ECO spectroscopy" (Dreyer et al. 2004; Berti et al. 2006b, 2016; Berti and Cardoso 2006; Meidam et al. 2014).

To exclude ECO models, one needs calculations of their vibration spectra. These are available for a wide class of objects, including boson stars (Berti and Cardoso 2006; Macedo et al. 2013a, b), gravastars (Pani et al. 2009; Mazur and Mottola 2015; Chirenti and Rezzolla 2016), wormholes (Konoplya and Zhidenko 2016; Nandi et al. 2017), or other quantum-corrected objects (Barceló et al. 2017; Brustein et al. 2017b). A major challenge in these tests is how to model spin effects properly, since few spinning ECO models are available and the study of their perturbations is much more involved than for Kerr BHs. In general, the post-merger signal from a distorted ECO might be qualitatively similar to that of a neutron-star merger, with several long-lived modes excited (Kokkotas and Schmidt 1999) and a waveform that is more involved than a simple superposition of damped sinusoids as in the case of BH QNMs.

As discussed previously in Sect. 4.2 and in Sect. 5.12 below, all these extra features are expected to become negligible in the $\epsilon \to 0$ limit: the *prompt ringdown* of an ultracompact ECOs should become indistinguishable from that of a BH in this limit, jeopardizing standard QNM tests.

5.11 Inspiral-merger-ringdown consistency

The full nonlinear structure of GR is encoded in the complete waveform from the inspiral and merger of compact objects. Thus, while isolated tests on separate dynamical stages are important, the ultimate test is that of consistency with the full GR prediction: is the full inspiral-merger-ringdown waveform compatible with that of a binary BH coalescence? Even when the SNR of a given detection is low, such tests can be performed, with some accuracy. Unfortunately, predictions for the coalescence

in theories other than GR and for objects other that BHs are practically unknown. The exceptions concern evolutions of neutron stars, boson stars, composite fluid systems, and axion stars (Liebling and Palenzuela 2012; Cardoso et al. 2016b; Bezares et al. 2017, 2019; Bezares and Palenzuela 2018; Helfer et al. 2017; Widdicombe et al. 2018; Clough et al. 2018) (see Sect. 4.6), and recent progress in BH mergers in modified gravity (Okounkova et al. 2017, 2019; Hirschmann et al. 2018; Witek et al. 2019).

A model-independent constraint comes from the high merger frequency of GW150914 (Abbott et al. (LIGO Scientific Collaboration and the Virgo Collaboration) 2016b), which was measured to be $\nu_{GW} \approx 150$ Hz. The total mass of this system is roughly $m_1 + m_2 \approx 66.2 \, M_\odot$. By assuming that the merger frequency corresponds to the Keplerian frequency at contact, when the binary is at orbital distance $r = 2m(1 + \epsilon)$, we obtain the upper bound

$$\epsilon < 0.74. \tag{107}$$

Agreement between the mass and spin of the final object as predicted from the inspiral stage and from a ringdown analysis can be used as a consistency check of GR (Abbott et al. (LIGO Scientific Collaboration and the Virgo Collaboration) 2016b; Cabero et al. 2018). For compact boson star mergers, it is possible to find configurations for which either the inspiral phase or the ringdown phase match approximately that of a BH coalescence, but not both (Bezares et al. 2017). This suggests that inspiral-merger-ringdown consistency tests can be very useful to distinguish such binaries. Thus, although the measurement errors on the mass and spin of the final remnant are currently large, the consistency of the ringdown waveform with the full inspiral-merger-ringdown template suggests that the remnant should at least be a ClePhO, i.e., places the bound $\epsilon \lesssim \mathcal{O}(0.01)$, the exact number requires a detailed, model-dependent analysis.

5.12 Tests with GW echoes

For binaries composed of ClePhOs, the GW signal generated during inspiral and merger is expected to be very similar to that by a BH binary with the same mass and spin. Indeed, the multipole moments of very compact objects approach those of Kerr when $\epsilon \rightarrow 0$, and so do the TLNs, etc. Constraining ϵ (or quantifying up to which point the vacuum Kerr is a description of the spacetime) is then a question of having sensitive detectors that can probe minute changes in waveforms. This would also require having sufficiently accurate waveform models to avoid systematics. However, there is a clear distinctive feature of horizonless objects: the appearance of late-time echoes in the waveforms (see Sect. 4.2). There has been some progress in modeling the echo waveform and data analysis strategies are in place to look for such late-time features; some strategies have been also implemented using real data (Abedi et al. 2017a, b; Conklin et al. 2018; Westerweck et al. 2018; Tsang et al. 2018; Nielsen et al. 2018; Lo et al. 2018; Wang et al. 2019a; Uchikata et al. 2019).

The ability to detect such signals depends on how much energy is converted from the main burst into echoes (i.e., on the relative amplitude between the first echo and

the prompt ringdown signal in Fig. 9). Depending on the reflectivity of the ECO, the energy contained in the echoes can exceed that of the standard ringdown alone (Mark et al. 2017; Testa and Pani 2018), see left panel of Fig. 17. This suggests that it is possible to detect or constrain echoes even when the ringdown is marginally detectable or below threshold, as in the case of EMRIs or for comparable-mass coalescences at small SNR.

Searches for echo signals in the detectors based on reliable templates can be used to find new physics, or to set very stringent constraints on several models using real data. Different groups with independent search techniques *have found* structure in many of the GW events, compatible with postmerger echoes (Abedi et al. 2017a, b; Ashton et al. 2016; Conklin et al. 2018; Westerweck et al. 2018). However, the statistical significance of such events has been put into question (Westerweck et al. 2018; Abedi et al. 2018). For GW150914, Abedi et al. (2017a), Ashton et al. (2016) and Conklin et al. (2018)—using independent search techniques—report evidence for the existence of postmerger echoes in the data. However, Nielsen et al. (2018) finds a lower significance and a Bayes factor indicating preference for noise over the echo hypothesis. For other GW events, there is agreement between different groups on the existence of postmerger features in the signal, found using echo waveforms. The interpretation of these features is under debate. An independent search in the LIGO-Virgo Catalog GWTC-1 found no statistical evidence for the presence of echoes within 0.1 s of the main burst (Uchikata et al. 2019).

Any realistic search is controlled by η [cf. Eq. (59)] *and* the time delay between main burst and echoes (Abedi et al. 2017a, b; Conklin et al. 2018; Westerweck et al. 2018; Tsang et al. 2018; Nielsen et al. 2018; Lo et al. 2018). Since the SNR of the postmerger signal is controlled by η on a integration timescale controlled by τ, even negative searches can be used to place strong constraints on ϵ (Westerweck et al. 2018; Nielsen et al. 2018).

Constraints on ϵ are currently limited by the low SNR. These constraints will greatly improve with next-generation GW detectors. A preliminary analysis in this direction (Testa and Pani 2018) [based on the template (61) valid only for nonspinning objects] suggests that perfectly-reflecting ECO models can be detected or ruled out at 5σ confidence level with SNR in the ringdown of $\rho_{\mathrm{ringdown}} \approx 10$. Excluding/detecting echoes for models with smaller values of the reflectivity will require SNRs in the postmerger phase of $\mathcal{O}(100)$. This will be achievable only with ground-based 3G detectors and the planned space mission LISA (Amaro-Seoane et al. 2017), see right panel of Fig. 17. Simple-minded ringdown searches [using as template an exponentially damped sinusoid (Abbott et al. (LIGO Scientific Collaboration) 2009)] can be used to look for echoes, separately from the main burst. For example, if the first echo carries 20% of the energy of the main ringdown stage, then it is detectable with a simple ringdown template. LISA will see at least one ringdown event per year, even for the most pessimistic population synthesis models used to estimate the rates (Berti et al. 2016). The proposed Einstein Telescope (Punturo et al. 2010) or Voyager-like (LIGO Scientific Collaboration 2015) 3G Earth-based detectors will also be able to distinguish ClePhOs from BHs with such simple-minded searches.

Overall, in a large region of the parameter space the signal is large enough to produce effects within reach of near-future GW detectors, even if the corrections occur at the
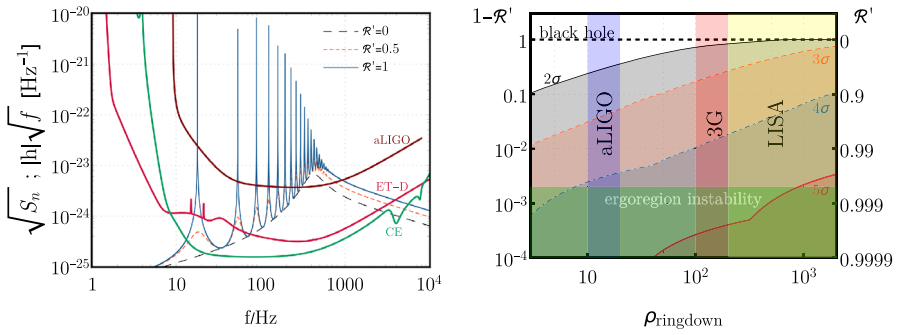
Fig. 17 Left: Representative example of ringdown + echo template [Eq. (61)] compared to the power spectral densities of various ground-based interferometers (Shoemaker 2010; Abbott et al. (LIGO Scientific Collaboration) 2017; Essick et al. 2017; Hild et al. 2011) as functions of the GW frequency f. We considered an object with $M = 30 M_\odot$, at a distance of 400 Mpc, with closeness parameter $\epsilon = 10^{-11}$, and various values of the reflectivity coefficient $\mathcal{R}'$ at the surface [see Eq. (62)]. The case $\mathcal{R}' = 0$ corresponds to the pure BH ringdown template. Right: Projected exclusion plot for the ECO reflectivity $\mathcal{R}'$ as a function of the SNR in the ringdown phase and at different σ confidence levels, assuming the ringdown template (61) based on the transfer-function representation and assuming a source near the ECO surface. Shaded areas represent regions that can be excluded at a given confidence level. Vertical bands are typical SNR achievable by aLIGO/Virgo, 3G, and LISA in the ringdown phase, whereas the horizontal band is the region excluded by the ergoregion instability, see Sect. 4.4.1. Adapted from Testa and Pani (2018)

"Planck scale" (by which we mean $\epsilon \sim 10^{-40}$). This is a truly remarkable prospect. As the sensitivity of GW detectors increases, the absence of echoes might be used to rule out ECO models, to set ever stringent upper bounds on the level of absorption in the object's interior, and generically to push tests of gravity closer and closer to the horizon scale, as now routinely done for other cornerstones of GR, e.g., in tests of the equivalence principle (Will 2014; Berti et al. 2015).

5.13 Stochastic background

Above in Sect. 5.5, we discussed possible features in the spin distribution of massive compact objects. If a large number of massive and dark objects are indeed horizonless and very compact, they will be subjected to the ergoregion instability (discussed in Sect. 4.4.1) which drains their rotational energy and transfers it to GWs. Thus, the entire universe would be radiating GWs, producing a (potentially) significant amount of stochastic GWs (Barausse et al. 2018; Fan and Chen 2018; Du and Chen 2018). Note that such background does *not* require binaries, isolated ECOs suffice [isolated compact objects are expected to be ~ 100 times more numerous than merging binaries (Dvorkin et al. 2016)].

The background can be characterized by its (dimensionless) energy spectrum

$$\Omega_{\rm GW} = \frac{1}{\rho_c} \frac{d\rho_{\rm gw}}{d \ln f_o}, \tag{108}$$
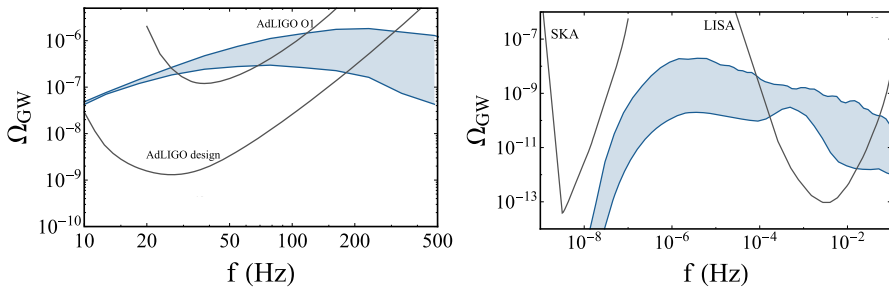
Fig. 18 Extragalactic stochastic background of GWs in the LIGO/Virgo (left panel), LISA and PTA bands (right panel) assuming all BH candidates to be horizonless, described by a Kerr exterior and Dirichlet conditions at the surface $r = r_+(1 + \epsilon)$, with $\epsilon = 10^{-40}$. The bands brackets different population models. The black lines are the power-law integrated curves computed using noise power spectral densities for: LISA with one year of observation time (Amaro-Seoane et al. 2017), LIGO's first observing runs (O1), LIGO at design sensitivity, and an SKA-based pulsar timing array. Image reproduced by permission from Barausse et al. (2018), copyright bythe authors

$\rho_{\rm gw}$ being the background's energy density, f_o the frequency measured at the detector and ρ_c the critical density of the Universe at the present time. Results for a simple ECO, modelled with Kerr exterior and Dirichlet conditions at its surface are shown in Fig. 18. The derived constraints assume all BH candidates are horizonless, the bound scales linearly with the fraction of ECOs in the population.

5.14 Motion within ECOs

In certain models, the ECO interior might be weakly interacting and a further discriminator would be the motion of test particles *within* the object. Among other effect, this can produce non-standard signals in EMRIs. As discussed in Sects. 4.5.4 and 4.5.5, this motion is driven by the self-gravity of the central object, accretion, and dynamical friction. The study of geodesic motion inside a solitonic boson stars was analyzed in Kesden et al. (2005). The effects of accretion and drag were included in Macedo et al. (2013b, a), Barausse et al. (2014, 2015). These effects cannot be directly translated into bounds on ϵ, but would be a smoking-gun signature for the existence of structures in supermassive ultracompact objects.

6 Discussion and observational bounds

The purpose of physics is to describe natural phenomena in the most accurate possible way. The most outrageous prediction of GR—that BHs should exist and be always described by the Kerr geometry—remains poorly quantified. It is a foundational issue, touching on questions such as singularity formation, quantum effects in gravity, the behavior of matter at extreme densities, and even DM physics. The quest to quantify the evidence for BHs can—in more than one way—be compared with the quest to quantify the equivalence principle, and needs to be complemented with tests of the Kerr nature of ultracompact dark objects. Table 3 summarizes the observational evidence for BHs.

Table 3 How well does the BH geometry describe the dark compact objects in our universe?

	Constraints		Source	References
	$\epsilon(\lesssim)$	$\frac{\nu}{\nu_\infty}(\gtrsim)$		
1a.	$\mathcal{O}(1)$	$\mathcal{O}(1)$	Sgr A* & M87	Doeleman et al. (2008), Doeleman (2012), Johannsen et al. (2016), Abuter et al. (GRAVITY Collaboration) (2018a), Akiyama et al. (2019)
1b.	0.74	1.5	GW150914	Abbott et al. (LIGO Scientific Collaboration and the Virgo Collaboration) (2016a)
2.	$\mathcal{O}(0.01)$	$\mathcal{O}(10)$	GW150914	Abbott et al. (LIGO Scientific Collaboration and the Virgo Collaboration) (2016a)
3.	$10^{-4.4}$	158	All with $M > 10^{7.5} M_\odot$	Lu et al. (2017)
4.	10^{-14}	10^7	Sgr A*	Lu et al. (2017)
5.	10^{-40}	10^{20}	All with $M < 100 M_\odot$	Barausse et al. (2018)
6.	10^{-47}	10^{23}	GW150914	Nielsen et al. (2018), Uchikata et al. (2019)
7*.	$e^{-10^4/\zeta}$	$e^{5000/\zeta}$	EMRIs	Babak et al. (2017), Barack and Cutler (2007), Pani and Maselli (2019)

	Effect and caveats
1a.	Uses detected orbiting hotspot around Sgr A* and "shadow" of Sgr A* and M87
	Spin effects are poorly understood; systematic uncertainties not quantified
1b.	Merger frequency of GW150914 and measurements of the masses
	Assumes merger frequency equal to Keplerian frequency at contact
2.	Consistency of ringdown with BH signal
	Large measurement errors on the QNM frequencies. Precise bounds are model dependent
	Bounds will improve significantly with detailed searches for post-merger echoes
3.	Lack of optical/UV transients from tidal disruption events
	Assumes: all objects are horizonless, have a hard surface, spherical symmetry, and isotropy

Table 3 continued

	Effect and caveats
4.	Uses absence of relative low luminosity from Sgr A*, compared to disk
	Spin effects and matter-radiation interaction matter poorly understood; assumes spherical symmetry
5.	Uses absence of GW stochastic background (from ergoregion instability)
	Assumes: hard surface (perfect reflection); exterior Kerr; all objects are horizonless
6.	Uses absence of GW echoes from post-merger object
	90% confidence level for $\eta > 0.9$, deteriorates for smaller η. Simplified echo template, limited range of priors
7*.	Projected EMRI constraints on the spin-induced quadrupole ($\zeta = (\delta\mathcal{M}_2/M^3)/10^{-4}$) and TLNs ($\zeta = k/10^{-4}$)
	Assumes saturation of Eq. (16) (for $\delta\mathcal{M}_2$) and Eq. (95) (for k) and order-unity coefficients in those equations
	Uses PN kludge waveforms, phenomenological deviation for $\mathcal{M}_2$, and simplified parameter estimation
	Models for which $\delta\mathcal{M}_2 \sim \epsilon^n$ or $k \sim \epsilon^n$ are much less constrained

This table quantifies the answer to this question, for selected objects, by *excluding* the presence of surfaces in the spacetime close to the gravitational radius of the object. The deviation from the vacuum Kerr geometry, of mass M and angular momentum $J = \chi M^2$, is measured with a dimensionless quantity ϵ, such that the structure is localized at a Boyer-Lindquist radius $r_+(1 + \epsilon)$, where $r_+ = M(1 + \sqrt{1 - \chi^2})$. For $\epsilon = 0$ the spacetime is described by vacuum GR all the way to the horizon. We also express the constraint as measured by the blueshift of a radial-directed photon ν/ν_∞ (on the equatorial plane, measured by locally non-rotating observers) as it travels from large distances to the last point down to which observations are compatible with vacuum. The constraints come from a variety of observations and tests provided in the references in the last column and interpreted as discussed in Sect. 5. Alternative quantities that can parametrize the deviation from the vacuum Kerr geometry are the light travel time from the light ring to the surface [Eq. (74)] or the proper distance between the light ring and the surface. Both quantities depend on ϵ and on the spin χ of the object, and scale as $\log \epsilon$ as $\epsilon \to 0$. Entries with an asterix refer to projected constraints

These bounds can be read in two different ways. On the one hand, they tell us how appropriate the Kerr metric is in describing some of the massive and dark objects in our universe. In other words, observations tell us that the Kerr description is compatible with observations at least down to $r = r_+(1 + \epsilon)$. Alternatively, one can view these numbers as constraints on exotic alternatives to BHs. In both cases, the constraint on ϵ can be translated into the ratio of frequencies [or redshift, as measured by locally non-rotating observers (Bardeen et al. 1972)] of a photon as it travels from infinity down to the farthest point down to which observations are compatible with vacuum.

Most of the constraints shown in Table 3 are associated with large systematics or modelling uncertainties. From a proper understanding of astrophysical environments and their interaction with ultracompact objects, the development of a solid theoretical framework, to a proper modeling of the coalescence of such objects and data analysis to see such events, the challenges are immense. The pay-off for facing these oustanding issues is to be able to quantify the statement that BHs exist in nature.

References

Abbott BP et al (LIGO Scientific Collaboration) (2009) Search for gravitational wave ringdowns from perturbed black holes in LIGO S4 data. Phys Rev D 80:062001. https://doi.org/10.1103/PhysRevD.80.062001. arXiv:0905.1654

Abbott BP et al (LIGO Scientific Collaboration and the Virgo Collaboration) (2016a) Observation of gravitational waves from a binary black hole merger. Phys Rev Lett 116:061102. https://doi.org/10.1103/PhysRevLett.116.061102. arXiv:1602.03837

Abbott BP et al (LIGO Scientific Collaboration and the Virgo Collaboration) (2016b) Tests of general relativity with GW150914. Phys Rev Lett 116:221101. https://doi.org/10.1103/PhysRevLett.116.221101. https://doi.org/10.1103/PhysRevLett.121.129902 [Erratum: Phys Rev Lett 121(12):129902 (2018)]. arXiv:1602.03841

Abbott BP et al (LIGO Scientific Collaboration) (2017) Exploring the sensitivity of next generation gravitational wave detectors. Class Quantum Grav 34:044001. https://doi.org/10.1088/1361-6382/aa51f4. arXiv:1607.08697

Abbott BP et al (LIGO Scientific Collaboration and the Virgo Collaboration) (2018a) GW170817: measurements of neutron star radii and equation of state. Phys Rev Lett 121:161101. https://doi.org/10.1103/PhysRevLett.121.161101. arXiv:1805.11581

Abbott BP et al (LIGO Scientific Collaboration and the Virgo Collaboration) (2018b) GWTC-1: a gravitational-wave transient catalog of compact binary mergers observed by LIGO and virgo during the first and second observing runs. ArXiv e-prints arXiv:1811.12907

Abbott BP et al (LIGO Scientific Collaboration and the Virgo Collaboration) (2019) Tests of general relativity with the binary black hole signals from the LIGO-virgo catalog GWTC-1. ArXiv e-prints arXiv:1903.04467

Abdelsalhin T, Gualtieri L, Pani P (2018) Post-Newtonian spin-tidal couplings for compact binaries. Phys Rev D 98:104046. https://doi.org/10.1103/PhysRevD.98.104046. arXiv:1805.01487

Abdujabbarov A, Juraev B, Ahmedov B, Stuchlík Z (2016) Shadow of rotating wormhole in plasma environment. Astrophys Space Sci 361:226. https://doi.org/10.1007/s10509-016-2818-9

Abedi J, Dykaar H, Afshordi N (2017a) Echoes from the Abyss: tentative evidence for Planck-scale structure at black hole horizons. Phys Rev D 96:082004. https://doi.org/10.1103/PhysRevD.96.082004. arXiv:1612.00266

Abedi J, Dykaar H, Afshordi N (2017b) Echoes from the Abyss: the holiday edition! ArXiv e-prints arXiv:1701.03485

Abedi J, Dykaar H, Afshordi N (2018) Comment on: "Low significance of evidence for black hole echoes in gravitational wave data". ArXiv e-prints arXiv:1803.08565

Abramowicz MA, Kluzniak W (2001) A precise determination of angular momentum in the black hole candidate GRO J1655-40. Astron Astrophys 374:L19. https://doi.org/10.1051/0004-6361:20010791. arXiv:astro-ph/0105077

Abramowicz MA, Kluzniak W, Lasota JP (2002) No observational proof of the black hole event-horizon. Astron Astrophys 396:L31–L34. https://doi.org/10.1051/0004-6361:20021645. arXiv:astro-ph/0207270

Abramowicz MA, Bulik T, Ellis GFR, Meissner KA, Wielgus M (2016) The electromagnetic afterglows of gravitational waves as a test for quantum gravity. ArXiv e-prints arXiv:1603.07830

Abuter R et al (GRAVITY Collaboration) (2018a) Detection of orbital motions near the last stable circular orbit of the massive black hole Sgr A*. Astron Astrophys 618:L10. https://doi.org/10.1051/0004-6361/201834294. arXiv:1810.12641

Abuter R et al (GRAVITY Collaboration) (2018b) Detection of the gravitational redshift in the orbit of the star S2 near the Galactic centre massive black hole. Astron Astrophys 615:L15. https://doi.org/10.1051/0004-6361/201833718. arXiv:1807.09409

Addazi A, Marciano A, Yunes N (2018) Can we probe Planckian corrections at the horizon scale with gravitational waves? ArXiv e-prints arXiv:1810.10417

Addazi A, Marciano A, Yunes N (2019) Gravitational instability of exotic compact objects. ArXiv e-prints arXiv:1905.08734

Afonso VI, Olmo GJ, Rubiera-Garcia D (2017) Scalar geons in Born Infeld gravity. J Cosmol Astropart Phys 1708(08):031. https://doi.org/10.1088/1475-7516/2017/08/031. arXiv:1705.01065

Afonso VI, Olmo GJ, Rubiera-Garcia D (2018) Mapping Ricci-based theories of gravity into general relativity. Phys Rev D 97:021503. https://doi.org/10.1103/PhysRevD.97.021503. arXiv:1801.10406

Akiyama K et al (2019) First M87 event horizon telescope results. I. The shadow of the supermassive black hole. Astrophys J 875:L1. https://doi.org/10.3847/2041-8213/ab0ec7

Alexander T (2005) Stellar processes near the massive black hole in the Galactic center. Phys Rep 419:65–142. https://doi.org/10.1016/j.physrep.2005.08.002. arXiv:astro-ph/0508106

Allahyari A, Firouzjahi H, Mashhoon B (2019) Quasinormal modes of a black hole with quadrupole moment. Phys Rev D 99:044005. https://doi.org/10.1103/PhysRevD.99.044005. arXiv:1812.03376

Almheiri A, Marolf D, Polchinski J, Sully J (2013) Black holes: complementarity or firewalls? J High Energy Phys 1302:062. https://doi.org/10.1007/JHEP02(2013)062. arXiv:1207.3123

Alvi K (2001) Energy and angular momentum flow into a black hole in a binary. Phys Rev D 64:104020. https://doi.org/10.1103/PhysRevD.64.104020. arXiv:gr-qc/0107080

Amaro-Seoane P et al (2017) Laser interferometer space antenna. ArXiv e-prints arXiv:1702.00786

Amin MA, Mocz P (2019) Formation, gravitational clustering and interactions of non-relativistic solitons in an expanding universe. ArXiv e-prints arXiv:1902.07261

Amorim A et al (GRAVITY Collaboration) (2019) Test of Einstein equivalence principle near the Galactic center supermassive black hole. Phys Rev Lett 122:101102. https://doi.org/10.1103/PhysRevLett.122.101102. arXiv:1902.04193

Andersson N, Kojima Y, Kokkotas KD (1996) On the oscillation spectra of ultracompact stars: an extensive survey of gravitational wave modes. Astrophys J 462:855. https://doi.org/10.1086/177199. arXiv:gr-qc/9512048

Andrade Z (2001) Trapped and excited w modes of stars with a phase transition and R greater than or equal to $R \geq 5M$. Phys Rev D 63:124002. https://doi.org/10.1103/PhysRevD.63.124002. arXiv:gr-qc/0103062

Andrade Z, Price RH (1999) Excitation of the odd parity quasinormal modes of compact objects. Phys Rev D 60:104037. https://doi.org/10.1103/PhysRevD.60.104037. arXiv:gr-qc/9902062

Andreasson H (2008) Sharp bounds on $2m/r$ of general spherically symmetric static objects. J Differ Equations 245:2243–2266. https://doi.org/10.1016/j.jde.2008.05.010. arXiv:gr-qc/0702137

Antoniadis J et al (2013) A massive pulsar in a compact relativistic binary. Science 340:6131. https://doi.org/10.1126/science.1233232. arXiv:1304.6875

Arkani-Hamed N, Dimopoulos S, Dvali GR (1998) The hierarchy problem and new dimensions at a millimeter. Phys Lett B 429:263–272. https://doi.org/10.1016/S0370-2693(98)00466-3. arXiv:hep-ph/9803315

Arzano M, Calcagni G (2016) What gravity waves are telling about quantum spacetime. Phys Rev D 93:124065. https://doi.org/10.1103/PhysRevD.93.124065, https://doi.org/10.1103/PhysRevD.94.049907 [Addendum: Phys Rev D 94(4):049907 (2016)]. arXiv:1604.00541

Ashton G, Birnholtz O, Cabero M, Capano C, Dent T, Krishnan B, Meadors GD, Nielsen AB, Nitz A, Westerweck J (2016) Comments on: "Echoes from the abyss: evidence for Planck-scale structure at black hole horizons". ArXiv e-prints arXiv:1612.05625

Babak S, Gair J, Sesana A, Barausse E, Sopuerta CF, Berry CPL, Berti E, Amaro-Seoane P, Petiteau A, Klein A (2017) Science with the space-based interferometer LISA. V: extreme mass-ratio inspirals. Phys Rev D 95:103012. https://doi.org/10.1103/PhysRevD.95.103012. arXiv:1703.09722

Baccetti V, Mann RB, Terno DR (2017) Do event horizons exist? Int J Mod Phys D 26:1743008. https://doi.org/10.1142/S0218271817430088, https://doi.org/10.1142/S0218271817170088. arXiv:1706.01180

Baccetti V, Mann RB, Terno DR (2018a) Role of evaporation in gravitational collapse. Class Quantum Grav 35:185005. https://doi.org/10.1088/1361-6382/aad70e. arXiv:1610.07839

Baccetti V, Murk S, Terno DR (2018b) Thin shell collapse in semiclassical gravity. ArXiv e-prints arXiv:1812.07727

Balasubramanian V, de Boer J, El-Showk S, Messamah I (2008) Black holes as effective geometries. Class Quantum Grav 25:214004. https://doi.org/10.1088/0264-9381/25/21/214004. arXiv:0811.0263

Bambi C (2012) A code to compute the emission of thin accretion disks in non-Kerr space–times and test the nature of black hole candidates. Astrophys J 761:174. https://doi.org/10.1088/0004-637X/761/2/174. arXiv:1210.5679

Bambi C (2013) Testing the space–time geometry around black hole candidates with the analysis of the broad Kα iron line. Phys Rev D 87:023007. https://doi.org/10.1103/PhysRevD.87.023007. arXiv:1211.2513

Bambi C (2014) Note on the Cardoso–Pani–Rico parametrization to test the Kerr black hole hypothesis. Phys Rev D 90:047503. https://doi.org/10.1103/PhysRevD.90.047503. arXiv:1408.0690

Bambi C (2017) Testing black hole candidates with electromagnetic radiation. Rev Mod Phys 89:025001. https://doi.org/10.1103/RevModPhys.89.025001. arXiv:1509.03884

Bambi C, Barausse E (2011) Constraining the quadrupole moment of stellar-mass black-hole candidates with the continuum fitting method. Astrophys J 731:121. https://doi.org/10.1088/0004-637X/731/2/121. arXiv:1012.2007

Bambi C, Malafarina D, Modesto L (2013) Non-singular quantum-inspired gravitational collapse. Phys Rev D 88:044009. https://doi.org/10.1103/PhysRevD.88.044009. arXiv:1305.4790

Banados M, Silk J, West SM (2009) Kerr black holes as particle accelerators to arbitrarily high energy. Phys Rev Lett 103:111102. https://doi.org/10.1103/PhysRevLett.103.111102. arXiv:0909.0169

Barack L, Cutler C (2007) Using LISA EMRI sources to test off-Kerr deviations in the geometry of massive black holes. Phys Rev D 75:042003. https://doi.org/10.1103/PhysRevD.75.042003. arXiv:gr-qc/0612029

Barack L et al (2018) Black holes, gravitational waves and fundamental physics: a roadmap. ArXiv e-prints arXiv:1806.05195

Barausse E, Cardoso V, Pani P (2014) Can environmental effects spoil precision gravitational-wave astrophysics? Phys Rev D 89:104059. https://doi.org/10.1103/PhysRevD.89.104059. arXiv:1404.7149

Barausse E, Cardoso V, Pani P (2015) Environmental effects for gravitational-wave astrophysics. J Phys Conf Ser 610:012044. https://doi.org/10.1088/1742-6596/610/1/012044. arXiv:1404.7140

Barausse E, Brito R, Cardoso V, Dvorkin I, Pani P (2018) The stochastic gravitational-wave background in the absence of horizons. Class Quantum Grav 35:20LT01. https://doi.org/10.1088/1361-6382/aae1de. arXiv:1805.08229

Barcelo C, Liberati S, Sonego S, Visser M (2008) Fate of gravitational collapse in semiclassical gravity. Phys Rev D 77:044032. https://doi.org/10.1103/PhysRevD.77.044032. arXiv:0712.1130

Barceló C, Liberati S, Sonego S, Visser M (2009) Black stars, not holes. Sci Am 301:38–45. https://doi.org/10.1038/scientificamerican1009-38

Barcelo C, Liberati S, Sonego S, Visser M (2011) Hawking-like radiation from evolving black holes and compact horizonless objects. J High Energy Phys 02:003. https://doi.org/10.1007/JHEP02(2011)003. arXiv:1011.5911

Barceló C, Carballo-Rubio R, Garay LJ (2016) Where does the physics of extreme gravitational collapse reside? Universe 2:7. https://doi.org/10.3390/universe2020007. arXiv:1510.04957

Barceló C, Carballo-Rubio R, Garay LJ (2017) Gravitational wave echoes from macroscopic quantum gravity effects. J High Energy Phys 05:054. https://doi.org/10.1007/JHEP05(2017)054. arXiv:1701.09156

Barceló C, Carballo-Rubio R, Liberati S (2019) Generalized no-hair theorems without horizons. ArXiv e-prints arXiv:1901.06388

Bardeen JM (1981) Black holes do evaporate thermally. Phys Rev Lett 46:382–385. https://doi.org/10.1103/PhysRevLett.46.382

Bardeen JM, Press WH, Teukolsky SA (1972) Rotating black holes: locally nonrotating frames, energy extraction, and scalar synchrotron radiation. Astrophys J 178:347. https://doi.org/10.1086/151796

Bayin SS (1982) Anisotropic fluid spheres in general relativity. Phys Rev D 26:1262. https://doi.org/10.1103/PhysRevD.26.1262

Bekenstein JD, Mukhanov VF (1995) Spectroscopy of the quantum black hole. Phys Lett B 360:7–12. https://doi.org/10.1016/0370-2693(95)01148-J. arXiv:gr-qc/9505012

Beltracchi P, Gondolo P (2019) Formation of dark energy stars. Phys Rev D 99:044037. https://doi.org/10.1103/PhysRevD.99.044037. arXiv:1810.12400

Beltran Jimenez J, Heisenberg L, Olmo GJ, Rubiera-Garcia D (2018) Born Infeld inspired modifications of gravity. Phys Rep 727:1–129. https://doi.org/10.1016/j.physrep.2017.11.001. arXiv:1704.03351

Bena I, Warner NP (2008) Black holes, black rings and their microstates. In: Supersymmetric mechanics: vol. 3. Lecture notes in physics, vol 755. Springer, Berlin, pp 1–92. https://doi.org/10.1007/978-3-540-79523-0_1. arXiv:hep-th/0701216

Bena I, Warner NP (2013) Resolving the structure of black holes: philosophizing with a hammer. ArXiv e-prints arXiv:1311.4538

Benavides-Gallego CA, Abdujabbarov A, Malafarina D, Ahmedov B, Bambi C (2019) Charged particle motion and electromagnetic field in γ spacetime. Phys Rev D 99:044012. https://doi.org/10.1103/PhysRevD.99.044012. arXiv:1812.04846

Bender CM, Orszag SA (1999) Advanced mathematical methods for scientists and engineers. Springer, New York

Bergé J, Brax P, Métris G, Pernot-Borràs M, Touboul P, Uzan JP (2018) MICROSCOPE mission: first constraints on the violation of the weak equivalence principle by a light scalar dilaton. Phys Rev Lett 120:141101. https://doi.org/10.1103/PhysRevLett.120.141101. arXiv:1712.00483

Berthiere C, Sarkar D, Solodukhin SN (2018) The fate of black hole horizons in semiclassical gravity. Phys Lett B 786:21–27. https://doi.org/10.1016/j.physletb.2018.09.027. arXiv:1712.09914

Berti E, Cardoso V (2006) Supermassive black holes or boson stars? Hair counting with gravitational wave detectors. Int J Mod Phys D 15:2209–2216. https://doi.org/10.1142/S0218271806009637. arXiv:gr-qc/0605101

Berti E, Cardoso V, Casals M (2006a) Eigenvalues and eigenfunctions of spin-weighted spheroidal harmonics in four and higher dimensions. Phys Rev D 73:024013. https://doi.org/10.1103/PhysRevD.73.024013. arXiv:gr-qc/0511111

Berti E, Cardoso V, Will CM (2006b) On gravitational-wave spectroscopy of massive black holes with the space interferometer LISA. Phys Rev D 73:064030. https://doi.org/10.1103/PhysRevD.73.064030. arXiv:gr-qc/0512160

Berti E, Cardoso V, Gonzalez JA, Sperhake U, Hannam M, Husa S, Bruegmann B (2007) Inspiral, merger and ringdown of unequal mass black hole binaries: a multipolar analysis. Phys Rev D 76:064034. https://doi.org/10.1103/PhysRevD.76.064034. arXiv:gr-qc/0703053

Berti E, Cardoso V, Starinets AO (2009) Quasinormal modes of black holes and black branes. Class Quantum Grav 26:163001. https://doi.org/10.1088/0264-9381/26/16/163001. arXiv:0905.2975

Berti E et al (2015) Testing general relativity with present and future astrophysical observations. Class Quantum Grav 32:243001. https://doi.org/10.1088/0264-9381/32/24/243001. arXiv:1501.07274

Berti E, Sesana A, Barausse E, Cardoso V, Belczynski K (2016) Spectroscopy of Kerr black holes with Earth- and space-based interferometers. Phys Rev Lett 117:101102. https://doi.org/10.1103/PhysRevLett.117.101102. arXiv:1605.09286

Bertone G, Fairbairn M (2008) Compact stars as dark matter probes. Phys Rev D 77:043515. https://doi.org/10.1103/PhysRevD.77.043515. arXiv:0709.1485

Bertone G, Tim Tait MP (2018) A new era in the search for dark matter. Nature 562:51–56. https://doi.org/10.1038/s41586-018-0542-z. arXiv:1810.01668

Bezares M, Palenzuela C (2018) Gravitational waves from dark boson star binary mergers. Class Quantum Grav 35:234002. https://doi.org/10.1088/1361-6382/aae87c. arXiv:1808.10732

Bezares M, Palenzuela C, Bona C (2017) Final fate of compact boson star mergers. Phys Rev D 95:124005. https://doi.org/10.1103/PhysRevD.95.124005. arXiv:1705.01071

Bezares M, Vigano D, Palenzuela C (2019) Signatures of dark matter cores in binary neutron star mergers. ArXiv e-prints arXiv:1905.08551

Bianchi E, Christodoulou M, D'Ambrosio F, Haggard HM, Rovelli C (2018) White holes as remnants: a surprising scenario for the end of a black hole. Class Quantum Grav 35:225003. https://doi.org/10.1088/1361-6382/aae550. arXiv:1802.04264

Binney J, Tremaine S (2011) Galactic dynamics. Princeton series in astrophysics, 2nd edn. Princeton University Press, Princeton

Binnington T, Poisson E (2009) Relativistic theory of tidal Love numbers. Phys Rev D 80:084018. https://doi.org/10.1103/PhysRevD.80.084018. arXiv:0906.1366

Birrell ND, Davies PCW (1984) Quantum fields in curved space. Cambridge monographs on mathematical physics. Cambridge Univ. Press, Cambridge. https://doi.org/10.1017/CBO9780511622632

Blanchet L (2006) Gravitational radiation from post-Newtonian sources and inspiralling compact binaries. Living Rev Relativ 9:4. https://doi.org/10.12942/lrr-2006-4

Blanchet L (2014) Gravitational radiation from post-Newtonian sources and inspiralling compact binaries. Living Rev Relativ 17:2. https://doi.org/10.12942/lrr-2014-2. arXiv:1310.1528

Blázquez-Salcedo JL, Macedo CFB, Cardoso V, Ferrari V, Gualtieri L, Khoo FS, Kunz J, Pani P (2016) Perturbed black holes in Einstein-dilaton–Gauss–Bonnet gravity: stability, ringdown, and gravitational-wave emission. Phys Rev D 94:104024. https://doi.org/10.1103/PhysRevD.94.104024. arXiv:1609.01286

Bowers RL, Liang EPT (1974) Anisotropic spheres in general relativity. Astrophys J 188:657. https://doi.org/10.1086/152760

Brito R, Cardoso V, Okawa H (2015a) Accretion of dark matter by stars. Phys Rev Lett 115:111301. https://doi.org/10.1103/PhysRevLett.115.111301. arXiv:1508.04773

Brito R, Cardoso V, Pani P (2015) Superradiance: energy extraction, black-hole bombs and implications for astrophysics and particle physics. Lecture notes in physics, vol 906. Springer, Cham. https://doi.org/10.1007/978-3-319-19000-6. arXiv:1501.06570

Brito R, Cardoso V, Herdeiro CAR, Radu E (2016a) Proca stars: gravitating Bose–Einstein condensates of massive spin 1 particles. Phys Lett B 752:291–295. https://doi.org/10.1016/j.physletb.2015.11.051. arXiv:1508.05395

Brito R, Cardoso V, Macedo CFB, Okawa H, Palenzuela C (2016b) Interaction between bosonic dark matter and stars. Phys Rev D 93:044045. https://doi.org/10.1103/PhysRevD.93.044045. arXiv:1512.00466

Broderick AE, Loeb A (2005) Imaging bright-spots in the accretion flow near the black hole horizon of Sgr A*. Mon Not R Astron Soc 363:353–362. https://doi.org/10.1111/j.1365-2966.2005.09458.x. arXiv:astro-ph/0506433

Broderick AE, Loeb A (2006) Imaging optically-thin hot spots near the black hole horizon of Sgr A* at radio and near-infrared wavelengths. Mon Not R Astron Soc 367:905–916. https://doi.org/10.1111/j.1365-2966.2006.10152.x. arXiv:astro-ph/0509237

Broderick AE, Narayan R (2006) On the nature of the compact dark mass at the Galactic center. Astrophys J 638:L21–L24. https://doi.org/10.1086/500930. arXiv:astro-ph/0512211

Broderick AE, Narayan R (2007) Where are all the gravastars? Limits upon the gravastar model from accreting black holes. Class Quantum Grav 24:659–666. https://doi.org/10.1088/0264-9381/24/3/009. arXiv:gr-qc/0701154

Broderick AE, Loeb A, Narayan R (2009) The event horizon of Sagittarius A*. Astrophys J 701:1357–1366. https://doi.org/10.1088/0004-637X/701/2/1357. arXiv:0903.1105

Broderick AE, Johannsen T, Loeb A, Psaltis D (2014) Testing the no-hair theorem with event horizon telescope observations of Sagittarius A*. Astrophys J 784:7. https://doi.org/10.1088/0004-637X/784/1/7. arXiv:1311.5564

Bronnikov KA, Konoplya RA, Zhidenko A (2012) Instabilities of wormholes and regular black holes supported by a phantom scalar field. Phys Rev D 86:024028. https://doi.org/10.1103/PhysRevD.86.024028. arXiv:1205.2224

Brustein R, Medved AJM (2017) Black holes as collapsed polymers. Fortschr Phys 65:0114. https://doi.org/10.1002/prop.201600114. arXiv:1602.07706

Brustein R, Medved AJM (2018) Quantum hair of black holes out of equilibrium. Phys Rev D 97:044035. https://doi.org/10.1103/PhysRevD.97.044035. arXiv:1709.03566

Brustein R, Medved AJM (2019) Resisting collapse: how matter inside a black hole can withstand gravity. Phys Rev D 99:064019. https://doi.org/10.1103/PhysRevD.99.064019. arXiv:1805.11667

Brustein R, Medved AJM, Yagi K (2017a) Discovering the interior of black holes. Phys Rev D 96:124021. https://doi.org/10.1103/PhysRevD.96.124021. arXiv:1701.07444

Brustein R, Medved AJM, Yagi K (2017b) When black holes collide: probing the interior composition by the spectrum of ringdown modes and emitted gravitational waves. Phys Rev D 96:064033. https://doi.org/10.1103/PhysRevD.96.064033. arXiv:1704.05789

Brustein R, Medved AJM, Yagi K (2018) Lower limit on the entropy of black holes as inferred from gravitational wave observations. ArXiv e-prints arXiv:1811.12283

Buchdahl HA (1959) General relativistic fluid spheres. Phys Rev 116:1027. https://doi.org/10.1103/PhysRev.116.1027

Bueno P, Cano PA, Goelen F, Hertog T, Vercnocke B (2018) Echoes of Kerr-like wormholes. Phys Rev D 97:024040. https://doi.org/10.1103/PhysRevD.97.024040. arXiv:1711.00391

Buonanno A, Cook GB, Pretorius F (2007) Inspiral, merger and ring-down of equal-mass black-hole binaries. Phys Rev D 75:124018. https://doi.org/10.1103/PhysRevD.75.124018. arXiv:gr-qc/0610122

Buoninfante L, Mazumdar A (2019) Nonlocal star as a blackhole mimicker. ArXiv e-prints arXiv:1903.01542

Buoninfante L, Koshelev AS, Lambiase G, Marto J, Mazumdar A (2018) Conformally-flat, non-singular static metric in infinite derivative gravity. J Cosmol Astropart Phys 1806(06):014. https://doi.org/10.1088/1475-7516/2018/06/014. arXiv:1804.08195

Burgess CP, Plestid R, Rummel M (2018) Effective field theory of black hole echoes. J High Energy Phys 09:113. https://doi.org/10.1007/JHEP09(2018)113. arXiv:1808.00847

Cabero M, Capano CD, Fischer-Birnholtz O, Krishnan B, Nielsen AB, Nitz AH, Biwer CM (2018) Observational tests of the black hole area increase law. Phys Rev D 97:124069. https://doi.org/10.1103/PhysRevD.97.124069. arXiv:1711.09073

Canuto V, Chitre SM (1974) Crystallization of dense neutron matter. Phys Rev D 9:1587–1613. https://doi.org/10.1103/PhysRevD.9.1587

Cao Z, Cardenas-Avendano A, Zhou M, Bambi C, Herdeiro CAR, Radu E (2016) Iron $K\alpha$ line of boson stars. J Cosmol Astropart Phys 1610(10):003. https://doi.org/10.1088/1475-7516/2016/10/003. arXiv:1609.00901

Carballo-Rubio R (2018) Stellar equilibrium in semiclassical gravity. Phys Rev Lett 120:061102. https://doi.org/10.1103/PhysRevLett.120.061102. arXiv:1706.05379

Carballo-Rubio R, Di Filippo F, Liberati S, Visser M (2018a) Phenomenological aspects of black holes beyond general relativity. Phys Rev D 98:124009. https://doi.org/10.1103/PhysRevD.98.124009. arXiv:1809.08238

Carballo-Rubio R, Kumar P, Lu W (2018b) Seeking observational evidence for the formation of trapping horizons in astrophysical black holes. Phys Rev D 97:123012. https://doi.org/10.1103/PhysRevD.97.123012. arXiv:1804.00663

Cardenas-Avendano A, Godfrey J, Yunes N, Lohfink A (2019) Experimental relativity with accretion disk observations. ArXiv e-prints arXiv:1903.04356

Cardoso V, Gualtieri L (2009) Perturbations of Schwarzschild black holes in dynamical Chern–Simons modified gravity. Phys Rev D 80:064008. https://doi.org/10.1103/PhysRevD.81.089903, https://doi.org/10.1103/PhysRevD.80.064008 [Erratum: Phys Rev D 81:089903 (2010)]. arXiv:0907.5008

Cardoso V, Gualtieri L (2016) Testing the black hole no-hair hypothesis. Class Quantum Grav 33:174001. https://doi.org/10.1088/0264-9381/33/17/174001. arXiv:1607.03133

Cardoso V, Pani P (2013) Tidal acceleration of black holes and superradiance. Class Quantum Grav 30:045011. https://doi.org/10.1088/0264-9381/30/4/045011. arXiv:1205.3184

Cardoso V, Pani P (2017a) Tests for the existence of black holes through gravitational wave echoes. Nature Astron 1:586–591. https://doi.org/10.1038/s41550-017-0225-y. arXiv:1709.01525

Cardoso V, Pani P (2017b) The observational evidence for horizons: from echoes to precision gravitational-wave physics. ArXiv e-prints arXiv:1707.03021

Cardoso V, Dias OJC, Hovdebo JL, Myers RC (2006) Instability of non-supersymmetric smooth geometries. Phys Rev D 73:064031. https://doi.org/10.1103/PhysRevD.73.064031. arXiv:hep-th/0512277

Cardoso V, Pani P, Cadoni M, Cavaglia M (2008a) Ergoregion instability of ultracompact astrophysical objects. Phys Rev D 77:124044. https://doi.org/10.1103/PhysRevD.77.124044. arXiv:0709.0532

Cardoso V, Pani P, Cadoni M, Cavaglia M (2008b) Instability of hyper-compact Kerr-like objects. Class Quantum Grav 25:195010. https://doi.org/10.1088/0264-9381/25/19/195010. arXiv:0808.1615

Cardoso V, Miranda AS, Berti E, Witek H, Zanchin VT (2009) Geodesic stability, Lyapunov exponents and quasinormal modes. Phys Rev D 79:064016. https://doi.org/10.1103/PhysRevD.79.064016. arXiv:0812.1806

Cardoso V, Crispino LCB, Macedo CFB, Okawa H, Pani P (2014) Light rings as observational evidence for event horizons: long-lived modes, ergoregions and nonlinear instabilities of ultracompact objects. Phys Rev D 90:044069. https://doi.org/10.1103/PhysRevD.90.044069. arXiv:1406.5510

Cardoso V, Franzin E, Pani P (2016a) Is the gravitational-wave ringdown a probe of the event horizon? Phys Rev Lett 116:171101. https://doi.org/10.1103/PhysRevLett.116.171101. arXiv:1602.07309

Cardoso V, Hopper S, Macedo CFB, Palenzuela C, Pani P (2016b) Gravitational-wave signatures of exotic compact objects and of quantum corrections at the horizon scale. Phys Rev D 94:084031. https://doi.org/10.1103/PhysRevD.94.084031. arXiv:1608.08637

Cardoso V, Franzin E, Maselli A, Pani P, Raposo G (2017) Testing strong-field gravity with tidal Love numbers. Phys Rev D 95:084014. https://doi.org/10.1103/PhysRevD.95.084014. arXiv:1701.01116

Cardoso V, Costa JL, Destounis K, Hintz P, Jansen A (2018a) Quasinormal modes and strong cosmic censorship. Phys Rev Lett 120:031103. https://doi.org/10.1103/PhysRevLett.120.031103. arXiv:1711.10502

Cardoso V, Kimura M, Maselli A, Senatore L (2018b) Black holes in an effective field theory extension of general relativity. Phys Rev Lett 121:251105. https://doi.org/10.1103/PhysRevLett.121.251105. arXiv:1808.08962

Cardoso V, Foit VF, Kleban M (2019a) Gravitational wave echoes from black hole area quantization. ArXiv e-prints arXiv:1902.10164

Cardoso V, del Río A, Kimura M (2019b) Distinguishing black holes from horizonless objects through the excitation of resonances (in preparation)

Carloni S, Vernieri D (2018) Covariant Tolman–Oppenheimer–Volkoff equations. II. The anisotropic case. Phys Rev D 97:124057. https://doi.org/10.1103/PhysRevD.97.124057. arXiv:1709.03996

Carter B (1971) Axisymmetric black hole has only two degrees of freedom. Phys Rev Lett 26:331–333. https://doi.org/10.1103/PhysRevLett.26.331

Carter B, Langlois D (1998) Relativistic models for superconducting superfluid mixtures. Nucl Phys B 531:478–504. https://doi.org/10.1016/S0550-3213(98)00430-1. arXiv:gr-qc/9806024

Cattoen C, Faber T, Visser M (2005) Gravastars must have anisotropic pressures. Class Quantum Grav 22:4189–4202. https://doi.org/10.1088/0264-9381/22/20/002. arXiv:gr-qc/0505137

CENTRA (2019) Webpage with Mathematica notebooks and numerical quasinormal mode tables. http://centra.tecnico.ulisboa.pt/network/grit/files/. See also http://www.darkgra.org

Chakraborty S, Lochan K (2019) Decoding infrared imprints of quantum origins of black holes. Phys Lett B 789:276–286. https://doi.org/10.1016/j.physletb.2018.12.028. arXiv:1711.10660

Chambers KC et al (2016) The Pan-STARRS1 surveys. ArXiv e-prints arXiv:1612.05560

Chandrasekhar S (1983) The mathematical theory of black holes. Oxford University Press, New York

Chandrasekhar S, Detweiler SL (1975) The quasi-normal modes of the Schwarzschild black hole. Proc R Soc London, Ser A 344:441–452. https://doi.org/10.1098/rspa.1975.0112

Chandrasekhar S, Ferrari V (1991) On the non-radial oscillations of a star. III. A reconsideration of the axial modes. Proc R Soc London, Ser A 434(1891):449–457. https://doi.org/10.1098/rspa.1991.0104

Chatziioannou K et al (2019) On the properties of the massive binary black hole merger GW170729. ArXiv e-prints arXiv:1903.06742

Chen P, Unruh WG, Wu CH, Yeom DH (2018) Pre-Hawking radiation cannot prevent the formation of apparent horizon. Phys Rev D 97:064045. https://doi.org/10.1103/PhysRevD.97.064045. arXiv:1710.01533

Chen B, Chen Y, Ma Y, Lo KLR, Sun L (2019) Instability of exotic compact objects and its implications for gravitational-wave echoes. ArXiv e-prints arXiv:1902.08180

Chianese M, Di Grezia E, Manfredonia M, Miele G (2017) Characterising exotic matter driving wormholes. Eur Phys J Plus 132:164. https://doi.org/10.1140/epjp/i2017-11475-y. arXiv:1701.08770

Chirenti CBMH, Rezzolla L (2007) How to tell a gravastar from a black hole. Class Quantum Grav 24:4191–4206. https://doi.org/10.1088/0264-9381/24/16/013. arXiv:0706.1513

Chirenti CBMH, Rezzolla L (2008) On the ergoregion instability in rotating gravastars. Phys Rev D 78:084011. https://doi.org/10.1103/PhysRevD.78.084011. arXiv:0808.4080

Chirenti C, Rezzolla L (2016) Did GW150914 produce a rotating gravastar? Phys Rev D 94:084016. https://doi.org/10.1103/PhysRevD.94.084016. arXiv:1602.08759

Choptuik MW, Pretorius F (2010) Ultra relativistic particle collisions. Phys Rev Lett 104:111101. https://doi.org/10.1103/PhysRevLett.104.111101. arXiv:0908.1780

Choptuik M, Masachs R, Way B (2019) Multi-oscillating boson stars. ArXiv e-prints arXiv:1904.02168

Chowdhury BD, Mathur SD (2008) Radiation from the non-extremal fuzzball. Class Quantum Grav 25:135005. https://doi.org/10.1088/0264-9381/25/13/135005. arXiv:0711.4817

Chruściel PT, Costa JL, Heusler M (2012) Stationary black holes: uniqueness and beyond. Living Rev Relativ 15:7. https://doi.org/10.12942/lrr-2012-7. arXiv:1205.6112

Clifton T, Ferreira PG, Padilla A, Skordis C (2012) Modified gravity and cosmology. Phys Rep 513:1–189. https://doi.org/10.1016/j.physrep.2012.01.001. arXiv:1106.2476

Clough K, Dietrich T, Niemeyer JC (2018) Axion star collisions with black holes and neutron stars in full 3D numerical relativity. Phys Rev D 98:083020. https://doi.org/10.1103/PhysRevD.98.083020. arXiv:1808.04668

Colpi M, Shapiro SL, Wasserman I (1986) Boson stars: gravitational equilibria of selfinteracting scalar fields. Phys Rev Lett 57:2485–2488. https://doi.org/10.1103/PhysRevLett.57.2485

Comins N, Schutz BF (1978) On the ergoregion instability. Proc R Soc London, Ser A 364(1717):211–226

Conklin RS, Holdom B (2019) Gravitational wave "Echo" spectra. ArXiv e-prints arXiv:1905.09370

Conklin RS, Holdom B, Ren J (2018) Gravitational wave echoes through new windows. Phys Rev D 98:044021. https://doi.org/10.1103/PhysRevD.98.044021. arXiv:1712.06517

Correia MR, Cardoso V (2018) Characterization of echoes: a Dyson-series representation of individual pulses. Phys Rev D 97:084030. https://doi.org/10.1103/PhysRevD.97.084030. arXiv:1802.07735

Cunha PVP, Herdeiro CAR (2018) Shadows and strong gravitational lensing: a brief review. Gen Relativ Gravit 50:42. https://doi.org/10.1007/s10714-018-2361-9. arXiv:1801.00860

Cunha PVP, Herdeiro CAR, Radu E, Runarsson HF (2015) Shadows of Kerr black holes with scalar hair. Phys Rev Lett 115:211102. https://doi.org/10.1103/PhysRevLett.115.211102. arXiv:1509.00021

Cunha PVP, Berti E, Herdeiro CAR (2017a) Light-ring stability for ultracompact objects. Phys Rev Lett 119:251102. https://doi.org/10.1103/PhysRevLett.119.251102. arXiv:1708.04211

Cunha PVP, Font JA, Herdeiro C, Radu E, Sanchis-Gual N, Zilhão M (2017b) Lensing and dynamics of ultracompact bosonic stars. Phys Rev D 96:104040. https://doi.org/10.1103/PhysRevD.96.104040. arXiv:1709.06118

Cunha PVP, Herdeiro CAR, Rodriguez MJ (2018) Does the black hole shadow probe the event horizon geometry? Phys Rev D 97:084020. https://doi.org/10.1103/PhysRevD.97.084020. arXiv:1802.02675

Curiel E (2019) The many definitions of a black hole. Nature Astron 3:27–34. https://doi.org/10.1038/s41550-018-0602-1. arXiv:1808.01507

Cuyubamba MA, Konoplya RA, Zhidenko A (2018) No stable wormholes in Einstein-dilaton–Gauss–Bonnet theory. Phys Rev D 98:044040. https://doi.org/10.1103/PhysRevD.98.044040. arXiv:1804.11170

Dafermos M (2005) The Interior of charged black holes and the problem of uniqueness in general relativity. Commun Pure Appl Math 58:0445–0504 arXiv:gr-qc/0307013

Dafermos M, Rodnianski I (2013) Lectures on black holes and linear waves. Clay Math Proc 17:97–205 arXiv:0811.0354

Damour T (1982) Surface effects in black hole physics. In: Ruffini R (ed) Proceedings of the second Marcel Grossmann meeting on general relativity. North-Holland, Amsterdam, pp 587–608

Damour T (1983) Gravitational radiation and the motion of compact bodies. In: Deruelle N, Piran T (eds) Rayonnement gravitationnel/gravitational radiation, proceedings of the Les Houches summer school, 2–21 June 1982. North-Holland, Amsterdam (see Section V of Damour's contribution for the first published calculation of the TLNs of black holes)

Damour T, Nagar A (2009) Relativistic tidal properties of neutron stars. Phys Rev D 80:084035. https://doi.org/10.1103/PhysRevD.80.084035. arXiv:0906.0096

Damour T, Solodukhin SN (2007) Wormholes as black hole foils. Phys Rev D 76:024016. https://doi.org/10.1103/PhysRevD.76.024016. arXiv:0704.2667

Danielsson U, Giri S (2018) Observational signatures from horizonless black shells imitating rotating black holes. J High Energy Phys 07:070. https://doi.org/10.1007/JHEP07(2018)070. arXiv:1712.00511

Danielsson UH, Dibitetto G, Giri S (2017) Black holes as bubbles of AdS. J High Energy Phys 10:171. https://doi.org/10.1007/JHEP10(2017)171. arXiv:1705.10172

Das SR, Mathur SD (2000) The quantum physics of black holes: results from string theory. Annu Rev Nucl Part Sci 50:153–206. https://doi.org/10.1146/annurev.nucl.50.1.153. arXiv:gr-qc/0105063

Datta S, Bose S (2019) Probing the nature of central objects in extreme-mass-ratio inspirals with gravitational waves. ArXiv e-prints arXiv:1902.01723

David JR, Mandal G, Wadia SR (2002) Microscopic formulation of black holes in string theory. Phys Rep 369:549–686. https://doi.org/10.1016/S0370-1573(02)00271-5. arXiv:hep-th/0203048

Davis M, Ruffini R, Press WH, Price RH (1971) Gravitational radiation from a particle falling radially into a Schwarzschild black hole. Phys Rev Lett 27:1466–1469. https://doi.org/10.1103/PhysRevLett.27.1466

Davis M, Ruffini R, Tiomno J (1972) Pulses of gravitational radiation of a particle falling radially into a Schwarzschild black hole. Phys Rev D 5:2932–2935. https://doi.org/10.1103/PhysRevD.5.2932

Deliyergiyev M, Del Popolo A, Tolos L, Le Delliou M, Lee X, Burgio F (2019) Dark compact objects: an extensive overview. Phys Rev D 99:063015. https://doi.org/10.1103/PhysRevD.99.063015. arXiv:1903.01183

Detweiler S (1977) On resonant oscillations of a rapidly rotating black hole. Proc R Soc London, Ser A 352:381–395. https://doi.org/10.1098/rspa.1977.0005

Dev K, Gleiser M (2002) Anisotropic stars: exact solutions. Gen Relativ Gravit 34:1793–1818. https://doi.org/10.1023/A:1020707906543. arXiv:astro-ph/0012265

Dev K, Gleiser M (2003) Anisotropic stars. 2. Stability. Gen Relativ Gravit 35:1435–1457. https://doi.org/10.1023/A:1024534702166. arXiv:gr-qc/0303077

Di Giovanni F, Sanchis-Gual N, Herdeiro CAR, Font JA (2018) Dynamical formation of Proca stars and quasistationary solitonic objects. Phys Rev D 98:064044. https://doi.org/10.1103/PhysRevD.98.064044. arXiv:1803.04802

Di Matteo T, Allen SW, Fabian AC, Wilson AS, Young AJ (2003) Accretion onto the supermassive black hole in M87. Astrophys J 582:133–140. https://doi.org/10.1086/344504. arXiv:astro-ph/0202238

Dietrich T, Ossokine S, Clough K (2019) Full 3D numerical relativity simulations of neutron star boson star collisions with BAM. Class Quantum Grav 36:025002. https://doi.org/10.1088/1361-6382/aaf43e. arXiv:1807.06959

Doeleman S et al (2008) Event-horizon-scale structure in the supermassive black hole candidate at the Galactic centre. Nature 455:78. https://doi.org/10.1038/nature07245. arXiv:0809.2442

Doeleman SS et al (2012) Jet launching structure resolved near the supermassive black hole in M87. Science 338:355. https://doi.org/10.1126/science.1224768. arXiv:1210.6132

Doneva DD, Yazadjiev SS (2012) Gravitational wave spectrum of anisotropic neutron stars in Cowling approximation. Phys Rev D 85:124023. https://doi.org/10.1103/PhysRevD.85.124023. arXiv:1203.3963

Dreyer O, Kelly BJ, Krishnan B, Finn LS, Garrison D, Lopez-Aleman R (2004) Black hole spectroscopy: testing general relativity through gravitational wave observations. Class Quantum Grav 21:787–804. https://doi.org/10.1088/0264-9381/21/4/003. arXiv:gr-qc/0309007

Droste J (1917) The field of a single centre in Einstein's theory of gravitation, and the motion of a particle in that field. Proc R Neth Acad Arts Sci 19:197–215

Du SM, Chen Y (2018) Searching for near-horizon quantum structures in the binary black-hole stochastic gravitational-wave background. Phys Rev Lett 121:051105. https://doi.org/10.1103/PhysRevLett.121.051105. arXiv:1803.10947

Dvali G, Gomez C (2013) Black hole's 1/N hair. Phys Lett B 719:419–423. https://doi.org/10.1016/j.physletb.2013.01.020. arXiv:1203.6575

Dvali G, Gomez C (2013b) Black hole's quantum N-portrait. Fortschr Phys 61:742–767. https://doi.org/10.1002/prop.201300001. arXiv:1112.3359

Dvorkin I, Vangioni E, Silk J, Uzan JP, Olive KA (2016) Metallicity-constrained merger rates of binary black holes and the stochastic gravitational wave background. Mon Not R Astron Soc 461:3877–3885. https://doi.org/10.1093/mnras/stw1477. arXiv:1604.04288

Dwyer S, Sigg D, Ballmer SW, Barsotti L, Mavalvala N, Evans M (2015) Gravitational wave detector with cosmological reach. Phys Rev D 91:082001. https://doi.org/10.1103/PhysRevD.91.082001

Eardley DM, Giddings SB (2002) Classical black hole production in high-energy collisions. Phys Rev D 66:044011. https://doi.org/10.1103/PhysRevD.66.044011. arXiv:gr-qc/0201034

Eckart A, Huttemann A, Kiefer C, Britzen S, Zajacek M, Lammerzahl C, Stockler M, Valencia SM, Karas V, Garcia Marin M (2017) The Milky Way's supermassive black hole: how good a case is it? Found Phys 47:553–624. https://doi.org/10.1007/s10701-017-0079-2. arXiv:1703.09118

Eda K, Itoh Y, Kuroyanagi S, Silk J (2015) Gravitational waves as a probe of dark matter minispikes. Phys Rev D 91:044045. https://doi.org/10.1103/PhysRevD.91.044045. arXiv:1408.3534

Einstein A, Rosen N (1935) The particle problem in the general theory of relativity. Phys Rev 48:73–77. https://doi.org/10.1103/PhysRev.48.73

Ellis J, Hektor A, Hütsi G, Kannike K, Marzola L, Raidal M, Vaskonen V (2018) Search for dark matter effects on gravitational signals from neutron star mergers. Phys Lett B 781:607–610. https://doi.org/10.1016/j.physletb.2018.04.048. arXiv:1710.05540

Emparan R, Grumiller D, Tanabe K (2013) Large-D gravity and low-D strings. Phys Rev Lett 110:251102. https://doi.org/10.1103/PhysRevLett.110.251102. arXiv:1303.1995

Eperon FC (2017) Geodesics in supersymmetric microstate geometries. Class Quantum Grav 34:165003. https://doi.org/10.1088/1361-6382/aa7bfe. arXiv:1702.03975

Eperon FC, Reall HS, Santos JE (2016) Instability of supersymmetric microstate geometries. JHEP 10:031. https://doi.org/10.1007/JHEP10(2016)031. arXiv:1607.06828

Essick R, Vitale S, Evans M (2017) Frequency-dependent responses in third generation gravitational-wave detectors. Phys Rev D 96:084004. https://doi.org/10.1103/PhysRevD.96.084004. arXiv:1708.06843

Fabian AC, Rees MJ, Stella L, White NE (1989) X-ray fluorescence from the inner disc in Cygnus X-1. Mon Not R Astron Soc 238(3):729–736

Falcke H, Markoff SB (2013) Toward the event horizon: the supermassive black hole in the Galactic center. Class Quantum Grav 30:244003. https://doi.org/10.1088/0264-9381/30/24/244003. arXiv:1311.1841

Fan XL, Chen YB (2018) Stochastic gravitational-wave background from spin loss of black holes. Phys Rev D 98:044020. https://doi.org/10.1103/PhysRevD.98.044020. arXiv:1712.00784

Ferrari V, Kokkotas KD (2000) Scattering of particles by neutron stars: time evolutions for axial perturbations. Phys Rev D 62:107504. https://doi.org/10.1103/PhysRevD.62.107504. arXiv:gr-qc/0008057

Ferrari V, Mashhoon B (1984) New approach to the quasinormal modes of a black hole. Phys Rev D 30:295–304. https://doi.org/10.1103/PhysRevD.30.295

Foit VF, Kleban M (2019) Testing quantum black holes with gravitational waves. Class Quantum Grav 36:035006. https://doi.org/10.1088/1361-6382/aafcba. arXiv:1611.07009

Franchini N, Pani P, Maselli A, Gualtieri L, Herdeiro CAR, Radu E, Ferrari V (2017) Constraining black holes with light boson hair and boson stars using epicyclic frequencies and quasiperiodic oscillations. Phys Rev D 95:124025. https://doi.org/10.1103/PhysRevD.95.124025. arXiv:1612.00038

Franzin E, Cadoni M, Tuveri M (2018) Sine-Gordon solitonic scalar stars and black holes. Phys Rev D 97:124018. https://doi.org/10.1103/PhysRevD.97.124018. arXiv:1805.08976

Friedberg R, Lee TD, Pang Y (1987) Scalar soliton stars and black holes. Phys Rev D 35:3658. https://doi.org/10.1103/PhysRevD.35.3658

Friedman JL (1978a) Ergosphere instability. Commun Math Phys 63(3):243–255

Friedman JL (1978b) Generic instability of rotating relativistic stars. Commun Math Phys 62:247–278. https://doi.org/10.1007/BF01202527

Fujita R (2012) Gravitational radiation for extreme mass ratio inspirals to the 14th post-Newtonian order. Prog Theor Phys 127:583–590. https://doi.org/10.1143/PTP.127.583. arXiv:1104.5615

Gair JR, Vallisneri M, Larson SL, Baker JG (2013) Testing general relativity with low-frequency, space-based gravitational-wave detectors. Living Rev Relativ 16:7. https://doi.org/10.12942/lrr-2013-7. arXiv:1212.5575

Garfinkle D, Mann RB, Vuille C (2003) Critical collapse of a massive vector field. Phys Rev D 68:064015. https://doi.org/10.1103/PhysRevD.68.064015. arXiv:gr-qc/0305014

Genzel R, Eisenhauer F, Gillessen S (2010) The Galactic center massive black hole and nuclear star cluster. Rev Mod Phys 82:3121–3195. https://doi.org/10.1103/RevModPhys.82.3121. arXiv:1006.0064

Geroch RP (1970) Multipole moments. II. Curved space. J Math Phys 11:2580–2588. https://doi.org/10.1063/1.1665427

Ghersi JTG, Frolov AV, Dobre DA (2019) Echoes from the scattering of wavepackets on wormholes. ArXiv e-prints arXiv:1901.06625

Giddings SB (1992) Black holes and massive remnants. Phys Rev D 46:1347–1352. https://doi.org/10.1103/PhysRevD.46.1347. arXiv:hep-th/9203059

Giddings SB (2011) Nonlocality versus complementarity: a conservative approach to the information problem. Class Quantum Grav 28:025002. https://doi.org/10.1088/0264-9381/28/2/025002. arXiv:0911.3395

Giddings SB (2012) Black holes, quantum information, and unitary evolution. Phys Rev D 85:124063. https://doi.org/10.1103/PhysRevD.85.124063. arXiv:1201.1037

Giddings SB (2013) Nonviolent information transfer from black holes: a field theory parametrization. Phys Rev D 88:024018. https://doi.org/10.1103/PhysRevD.88.024018. arXiv:1302.2613

Giddings SB (2014) Possible observational windows for quantum effects from black holes. Phys Rev D 90:124033. https://doi.org/10.1103/PhysRevD.90.124033. arXiv:1406.7001

Giddings SB (2016) Gravitational wave tests of quantum modifications to black hole structure: with post-GW150914 update. Class Quantum Grav 33:235010. https://doi.org/10.1088/0264-9381/33/23/235010. arXiv:1602.03622

Giddings SB (2017a) Astronomical tests for quantum black hole structure. Nature Astron 1:0067. https://doi.org/10.1038/s41550-017-0067. arXiv:1703.03387

Giddings SB (2017) Nonviolent unitarization: basic postulates to soft quantum structure of black holes. J High Energy Phys 12:047. https://doi.org/10.1007/JHEP12(2017)047. arXiv:1701.08765

Giddings SB, Koren S, Treviño G (2019) Exploring strong-field deviations from general relativity via gravitational waves. ArXiv e-prints arXiv:1904.04258

Gimon EG, Hořava P (2009) Astrophysical violations of the Kerr bound as a possible signature of string theory. Phys Lett B 672:299–302. https://doi.org/10.1016/j.physletb.2009.01.026. arXiv:0706.2873

Giudice GF, McCullough M, Urbano A (2016) Hunting for dark particles with gravitational waves. JCAP 1610(10):001. https://doi.org/10.1088/1475-7516/2016/10/001. arXiv:1605.01209

Giusto S, Mathur SD, Saxena A (2005) 3-Charge geometries and their CFT duals. Nucl Phys B 710:425–463. https://doi.org/10.1016/j.nuclphysb.2005.01.009. arXiv:hep-th/0406103

Glampedakis K, Pappas G (2018a) How well can ultracompact bodies imitate black hole ringdowns? Phys Rev D 97:041502. https://doi.org/10.1103/PhysRevD.97.041502. arXiv:1710.02136

Glampedakis K, Pappas G (2018b) The absence of spherical photon orbits as a diagnostic of non-Kerr spacetimes. ArXiv e-prints arXiv:1806.09333

Gleiser M, Watkins R (1989) Gravitational stability of scalar matter. Nucl Phys B 319:733. https://doi.org/10.1016/0550-3213(89)90627-5

Goddi C et al (2016) BlackHoleCam: fundamental physics of the Galactic center. Int J Mod Phys D 26:1730001. https://doi.org/10.1142/S0218271817300014. arXiv:1606.08879

Goldman I, Nussinov S (1989) Weakly interacting massive particles and neutron stars. Phys Rev D 40:3221–3230. https://doi.org/10.1103/PhysRevD.40.3221

Gonzalez JA, Guzman FS, Sarbach O (2009a) Instability of wormholes supported by a ghost scalar field. I. Linear stability analysis. Class Quantum Grav 26:015010. https://doi.org/10.1088/0264-9381/26/1/015010. arXiv:0806.0608

Gonzalez JA, Guzman FS, Sarbach O (2009b) Instability of wormholes supported by a ghost scalar field. II. Nonlinear evolution. Class Quantum Grav 26:015011. https://doi.org/10.1088/0264-9381/26/1/015011. arXiv:0806.1370

Gould A, Draine BT, Romani RW, Nussinov S (1990) Neutron stars: graveyard of charged dark matter. Phys Lett B 238:337. https://doi.org/10.1016/0370-2693(90)91745-W

Gracia-Linares M, Guzman FS (2016) Accretion of supersonic winds on boson stars. Phys Rev D 94:064077. https://doi.org/10.1103/PhysRevD.94.064077. arXiv:1609.06398

Grandclément P (2017) Light rings and light points of boson stars. Phys Rev D 95:084011. https://doi.org/10.1103/PhysRevD.95.084011. arXiv:1612.07507

Guo B, Hampton S, Mathur SD (2018) Can we observe fuzzballs or firewalls? J High Energy Phys 07:162. https://doi.org/10.1007/JHEP07(2018)162. arXiv:1711.01617

Gürlebeck N (2015) No-hair theorem for black holes in astrophysical environments. Phys Rev Lett 114:151102. https://doi.org/10.1103/PhysRevLett.114.151102. arXiv:1503.03240

Guth AH, Hertzberg MP, Prescod-Weinstein C (2015) Do dark matter axions form a condensate with long-range correlation? Phys Rev D 92:103513. https://doi.org/10.1103/PhysRevD.92.103513. arXiv:1412.5930

Guven J, O'Murchadha N (1999) Bounds on 2m/R for static spherical objects. Phys Rev D 60:084020. https://doi.org/10.1103/PhysRevD.60.084020. arXiv:gr-qc/9903067

Hannuksela OA, Wong KWK, Brito R, Berti E, Li TGF (2019) Probing the existence of ultralight bosons with a single gravitational-wave measurement. Nature Astron. https://doi.org/10.1038/s41550-019-0712-4. arXiv:1804.09659

Hansen R (1974) Multipole moments of stationary space–times. J Math Phys 15:46–52. https://doi.org/10.1063/1.1666501

Harada T, Iguchi H, Ki Nakao (2000) Naked singularity explosion. Phys Rev D 61:101502. https://doi.org/10.1103/PhysRevD.61.101502. arXiv:gr-qc/0003036

Harada T, Cardoso V, Miyata D (2019) Particle creation in gravitational collapse to a horizonless compact object. Phys Rev D 99:044039. https://doi.org/10.1103/PhysRevD.99.044039. arXiv:1811.05179

Hartle JB (1973) Tidal friction in slowly rotating black holes. Phys Rev D 8:1010–1024. https://doi.org/10.1103/PhysRevD.8.1010

Hawking SW (1971) Gravitational radiation from colliding black holes. Phys Rev Lett 26:1344–1346. https://doi.org/10.1103/PhysRevLett.26.1344

Hawking SW, Ellis GFR (2011) The large scale structure of space–time. Cambridge monographs on mathematical physics. Cambridge University Press, Cambridge

Helfer T, Marsh DJE, Clough K, Fairbairn M, Lim EA, Becerril R (2017) Black hole formation from axion stars. J Cosmol Astropart Phys 1703(03):055. https://doi.org/10.1088/1475-7516/2017/03/055. arXiv:1609.04724

Helfer T, Lim EA, Garcia MAG, Amin MA (2019) Gravitational wave emission from collisions of compact scalar solitons. Phys Rev D 99:044046. https://doi.org/10.1103/PhysRevD.99.044046. arXiv:1802.06733

Henriques AB, Mendes LE (2005) Boson-fermion stars: exploring different configurations. Astrophys Space Sci 300:367–379. https://doi.org/10.1007/s10509-005-4512-1. arXiv:astro-ph/0301015

Henriques A, Liddle AR, Moorhouse R (1989) Combined boson-fermion stars. Phys Lett B 233:99. https://doi.org/10.1016/0370-2693(89)90623-0

Henriques A, Liddle AR, Moorhouse R (1990) Combined boson-fermion stars: configurations and stability. Nucl Phys B 337:737. https://doi.org/10.1016/0550-3213(90)90514-E

Herdeiro CAR, Lemos JPS (2018) The black hole fifty years after: genesis of the name. ArXiv e-prints arXiv:1811.06587

Herrera L, Di Prisco A, Martin J, Ospino J, Santos NO, Troconis O (2004) Spherically symmetric dissipative anisotropic fluids: a general study. Phys Rev D 69:084026. https://doi.org/10.1103/PhysRevD.69.084026. arXiv:gr-qc/0403006

Hertog T, Hartle J (2017) Observational implications of fuzzball formation. ArXiv e-prints arXiv:1704.02123

Heusler M (1998) Stationary black holes: uniqueness and beyond. Living Rev Relativ 1:6. https://doi.org/10.12942/lrr-1998-6

Hild S et al (2011) Sensitivity studies for third-generation gravitational wave observatories. Class Quantum Grav 28:094013. https://doi.org/10.1088/0264-9381/28/9/094013. arXiv:1012.0908

Hillebrandt W, Steinmetz KO (1976) Anisotropic neutron star models: stability against radial and nonradial pulsations. A&A 53:283–287

Hinderer T, Lackey BD, Lang RN, Read JS (2010) Tidal deformability of neutron stars with realistic equations of state and their gravitational wave signatures in binary inspiral. Phys Rev D 81(12):101–12

Hirschmann EW, Lehner L, Liebling SL, Palenzuela C (2018) Black hole dynamics in Einstein–Maxwell-dilaton theory. Phys Rev D 97:064032. https://doi.org/10.1103/PhysRevD.97.064032. arXiv:1706.09875

Hod S (2017) Onset of superradiant instabilities in rotating spacetimes of exotic compact objects. J High Energy Phys 06:132. https://doi.org/10.1007/JHEP06(2017)132. arXiv:1704.05856

Hohmann M, Pfeifer C, Raidal M, Veermäe H (2018) Wormholes in conformal gravity. J Cosmol Astropart Phys 1810(10):003. https://doi.org/10.1088/1475-7516/2018/10/003. arXiv:1802.02184

Holdom B, Ren J (2016) QCD analogy for quantum gravity. Phys Rev D 93:124030. https://doi.org/10.1103/PhysRevD.93.124030. arXiv:1512.05305

Holdom B, Ren J (2017) Not quite a black hole. Phys Rev D 95:084034. https://doi.org/10.1103/PhysRevD.95.084034. arXiv:1612.04889

Honda EP, Choptuik MW (2002) Fine structure of oscillons in the spherically symmetric φ^4 Klein–Gordon model. Phys Rev D 65:084037. https://doi.org/10.1103/PhysRevD.65.084037. arXiv:hep-ph/0110065

Hoormann JK, Beheshtipour B, Krawczynski H (2016) Testing general relativity's no-hair theorem with X-ray observations of black holes. Phys Rev D 93:044020. https://doi.org/10.1103/PhysRevD.93.044020. arXiv:1601.02055

Horowitz CJ, Reddy S (2019) Gravitational waves from compact dark objects in neutron stars. ArXiv e-prints arXiv:1902.04597

Hughes SA (2001) Evolution of circular, nonequatorial orbits of Kerr black holes due to gravitational wave emission. II. Inspiral trajectories and gravitational wave forms. Phys Rev D 64:064004. https://doi.org/10.1103/PhysRevD.64.064004 [Erratum: Phys Rev D 88:109902 (2013)]. arXiv:gr-qc/0104041

Hui L, Ostriker JP, Tremaine S, Witten E (2017) Ultralight scalars as cosmological dark matter. Phys Rev D 95:043541. https://doi.org/10.1103/PhysRevD.95.043541. arXiv:1610.08297

Isayev AA (2018) Comment on "Covariant Tolman–Oppenheimer–Volkoff equations. II. The anisotropic case". Phys Rev D 98:088503. https://doi.org/10.1103/PhysRevD.98.088503. arXiv:1808.05699

Iyer BR, Vishveshwara CV, Dhurandhar SV (1985) Ultracompact ($R < 3M$) objects in general relativity. Class Quantum Grav 2:219–228. https://doi.org/10.1088/0264-9381/2/2/013

Jetzer P (1992) Boson stars. Phys Rep 220:163–227. https://doi.org/10.1016/0370-1573(92)90123-H

Jiang J, Bambi C, Steiner JF (2015) Using iron line reverberation and spectroscopy to distinguish Kerr and non-Kerr black holes. J Cosmol Astropart Phys 1505(05):025. https://doi.org/10.1088/1475-7516/2015/05/025. arXiv:1406.5677

Jiménez Forteza X, Abdelsalhin T, Pani P, Gualtieri L (2018) Impact of high-order tidal terms on binary neutron-star waveforms. Phys Rev D 98:124014. https://doi.org/10.1103/PhysRevD.98.124014. arXiv:1807.08016

Johannsen T (2014) X-ray probes of black hole accretion disks for testing the no-hair theorem. Phys Rev D 90:064002. https://doi.org/10.1103/PhysRevD.90.064002. arXiv:1501.02815

Johannsen T (2016a) Sgr A* and general relativity. Class Quantum Grav 33:113001. https://doi.org/10.1088/0264-9381/33/11/113001. arXiv:1512.03818

Johannsen T (2016b) Testing the no-hair theorem with observations of black holes in the electromagnetic spectrum. Class Quantum Grav 33:124001. https://doi.org/10.1088/0264-9381/33/12/124001. arXiv:1602.07694

Johannsen T, Psaltis D (2010) Testing the no-hair theorem with observations in the electromagnetic spectrum: I. Properties of a quasi-Kerr spacetime. Astrophys J 716:187–197. https://doi.org/10.1088/0004-637X/716/1/187. arXiv:1003.3415

Johannsen T, Psaltis D (2013) Testing the no-hair theorem with observations in the electromagnetic spectrum. IV. Relativistically broadened iron lines. Astrophys J 773:57. https://doi.org/10.1088/0004-637X/773/1/57. arXiv:1202.6069

Johannsen T, Broderick AE, Plewa PM, Chatzopoulos S, Doeleman SS, Eisenhauer F, Fish VL, Genzel R, Gerhard O, Johnson MD (2016) Testing general relativity with the shadow size of Sgr A*. Phys Rev Lett 116:031101. https://doi.org/10.1103/PhysRevLett.116.031101. arXiv:1512.02640

John F (1981) Blow-up for quasi-linear wave equations in three space dimensions. Commun Pure Appl Math 34:29–51

Johnson-Mcdaniel NK, Mukherjee A, Kashyap R, Ajith P, Del Pozzo W, Vitale S (2018) Constraining black hole mimickers with gravitational wave observations. ArXiv e-prints arXiv:1804.08026

Kanti P, Kleihaus B, Kunz J (2011) Wormholes in dilatonic Einstein–Gauss–Bonnet theory. Phys Rev Lett 107:271101. https://doi.org/10.1103/PhysRevLett.107.271101. arXiv:1108.3003

Kaplan DE, Rajendran S (2019) Firewalls in general relativity. Phys Rev D 99:044033. https://doi.org/10.1103/PhysRevD.99.044033. arXiv:1812.00536

Kastha S, Gupta A, Arun KG, Sathyaprakash BS, Van Den Broeck C (2018) Testing the multipole structure of compact binaries using gravitational wave observations. Phys Rev D 98:124033. https://doi.org/10.1103/PhysRevD.98.124033. arXiv:1809.10465

Kaup DJ (1968) Klein–Gordon geon. Phys Rev 172:1331–1342. https://doi.org/10.1103/PhysRev.172.1331

Kawai H, Matsuo Y, Yokokura Y (2013) A self-consistent model of the black hole evaporation. Int J Mod Phys A 28:1350050. https://doi.org/10.1142/S0217751X13500504. arXiv:1302.4733

Keir J (2016) Slowly decaying waves on spherically symmetric spacetimes and ultracompact neutron stars. Class Quantum Grav 33:135009. https://doi.org/10.1088/0264-9381/33/13/135009. arXiv:1404.7036

Kelner SR, Aharonian FA, Bugayov VV (2006) Energy spectra of gamma-rays, electrons and neutrinos produced at proton–proton interactions in the very high energy regime. Phys Rev D 74:034018. https://doi.org/10.1103/PhysRevD.74.034018, https://doi.org/10.1103/PhysRevD.79.039901 [Erratum: Phys Rev D 79:039901 (2009)]. arXiv:astro-ph/0606058

Kesden M, Gair J, Kamionkowski M (2005) Gravitational-wave signature of an inspiral into a supermassive horizonless object. Phys Rev D 71:044015. https://doi.org/10.1103/PhysRevD.71.044015. arXiv:astro-ph/0411478

Khanna G, Price RH (2017) Black hole ringing, quasinormal modes, and light rings. Phys Rev D 95:081501. https://doi.org/10.1103/PhysRevD.95.081501. arXiv:1609.00083

Khaybullina A, Tuleganova G (2019) Stability of Schwarzschild-$f(R)$ gravity thin-shell wormholes. Mod Phys Lett A 34:1950006. https://doi.org/10.1142/S0217732319500068. arXiv:1810.09222

Khlopov M, Malomed BA, Zeldovich IB (1985) Gravitational instability of scalar fields and formation of primordial black holes. Mon Not R Astron Soc 215:575–589

Kippenhahn R, Weigert A, Weiss A (2012) Stellar structure and evolution. Springer, Berlin

Klainerman S, Szeftel J (2017) Global nonlinear stability of Schwarzschild spacetime under polarized perturbations. ArXiv e-prints arXiv:1711.07597

Kokkotas KD (1995) Pulsating relativistic stars. In: Relativistic gravitation and gravitational radiation. Proceedings, School of Physics, Les Houches, France, 26 September–6 October 1995, pp 89–102. arXiv:gr-qc/9603024

Kokkotas KD, Schmidt BG (1999) Quasinormal modes of stars and black holes. Living Rev Relativ 2:2. https://doi.org/10.12942/lrr-1999-2. arXiv:gr-qc/9909058

Kokkotas KD, Ruoff J, Andersson N (2004) The w-mode instability of ultracompact relativistic stars. Phys Rev D 70:043003. https://doi.org/10.1103/PhysRevD.70.043003. arXiv:astro-ph/0212429

Kong L, Li Z, Bambi C (2014) Constraints on the spacetime geometry around 10 stellar-mass black hole candidates from the disk's thermal spectrum. Astrophys J 797:78. https://doi.org/10.1088/0004-637X/797/2/78. arXiv:1405.1508

Konoplya RA, Stuchlík Z (2017) Are eikonal quasinormal modes linked to the unstable circular null geodesics? Phys Lett B 771:597–602. https://doi.org/10.1016/j.physletb.2017.06.015. arXiv:1705.05928

Konoplya RA, Zhidenko A (2016) Wormholes versus black holes: quasinormal ringing at early and late times. J Cosmol Astropart Phys 1612(12):043. https://doi.org/10.1088/1475-7516/2016/12/043. arXiv:1606.00517

Konoplya RA, Stuchlík Z, Zhidenko A (2019) Echoes of compact objects: new physics near the surface and matter at a distance. Phys Rev D 99:024007. https://doi.org/10.1103/PhysRevD.99.024007. arXiv:1810.01295

Koshelev AS, Mazumdar A (2017) Do massive compact objects without event horizon exist in infinite derivative gravity? Phys Rev D 96:084069. https://doi.org/10.1103/PhysRevD.96.084069. arXiv:1707.00273

Krishnendu NV, Arun KG, Mishra CK (2017) Testing the binary black hole nature of a compact binary coalescence. Phys Rev Lett 119:091101. https://doi.org/10.1103/PhysRevLett.119.091101. arXiv:1701.06318

Krishnendu NV, Mishra CK, Arun KG (2019) Spin-induced deformations and tests of binary black hole nature using third-generation detectors. Phys Rev D 99:064008. https://doi.org/10.1103/PhysRevD.99.064008. arXiv:1811.00317

Lai KH, Li TGF (2018) Constraining black-hole horizon effects by LIGO-Virgo detections of inspiralling binary black holes. Phys Rev D 98:084059. https://doi.org/10.1103/PhysRevD.98.084059. arXiv:1807.01840

Landry P, Poisson E (2015) Tidal deformation of a slowly rotating material body. External metric. Phys Rev D 91:104018. https://doi.org/10.1103/PhysRevD.91.104018. arXiv:1503.07366

Lattimer JM, Prakash M (2007) Neutron star observations: prognosis for equation of state constraints. Phys Rep 442:109–165. https://doi.org/10.1016/j.physrep.2007.02.003. arXiv:astro-ph/0612440

Lee TD, Pang Y (1989) Stability of mini-boson stars. Nucl Phys B 315:477. https://doi.org/10.1016/0550-3213(89)90365-9

Lemos JPS, Weinberg EJ (2004) Quasiblack holes from extremal charged dust. Phys Rev D 69:104004. https://doi.org/10.1103/PhysRevD.69.104004. arXiv:gr-qc/0311051

Lemos JPS, Zaslavskii OB (2008) Black hole mimickers: regular versus singular behavior. Phys Rev D 78:024040. https://doi.org/10.1103/PhysRevD.78.024040. arXiv:0806.0845

Lemos JPS, Lobo FSN, Quinet de Oliveira S (2003) Morris–Thorne wormholes with a cosmological constant. Phys Rev D 68:064004. https://doi.org/10.1103/PhysRevD.68.064004. arXiv:gr-qc/0302049

Letelier PS (1980) Anisotropic fluids with two-perfect-fluid components. Phys Rev D 22:807. https://doi.org/10.1103/PhysRevD.22.807

Leung SC, Chu MC, Lin LM (2011) Dark-matter admixed neutron stars. Phys Rev D 84:107301. https://doi.org/10.1103/PhysRevD.84.107301. arXiv:1111.1787

Leung SC, Chu MC, Lin LM, Wong KW (2013) Dark-matter admixed white dwarfs. Phys Rev D 87:123506. https://doi.org/10.1103/PhysRevD.87.123506. arXiv:1305.6142

Li ZP, Piao YS (2019) Mixing of gravitational wave echoes. ArXiv e-prints arXiv:1904.05652

Li LX, Zimmerman ER, Narayan R, McClintock JE (2005) Multi-temperature blackbody spectrum of a thin accretion disk around a Kerr black hole: model computations and comparison with observations. Astrophys J Suppl Ser 157:335–370. https://doi.org/10.1086/428089. arXiv:astro-ph/0411583

Liebling SL, Palenzuela C (2012) Dynamical boson stars. Living Rev Relativ 15:6. https://doi.org/10.12942/lrr-2012-6. arXiv:1202.5809

LIGO Scientific Collaboration (2015) LIGO instrument science white paper. https://dcc.ligo.org/LIGO-T1500290-v2/public

Lin K, Qian WL, Fan X, Zhang H (2019) Tail wavelets in the merger of binary compact objects. ArXiv e-prints arXiv:1903.09039

Lo RKL, Li TGF, Weinstein AJ (2018) Template-based gravitational-wave echoes search using Bayesian model selection. ArXiv e-prints arXiv:1811.07431

Lopes L, Henriques A (1992) Boson-fermion stars: going to larger boson masses. Phys Lett B 285:80–84. https://doi.org/10.1016/0370-2693(92)91303-Q

Lu W, Kumar P, Narayan R (2017) Stellar disruption events support the existence of the black hole event horizon. Mon Not R Astron Soc 468:910–919. https://doi.org/10.1093/mnras/stx542. arXiv:1703.00023

Lunin O, Mathur SD (2002a) AdS/CFT duality and the black hole information paradox. Nucl Phys B 623:342–394. https://doi.org/10.1016/S0550-3213(01)00620-4. arXiv:hep-th/0109154

Lunin O, Mathur SD (2002b) Statistical interpretation of Bekenstein entropy for systems with a stretched horizon. Phys Rev Lett 88:211303. https://doi.org/10.1103/PhysRevLett.88.211303. arXiv:hep-th/0202072

Lynden-Bell D (1969) Galactic nuclei as collapsed old quasars. Nature 223:690. https://doi.org/10.1038/223690a0

Macedo CFB, Pani P, Cardoso V, Crispino LCB (2013a) Astrophysical signatures of boson stars: quasinormal modes and inspiral resonances. Phys Rev D 88:064046. https://doi.org/10.1103/PhysRevD.88.064046. arXiv:1307.4812

Macedo CFB, Pani P, Cardoso V, Crispino LCB (2013b) Into the lair: gravitational-wave signatures of dark matter. Astrophys J 774:48. https://doi.org/10.1088/0004-637X/774/1/48. arXiv:1302.2646

Macedo CFB, Stratton T, Dolan S, Crispino LCB (2018) Spectral lines of extreme compact objects. Phys Rev D 98:104034. https://doi.org/10.1103/PhysRevD.98.104034. arXiv:1807.04762

Maggio E, Pani P, Ferrari V (2017) Exotic compact objects and how to quench their ergoregion instability. Phys Rev D 96:104047. https://doi.org/10.1103/PhysRevD.96.104047. arXiv:1703.03696

Maggio E, Cardoso V, Dolan SR, Pani P (2019) Ergoregion instability of exotic compact objects: electromagnetic and gravitational perturbations and the role of absorption. Phys Rev D 99:064007. https://doi.org/10.1103/PhysRevD.99.064007. arXiv:1807.08840

Mak MK, Harko T (2003) Anisotropic stars in general relativity. Proc R Soc London, Ser A 459:393–408. https://doi.org/10.1098/rspa.2002.1014. arXiv:gr-qc/0110103

Malafarina D (2017) Classical collapse to black holes and quantum bounces: a review. Universe 3:48. https://doi.org/10.3390/universe3020048. arXiv:1703.04138

Malafarina D, Joshi PS (2016) Electromagnetic counterparts to gravitational waves from black hole mergers and naked singularities. ArXiv e-prints arXiv:1603.02848

Maldacena J, Milekhin A, Popov F (2018) Traversable wormholes in four dimensions. ArXiv e-prints arXiv:1807.04726

Mannarelli M, Tonelli F (2018) Gravitational wave echoes from strange stars. Phys Rev D 97:123010. https://doi.org/10.1103/PhysRevD.97.123010. arXiv:1805.02278

Mark Z, Zimmerman A, Du SM, Chen Y (2017) A recipe for echoes from exotic compact objects. Phys Rev D 96:084002. https://doi.org/10.1103/PhysRevD.96.084002. arXiv:1706.06155

Marsh DJE (2016) Axion cosmology. Phys Rep 643:1–79. https://doi.org/10.1016/j.physrep.2016.06.005. arXiv:1510.07633

Maselli A, Gualtieri L, Ferrari V (2013) Constraining the equation of state of nuclear matter with gravitational wave observations: tidal deformability and tidal disruption. Phys Rev D 88:104040

Maselli A, Pnigouras P, Nielsen NG, Kouvaris C, Kokkotas KD (2017a) Dark stars: gravitational and electromagnetic observables. Phys Rev D 96:023005. https://doi.org/10.1103/PhysRevD.96.023005. arXiv:1704.07286

Maselli A, Völkel SH, Kokkotas KD (2017b) Parameter estimation of gravitational wave echoes from exotic compact objects. Phys Rev D 96:064045. https://doi.org/10.1103/PhysRevD.96.064045. arXiv:1708.02217

Maselli A, Pani P, Cardoso V, Abdelsalhin T, Gualtieri L, Ferrari V (2018a) From micro to macro and back: probing near-horizon quantum structures with gravitational waves. ArXiv e-prints arXiv:1811.03689

Maselli A, Pani P, Cardoso V, Abdelsalhin T, Gualtieri L, Ferrari V (2018b) Probing Planckian corrections at the horizon scale with LISA binaries. Phys Rev Lett 120:081101. https://doi.org/10.1103/PhysRevLett.120.081101. arXiv:1703.10612

Mathur SD (2005) The fuzzball proposal for black holes: an elementary review. Fortschr Phys 53:793–827. https://doi.org/10.1002/prop.200410203. arXiv:hep-th/0502050

Mathur SD (2008) Fuzzballs and the information paradox: a summary and conjectures. ArXiv e-prints arXiv:0810.4525

Mathur SD (2009) The information paradox: a pedagogical introduction. Class Quantum Grav 26:224001. https://doi.org/10.1088/0264-9381/26/22/224001. arXiv:0909.1038

Mathur SD, Turton D (2014) Comments on black holes I: the possibility of complementarity. J High Energy Phys 01:034. https://doi.org/10.1007/JHEP01(2014)034. arXiv:1208.2005

Mazur PO, Mottola E (2001) Gravitational condensate stars: an alternative to black holes. ArXiv e-prints arXiv:gr-qc/0109035

Mazur PO, Mottola E (2004) Gravitational vacuum condensate stars. Proc Natl Acad Sci USA 101:9545–9550. https://doi.org/10.1073/pnas.0402717101. arXiv:gr-qc/0407075

Mazur PO, Mottola E (2015) Surface tension and negative pressure interior of a non-singular "black hole". Class Quantum Grav 32:215024. https://doi.org/10.1088/0264-9381/32/21/215024. arXiv:1501.03806

McClintock JE, Narayan R, Rybicki GB (2004) On the lack of thermal emission from the quiescent black hole XTE J1118+480: evidence for the event horizon. Astrophys J 615:402–415. https://doi.org/10.1086/424474. arXiv:astro-ph/0403251

McClintock JE, Narayan R, Steiner JF (2014) Black hole spin via continuum fitting and the role of spin in powering transient jets. Space Sci Rev 183:295–322. https://doi.org/10.1007/s11214-013-0003-9. arXiv:1303.1583

Meidam J, Agathos M, Van Den Broeck C, Veitch J, Sathyaprakash BS (2014) Testing the no-hair theorem with black hole ringdowns using TIGER. Phys Rev D 90:064009. https://doi.org/10.1103/PhysRevD.90.064009. arXiv:1406.3201

Mendes RFP, Yang H (2017) Tidal deformability of boson stars and dark matter clumps. Class Quantum Grav 34:185001. https://doi.org/10.1088/1361-6382/aa842d. arXiv:1606.03035

Middleton M (2016) Black hole spin: theory and observation. In: Bambi C (ed) Astrophysics of black holes: from fundamental aspects to latest developments. Astrophysics and space science library, vol 440. Springer, Berlin, pp 99–151. https://doi.org/10.1007/978-3-662-52859-4_3. arXiv:1507.06153

Minamitsuji M (2018) Vector boson star solutions with a quartic order self-interaction. Phys Rev D 97:104023. https://doi.org/10.1103/PhysRevD.97.104023. arXiv:1805.09867

Mirbabayi M (2018) The quasinormal modes of quasinormal modes. ArXiv e-prints arXiv:1807.04843

Molina C, Pani P, Cardoso V, Gualtieri L (2010) Gravitational signature of Schwarzschild black holes in dynamical Chern–Simons gravity. Phys Rev D 81:124021. https://doi.org/10.1103/PhysRevD.81.124021. arXiv:1004.4007

Moore CJ, Gair JR (2015) Testing the no-hair property of black holes with X-ray observations of accretion disks. Phys Rev D 92:024039. https://doi.org/10.1103/PhysRevD.92.024039. arXiv:1507.02998

Moore CJ, Chua AJK, Gair JR (2017) Gravitational waves from extreme mass ratio inspirals around bumpy black holes. Class Quantum Grav 34:195009. https://doi.org/10.1088/1361-6382/aa85fa. arXiv:1707.00712

Morris MS, Thorne KS (1988) Wormholes in space–time and their use for interstellar travel: a tool for teaching general relativity. Am J Phys 56:395–412. https://doi.org/10.1119/1.15620

Moschidis G (2016) A proof of Friedman's ergosphere instability for scalar waves. ArXiv e-prints arXiv:1608.02035

Mottola E, Vaulin R (2006) Macroscopic effects of the quantum trace anomaly. Phys Rev D 74:064004. https://doi.org/10.1103/PhysRevD.74.064004. arXiv:gr-qc/0604051

Myers RC (1997) Pure states don't wear black. Gen Relativ Gravit 29:1217–1222. https://doi.org/10.1023/A:1018855611972. arXiv:gr-qc/9705065

Nakano H, Sago N, Tagoshi H, Tanaka T (2017) Black hole ringdown echoes and howls. Prog Theor Exp Phys 2017(7):071E01. https://doi.org/10.1093/ptep/ptx093. arXiv:1704.07175

Nakao Ki, Yoo CM, Harada T (2019) Gravastar formation: what can be the evidence of a black hole? Phys Rev D 99:044027. https://doi.org/10.1103/PhysRevD.99.044027. arXiv:1809.00124

Nandi KK, Izmailov RN, Yanbekov AA, Shayakhmetov AA (2017) Ring-down gravitational waves and lensing observables: how far can a wormhole mimic those of a black hole? Phys Rev D 95:104011. https://doi.org/10.1103/PhysRevD.95.104011. arXiv:1611.03479

Nandi KK, Izmailov RN, Zhdanov ER, Bhattacharya A (2018) Strong field lensing by Damour–Solodukhin wormhole. J Cosmol Astropart Phys 1807(07):027. https://doi.org/10.1088/1475-7516/2018/07/027. arXiv:1805.04679

Narain G, Schaffner-Bielich J, Mishustin IN (2006) Compact stars made of fermionic dark matter. Phys Rev D 74:063003. https://doi.org/10.1103/PhysRevD.74.063003. arXiv:astro-ph/0605724

Narayan R, Heyl JS (2002) On the lack of type I X-ray bursts in black hole X-ray binaries: evidence for the event horizon? Astrophys J 574:L139–L142. https://doi.org/10.1086/342502. arXiv:astro-ph/0203089

Narayan R, McClintock JE (2008) Advection-dominated accretion and the black hole event horizon. New Astron Rev 51:733–751. https://doi.org/10.1016/j.newar.2008.03.002. arXiv:0803.0322

Narayan R, Garcia MR, McClintock JE (1997) Advection dominated accretion and black hole event horizons. Astrophys J 478:L79–L82. https://doi.org/10.1086/310554. arXiv:astro-ph/9701139

Nedkova PG, Tinchev VK, Yazadjiev SS (2013) Shadow of a rotating traversable wormhole. Phys Rev D 88:124019. https://doi.org/10.1103/PhysRevD.88.124019. arXiv:1307.7647

Nielsen AB, Capano CD, Birnholtz O, Westerweck J (2018) Parameter estimation for black hole echo signals and their statistical significance. ArXiv e-prints arXiv:1811.04904

Novikov ID, Thorne KS (1973) Astrophysics and black holes. In: DeWitt C, DeWitt B (eds) Black holes (Les astres occlus). Gordon and Breach, New York, pp 343–450

Ohgami T, Sakai N (2015) Wormhole shadows. Phys Rev D 91:124020. https://doi.org/10.1103/PhysRevD.91.124020. arXiv:1704.07065

Okawa H, Cardoso V, Pani P (2014) Collapse of self-interacting fields in asymptotically flat spacetimes: do self-interactions render Minkowski spacetime unstable? Phys Rev D 89:041502. https://doi.org/10.1103/PhysRevD.89.041502. arXiv:1311.1235

Okounkova M, Stein LC, Scheel MA, Hemberger DA (2017) Numerical binary black hole mergers in dynamical Chern–Simons gravity: scalar field. Phys Rev D 96:044020. https://doi.org/10.1103/PhysRevD.96.044020. arXiv:1705.07924

Okounkova M, Scheel MA, Teukolsky SA (2019) Evolving metric perturbations in dynamical Chern–Simons gravity. Phys Rev D 99:044019. https://doi.org/10.1103/PhysRevD.99.044019. arXiv:1811.10713

Olivares H, Younsi Z, Fromm CM, De Laurentis M, Porth O, Mizuno Y, Falcke H, Kramer M, Rezzolla L (2018) How to tell an accreting boson star from a black hole. ArXiv e-prints arXiv:1809.08682

Oliveira LA, Cardoso V, Crispino LCB (2014) Ergoregion instability: the hydrodynamic vortex. Phys Rev D 89:124008. https://doi.org/10.1103/PhysRevD.89.124008. arXiv:1405.4038

Oshita N, Afshordi N (2019) Probing microstructure of black hole spacetimes with gravitational wave echoes. Phys Rev D 99:044002. https://doi.org/10.1103/PhysRevD.99.044002. arXiv:1807.10287

Oshita N, Wang Q, Afshordi N (2019) On reflectivity of quantum black hole horizons. ArXiv e-prints arXiv:1905.00464

Özel F, Freire P (2016a) Masses, radii, and the equation of state of neutron stars. Annu Rev Astron Astrophys 54:401–440. https://doi.org/10.1146/annurev-astro-081915-023322. arXiv:1603.02698

Özel F, Freire P (2016b) Neutron stars. http://xtreme.as.arizona.edu/NeutronStars/

Page DN, Thorne KS (1974) Disk-accretion onto a black hole. Time-averaged structure of accretion disk. Astrophys J 191:499–506

Palenzuela C, Lehner L, Liebling SL (2008) Orbital dynamics of binary boson star systems. Phys Rev D 77:044036. https://doi.org/10.1103/PhysRevD.77.044036. arXiv:0706.2435

Palenzuela C, Pani P, Bezares M, Cardoso V, Lehner L, Liebling S (2017) Gravitational wave signatures of highly compact boson star binaries. Phys Rev D 96:104058. https://doi.org/10.1103/PhysRevD.96.104058. arXiv:1710.09432

Pani P (2015) I-Love-Q relations for gravastars and the approach to the black-hole limit. Phys Rev D 92:124030. https://doi.org/10.1103/PhysRevD.92.124030. arXiv:1506.06050

Pani P, Ferrari V (2018) On gravitational-wave echoes from neutron-star binary coalescences. Class Quantum Grav 35:15LT01. https://doi.org/10.1088/1361-6382/aacb8f. arXiv:1804.01444

Pani P, Maselli A (2019) Love in extrema ratio. ArXiv e-prints arXiv:1905.03947

Pani P, Berti E, Cardoso V, Chen Y, Norte R (2009) Gravitational wave signatures of the absence of an event horizon. I. Nonradial oscillations of a thin-shell gravastar. Phys Rev D 80:124047. https://doi.org/10.1103/PhysRevD.80.124047. arXiv:0909.0287

Pani P, Barausse E, Berti E, Cardoso V (2010a) Gravitational instabilities of superspinars. Phys Rev D 82:044009. https://doi.org/10.1103/PhysRevD.82.044009. arXiv:1006.1863

Pani P, Berti E, Cardoso V, Chen Y, Norte R (2010b) Gravitational-wave signature of a thin-shell gravastar. J Phys Conf Ser 222:012032. https://doi.org/10.1088/1742-6596/222/1/012032

Pani P, Berti E, Cardoso V, Chen Y, Norte R (2010c) Gravitational-wave signatures of the absence of an event horizon. II. Extreme mass ratio inspirals in the spacetime of a thin-shell gravastar. Phys Rev D 81:084011. https://doi.org/10.1103/PhysRevD.81.084011. arXiv:1001.3031

Pani P, Gualtieri L, Ferrari V (2015a) Tidal Love numbers of a slowly spinning neutron star. Phys Rev D 92:124003. https://doi.org/10.1103/PhysRevD.92.124003. arXiv:1509.02171

Pani P, Gualtieri L, Maselli A, Ferrari V (2015b) Tidal deformations of a spinning compact object. Phys Rev D 92:024010. https://doi.org/10.1103/PhysRevD.92.024010. arXiv:1503.07365

Papadopoulos GO, Kokkotas KD (2018) Preserving Kerr symmetries in deformed spacetimes. Class Quantum Grav 35:185014. https://doi.org/10.1088/1361-6382/aad7f4. arXiv:1807.08594

Pappas G, Glampedakis K (2018) On the connection of spacetime separability and spherical photon orbits. ArXiv e-prints arXiv:1806.04091

Paranjape A, Padmanabhan T (2009) Radiation from collapsing shells, semiclassical backreaction and black hole formation. Phys Rev D 80:044011. https://doi.org/10.1103/PhysRevD.80.044011. arXiv:0906.1768

Patil M, Harada T, Ki Nakao, Joshi PS, Kimura M (2016) Infinite efficiency of the collisional Penrose process: can a overspinning Kerr geometry be the source of ultrahigh-energy cosmic rays and neutrinos? Phys Rev D 93:104015. https://doi.org/10.1103/PhysRevD.93.104015. arXiv:1510.08205

Peet AW (1998) The Bekenstein formula and string theory (N-brane theory). Class Quantum Grav 15:3291–3338. https://doi.org/10.1088/0264-9381/15/11/003. arXiv:hep-th/9712253

Penrose R (1969) Gravitational collapse: the role of general relativity. Riv Nuovo Cim 1:252–276 [Gen Rel Grav 34:1141 (2002)]

Penrose R (1978) Singularities of spacetime. In: Lebovitz NR, Reid WH, Vandervoort PO (eds) Theoretical principles in astrophysics and relativity. Chicago University Press, Chicago, pp 217–243

Pisano F, Tomazelli J (1996) Stars of WIMPs. Mod Phys Lett A 11:647–652. https://doi.org/10.1142/S0217732396000667. arXiv:gr-qc/9509022

Poisson E (2004) Absorption of mass and angular momentum by a black hole: time-domain formalisms for gravitational perturbations, and the small-hole/slow-motion approximation. Phys Rev D 70:084044. https://doi.org/10.1103/PhysRevD.70.084044. arXiv:gr-qc/0407050

Poisson E (2009) Tidal interaction of black holes and Newtonian viscous bodies. Phys Rev D 80:064029. https://doi.org/10.1103/PhysRevD.80.064029. arXiv:0907.0874

Poisson E (2015) Tidal deformation of a slowly rotating black hole. Phys Rev D 91:044004. https://doi.org/10.1103/PhysRevD.91.044004. arXiv:1411.4711

Poisson E, Will C (1953) Gravity: Newtonian, post-Newtonian, relativistic. Cambridge University Press, Cambridge

Popper K (1985) The problem of induction. In: Miller D (ed) Popper selections. Princeton University Press, Princeton, pp 101–117

Porto RA (2016) The tune of love and the nature(ness) of spacetime. Fortschr Phys 64:723–729. https://doi.org/10.1002/prop.201600064. arXiv:1606.08895

Posada C (2017) Slowly rotating supercompact Schwarzschild stars. Mon Not R Astron Soc 468:2128–2139. https://doi.org/10.1093/mnras/stx523. arXiv:1612.05290

Posada C, Chirenti C (2019) On the radial stability of ultra compact Schwarzschild stars beyond the Buchdahl limit. Class Quantum Grav 36:065004. https://doi.org/10.1088/1361-6382/ab0526. arXiv:1811.09589

Poschl G, Teller E (1933) Bemerkungen zur Quantenmechanik des anharmonischen Oszillators. Z Phys 83:143–151. https://doi.org/10.1007/BF01331132

Press WH, Spergel DN (1985) Capture by the sun of a galactic population of weakly interacting massive particles. Astrophys J 296:679–684. https://doi.org/10.1086/163485

Price RH, Khanna G (2017) Gravitational wave sources: reflections and echoes. Class Quantum Grav 34:225005. https://doi.org/10.1088/1361-6382/aa8f29. arXiv:1702.04833

Psaltis D (2008) Probes and tests of strong-field gravity with observations in the electromagnetic spectrum. Living Rev Relativ 11:9. https://doi.org/10.12942/lrr-2008-9. arXiv:0806.1531

Punturo M et al (2010) The Einstein telescope: a third-generation gravitational wave observatory. Class Quantum Grav 27:194002. https://doi.org/10.1088/0264-9381/27/19/194002

Quataert E, Narayan R, Reid MJ (1999) What is the accretion rate in Sagittarius A*? Astrophys J 517:L101–L104. https://doi.org/10.1086/312035

Quevedo H, Mashhoon B (1991) Generalization of Kerr spacetime. Phys Rev D 43:3902–3906. https://doi.org/10.1103/PhysRevD.43.3902

Raidal M, Solodukhin S, Vaskonen V, Veermäe H (2018) Light primordial exotic compact objects as all dark matter. Phys Rev D 97:123520. https://doi.org/10.1103/PhysRevD.97.123520. arXiv:1802.07728

Ramos O, Barausse E (2019) Constraints on Horava gravity from binary black hole observations. Phys Rev D 99:024034. https://doi.org/10.1103/PhysRevD.99.024034. arXiv:1811.07786

Randall L, Sundrum R (1999) An alternative to compactification. Phys Rev Lett 83:4690–4693. https://doi.org/10.1103/PhysRevLett.83.4690. arXiv:hep-th/9906064

Raposo G, Pani P, Bezares M, Palenzuela C, Cardoso V (2018) Anisotropic stars as ultracompact objects in general relativity. ArXiv e-prints arXiv:1811.07917

Raposo G, Pani P, Emparan R (2019) Exotic compact objects with soft hair. Phys Rev D 99:104050. https://doi.org/10.1103/PhysRevD.99.104050. arXiv:1812.07615

Reall H (2018) Viewpoint: a possible failure of determinism in general relativity. Physics 11:6

Ren J (2019) Anatomy of a burning 2-2-hole. ArXiv e-prints arXiv:1905.09973

Reynolds CS (2014) Measuring black hole spin using X-ray reflection spectroscopy. Space Sci Rev 183:277–294. https://doi.org/10.1007/s11214-013-0006-6. arXiv:1302.3260

Robinson D (2009) Four decades of black holes uniqueness theorems. Cambridge University Press, Cambridge

Ruderman M (1972) Pulsars: structure and dynamics. Annu Rev Astron Astrophys 10:427–476. https://doi.org/10.1146/annurev.aa.10.090172.002235

Ruffini R, Bonazzola S (1969) Systems of selfgravitating particles in general relativity and the concept of an equation of state. Phys Rev 187:1767–1783. https://doi.org/10.1103/PhysRev.187.1767

Ryan FD (1997) Spinning boson stars with large selfinteraction. Phys Rev D 55:6081–6091. https://doi.org/10.1103/PhysRevD.55.6081

Sabín C (2017) Quantum detection of wormholes. Sci Rep 7:716. https://doi.org/10.1038/s41598-017-00882-6. arXiv:1702.01720

Saida H, Fujisawa A, Yoo CM, Nambu Y (2016) Spherical polytropic balls cannot mimic black holes. Prog Theor Exp Phys 2016(4):043E02. https://doi.org/10.1093/ptep/ptw032. arXiv:1503.01840

Sakai N, Saida H, Tamaki T (2014) Gravastar shadows. Phys Rev D 90:104013. https://doi.org/10.1103/PhysRevD.90.104013. arXiv:1408.6929

Sakamoto K, Shiraishi K (1998) Exact solutions for boson fermion stars in (2+1)-dimensions. Phys Rev D 58:124017. https://doi.org/10.1103/PhysRevD.58.124017. arXiv:gr-qc/9806040

Saravani M, Afshordi N, Mann RB (2015) Empty black holes, firewalls, and the origin of Bekenstein–Hawking entropy. Int J Mod Phys D 23:1443007. https://doi.org/10.1142/S021827181443007X. arXiv:1212.4176

Sathyaprakash BS et al (2019) Extreme gravity and fundamental physics. ArXiv e-prints arXiv:1903.09221

Sawyer RF, Scalapino DJ (1973) Pion condensation in superdense nuclear matter. Phys Rev D 7:953–964. https://doi.org/10.1103/PhysRevD.7.953

Schunck F, Mielke E (2003) General relativistic boson stars. Class Quantum Grav 20:R301–R356 arXiv:0801.0307

Schwarzschild K (1916) On the gravitational field of a mass point according to Einstein's theory. Sitzungsber Preuss Akad Wiss Berlin (Math Phys) 1916:189–196 arXiv:physics/9905030

Sebastiani L, Vanzo L, Zerbini S (2018) On a WKB formula for echoes. ArXiv e-prints arXiv:1808.06939

Seidel E, Suen W (1991) Oscillating soliton stars. Phys Rev Lett 66:1659–1662. https://doi.org/10.1103/PhysRevLett.66.1659

Seidel E, Suen WM (1994) Formation of solitonic stars through gravitational cooling. Phys Rev Lett 72:2516–2519. https://doi.org/10.1103/PhysRevLett.72.2516. arXiv:gr-qc/9309015

Sennett N, Hinderer T, Steinhoff J, Buonanno A, Ossokine S (2017) Distinguishing boson stars from black holes and neutron stars from tidal interactions in inspiraling binary systems. Phys Rev D 96:024002. https://doi.org/10.1103/PhysRevD.96.024002. arXiv:1704.08651

Shaikh R (2018) Wormholes with nonexotic matter in Born–Infeld gravity. Phys Rev D 98:064033. https://doi.org/10.1103/PhysRevD.98.064033. arXiv:1807.07941

Shaikh R, Kar S (2016) Wormholes, the weak energy condition, and scalar–tensor gravity. Phys Rev D 94:024011. https://doi.org/10.1103/PhysRevD.94.024011. arXiv:1604.02857

Shaikh R, Banerjee P, Paul S, Sarkar T (2019) An analytical approach to strong gravitational lensing from ultra-compact objects. ArXiv e-prints arXiv:1903.08211

Shapiro SL, Teukolsky SA (1983) Black holes, white dwarfs, and neutron stars: the physics of compact objects. Wiley, New York

Shen T, Zhou M, Bambi C, Herdeiro CAR, Radu E (2016) Iron Kα line of Proca stars. ArXiv e-prints arXiv:1701.00192

Shiromizu T, Tomikawa Y, Izumi K, Yoshino H (2017) Area bound for a surface in a strong gravity region. Prog Theor Exp Phys 2017(3):033E01. https://doi.org/10.1093/ptep/ptx022. arXiv:1701.00564

Shoemaker D (2010) Advanced LIGO anticipated sensitivity curves. Technical report T0900288-v3, LIGO. https://dcc.ligo.org/LIGO-T0900288/public

Shoom AA (2017) Metamorphoses of a photon sphere. Phys Rev D 96:084056. https://doi.org/10.1103/PhysRevD.96.084056. arXiv:1708.00019

Silva HO, Macedo CFB, Berti E, Crispino LCB (2015) Slowly rotating anisotropic neutron stars in general relativity and scalar–tensor theory. Class Quantum Grav 32:145008. https://doi.org/10.1088/0264-9381/32/14/145008. arXiv:1411.6286

Sperhake U, Berti E, Cardoso V (2013) Numerical simulations of black-hole binaries and gravitational wave emission. C R Physique 14:306–317. https://doi.org/10.1016/j.crhy.2013.01.004. arXiv:1107.2819

Sperhake U, Berti E, Cardoso V, Pretorius F (2013b) Universality, maximum radiation and absorption in high-energy collisions of black holes with spin. Phys Rev Lett 111:041101. https://doi.org/10.1103/PhysRevLett.111.041101. arXiv:1211.6114

Starobinskij AA, Churilov SM (1973) Amplification of electromagnetic and gravitational waves scattered by a rotating black hole. Zh Eksp Teor Fiz 65:3–11

Stella L, Vietri M (1999) kHz quasi periodic oscillations in low mass X-ray binaries as probes of general relativity in the strong field regime. Phys Rev Lett 82:17–20. https://doi.org/10.1103/PhysRevLett.82.17. arXiv:astro-ph/9812124

Stella L, Vietri M, Morsink S (1999) Correlations in the QPO frequencies of low mass X-ray binaries and the relativistic precession model. Astrophys J 524:L63–L66. https://doi.org/10.1086/312291. arXiv:astro-ph/9907346

Stelle KS (1977) Renormalization of higher derivative quantum gravity. Phys Rev D 16:953–969. https://doi.org/10.1103/PhysRevD.16.953

Strominger A, Vafa C (1996) Microscopic origin of the Bekenstein–Hawking entropy. Phys Lett B 379:99–104. https://doi.org/10.1016/0370-2693(96)00345-0. arXiv:hep-th/9601029

Stuchlík Z, Schee J, Toshmatov B, Hladík J, Novotný J (2017) Gravitational instability of polytropic spheres containing region of trapped null geodesics: a possible explanation of central supermassive black holes in galactic halos. J Cosmol Astropart Phys 2017(06):056. https://doi.org/10.1088/1475-7516/2017/06/056. arXiv:1704.07713

't Hooft G (1974) A planar diagram theory for strong interactions. Nucl Phys B 72:461. https://doi.org/10.1016/0550-3213(74)90154-0

Tattersall OJ, Ferreira PG, Lagos M (2018) General theories of linear gravitational perturbations to a Schwarzschild Black Hole. Phys Rev D 97:044021. https://doi.org/10.1103/PhysRevD.97.044021. arXiv:1711.01992

Terno D (2019) Self-consistent description of a spherically-symmetric gravitational collapse. ArXiv e-prints arXiv:1903.04744

Testa A, Pani P (2018) Analytical template for gravitational-wave echoes: signal characterization and prospects of detection with current and future interferometers. Phys Rev D 98:044018. https://doi.org/10.1103/PhysRevD.98.044018. arXiv:1806.04253

Testa A, Maggio E, Bhagwat S, Pani P (2019) Analytical template for gravitational-wave echoes from spinning remnants (in preparation)

Teukolsky SA (1972) Rotating black holes: separable wave equations for gravitational and electromagnetic perturbations. Phys Rev Lett 29:1114–1118. https://doi.org/10.1103/PhysRevLett.29.1114

Teukolsky SA (1973) Perturbations of a rotating black hole. I. Fundamental equations for gravitational electromagnetic and neutrino field perturbations. Astrophys J 185:635–647. https://doi.org/10.1086/152444

Teukolsky SA, Press WH (1974) Perturbations of a rotating black hole. III. Interaction of the hole with gravitational and electromagnetic radiation. Astrophys J 193:443–461. https://doi.org/10.1086/153180

Thornburg J (2007) Event and apparent horizon finders for 3 + 1 numerical relativity. Living Rev Relativ 10:3. https://doi.org/10.12942/lrr-2007-3. arXiv:gr-qc/0512169

Thorne KS (1972) Nonspherical gravitational collapse: a short review. In: Klauder JR (ed) Magic without magic: John Archibald Wheeler. A collection of essays in honor of his sixtieth birthday. W.H. Freeman, San Francisco, pp 231–258

Tolos L, Schaffner-Bielich J (2015) Dark compact planets. Phys Rev D 92:123002. https://doi.org/10.1103/PhysRevD.92.123002. arXiv:1507.08197

Tominaga K, Saijo M, Ki Maeda (1999) Gravitational waves from a test particle scattered by a neutron star: axial mode case. Phys Rev D 60:024004. https://doi.org/10.1103/PhysRevD.60.024004. arXiv:gr-qc/9901040

Tominaga K, Saijo M, Ki Maeda (2001) Gravitational waves from a spinning particle scattered by a relativistic star: axial mode case. Phys Rev D 63:124012. https://doi.org/10.1103/PhysRevD.63.124012. arXiv:gr-qc/0009055

Tsang KW, Rollier M, Ghosh A, Samajdar A, Agathos M, Chatziioannou K, Cardoso V, Khanna G, Van Den Broeck C (2018) A morphology-independent data analysis method for detecting and characterizing gravitational wave echoes. Phys Rev D 98:024023. https://doi.org/10.1103/PhysRevD.98.024023. arXiv:1804.04877

Uchikata N, Yoshida S (2016) Slowly rotating thin shell gravastars. Class Quantum Grav 33:025005. https://doi.org/10.1088/0264-9381/33/2/025005. arXiv:1506.06485

Uchikata N, Yoshida S, Pani P (2016) Tidal deformability and I-Love-Q relations for gravastars with polytropic thin shells. Phys Rev D 94:064015. https://doi.org/10.1103/PhysRevD.94.064015. arXiv:1607.03593

Uchikata N, Nakano H, Narikawa T, Sago N, Tagoshi H, Tanaka T (2019) Searching for black hole echoes from the LIGO-Virgo Catalog GWTC-1. ArXiv e-prints arXiv:1906.00838

Unruh WG, Wald RM (2017) Information loss. Rep Prog Phys 80:092002. https://doi.org/10.1088/1361-6633/aa778e. arXiv:1703.02140

Urbano A, Veermäe H (2018) On gravitational echoes from ultracompact exotic stars. ArXiv e-prints arXiv:1810.07137

van der Klis M (2000) Millisecond oscillations in X-ray binaries. Ann Rev Astron Astrophys 38:717–760. https://doi.org/10.1146/annurev.astro.38.1.717. arXiv:astro-ph/0001167

Vicente R, Cardoso V, Lopes JC (2018) Penrose process, superradiance, and ergoregion instabilities. Phys Rev D 97:084032. https://doi.org/10.1103/PhysRevD.97.084032. arXiv:1803.08060

Vigeland SJ, Hughes SA (2010) Spacetime and orbits of bumpy black holes. Phys Rev D 81:024030. https://doi.org/10.1103/PhysRevD.81.024030. arXiv:0911.1756

Vilenkin A (1978) Exponential amplification of waves in the gravitational field of ultrarelativistic rotating body. Phys Lett B 78:301–303. https://doi.org/10.1016/0370-2693(78)90027-8

Vincent FH, Meliani Z, Grandclement P, Gourgoulhon E, Straub O (2016) Imaging a boson star at the Galactic center. Class Quantum Grav 33:105015. https://doi.org/10.1088/0264-9381/33/10/105015. arXiv:1510.04170

Vines J, Flanagan EE, Hinderer T (2011) Post-1-Newtonian tidal effects in the gravitational wave-form from binary inspirals. Phys Rev D 83:084051. https://doi.org/10.1103/PhysRevD.83.084051. arXiv:1101.1673

Visser M (1995) Lorentzian wormholes: from Einstein to Hawking. AIP Press/Springer, Woodbury

Visser M (1996) Lorentzian wormholes: from Einstein to Hawking. AIP, Woodbury

Visser M, Wiltshire DL (2004) Stable gravastars: an alternative to black holes? Class Quantum Grav 21:1135–1152. https://doi.org/10.1088/0264-9381/21/4/027. arXiv:gr-qc/0310107

Visser M, Barcelo C, Liberati S, Sonego S (2009) Small, dark, and heavy: but is it a black hole? In: Black holes in general relativity and string theory, 24–30 August 2008, Veli Lošinj, Croatia, SISSA, Trieste, PoS. https://doi.org/10.22323/1.075.0010. arXiv:0902.0346

Völkel SH (2018) Inverse spectrum problem for quasi-stationary states. J Phys Commun 2:025029. https://doi.org/10.1088/2399-6528/aaaee2. arXiv:1802.08684

Völkel SH, Kokkotas KD (2017a) A semi-analytic study of axial perturbations of ultra compact stars. Class Quantum Grav 34:125006. https://doi.org/10.1088/1361-6382/aa68cc. arXiv:1703.08156

Völkel SH, Kokkotas KD (2017b) Ultra compact stars: reconstructing the perturbation potential. Class Quantum Grav 34:175015. https://doi.org/10.1088/1361-6382/aa82de. arXiv:1704.07517

Völkel SH, Kokkotas KD (2018) Wormhole potentials and throats from quasi-normal modes. Class Quantum Grav 35:105018. https://doi.org/10.1088/1361-6382/aabce6. arXiv:1802.08525

Voronov BL, Tyutin IV (1984) On renormalization of R^2 gravitation. Yad Fiz 39:998–1010 in Russian

Wade M, Creighton JDE, Ochsner E, Nielsen AB (2013) Advanced LIGO's ability to detect apparent viola-tions of the cosmic censorship conjecture and the no-hair theorem through compact binary coalescence detections. Phys Rev D 88:083002. https://doi.org/10.1103/PhysRevD.88.083002. arXiv:1306.3901

Wald RM (1997) Gravitational collapse and cosmic censorship. In: Black holes, gravitational radiation and the universe: essays in honor of C.V. Vishveshwara, pp 69–85. https://doi.org/10.1007/978-94-017-0934-7_5. arXiv:gr-qc/9710068

Wald RM, Iyer V (1991) Trapped surfaces in the Schwarzschild geometry and cosmic censorship. Phys Rev D 44:R3719–R3722. https://doi.org/10.1103/PhysRevD.44.R3719

Wang Q, Afshordi N (2018) Black hole echology: the observer's manual. Phys Rev D 97:124044. https://doi.org/10.1103/PhysRevD.97.124044. arXiv:1803.02845

Wang YT, Li ZP, Zhang J, Zhou SY, Piao YS (2018a) Are gravitational wave ringdown echoes always equal-interval? Eur Phys J C 78:482. https://doi.org/10.1140/epjc/s10052-018-5974-y. arXiv:1802.02003

Wang YT, Zhang J, Piao YS (2018b) Primordial gravastar from inflation. ArXiv e-prints arXiv:1810.04885

Wang Q, Oshita N, Afshordi N (2019a) Echoes from quantum black holes. ArXiv e-prints arXiv:1905.00446

Wang YT, Zhang J, Zhou SY, Piao YS (2019b) On echo intervals in gravitational wave echo analysis. ArXiv e-prints arXiv:1904.00212

Westerweck J, Nielsen A, Fischer-Birnholtz O, Cabero M, Capano C, Dent T, Krishnan B, Meadors G, Nitz AH (2018) Low significance of evidence for black hole echoes in gravitational wave data. Phys Rev D 97:124037. https://doi.org/10.1103/PhysRevD.97.124037. arXiv:1712.09966

Widdicombe JY, Helfer T, Marsh DJE, Lim EA (2018) Formation of relativistic axion stars. J Cosmol Astropart Phys 1810(10):005. https://doi.org/10.1088/1475-7516/2018/10/005. arXiv:1806.09367

Wilkins DR, Fabian AC (2013) The origin of the lag spectra observed in AGN: reverberation and the propagation of X-ray source fluctuations. Mon Not R Astron Soc 430:247. https://doi.org/10.1093/mnras/sts591. arXiv:1212.2213

Will CM (2014) The confrontation between general relativity and experiment. Living Rev Relativ 17:4. https://doi.org/10.12942/lrr-2014-4. arXiv:1403.7377

Witek H, Gualtieri L, Pani P, Sotiriou TP (2019) Black holes and binary mergers in scalar Gauss–Bonnet gravity: scalar field dynamics. Phys Rev D 99:064035. https://doi.org/10.1103/PhysRevD.99.064035. arXiv:1810.05177

Yagi K, Yunes N (2015a) I-Love-Q anisotropically: universal relations for compact stars with scalar pressure anisotropy. Phys Rev D 91:123008. https://doi.org/10.1103/PhysRevD.91.123008

Yagi K, Yunes N (2015b) I-Love-Q anisotropically: universal relations for compact stars with scalar pressure anisotropy. Phys Rev D 91:123008. https://doi.org/10.1103/PhysRevD.91.123008. arXiv:1503.02726

Yagi K, Yunes N (2015c) Relating follicly-challenged compact stars to bald black holes: a link between two no-hair properties. Phys Rev D 91:103003. https://doi.org/10.1103/PhysRevD.91.103003. arXiv:1502.04131

Yagi K, Yunes N (2016) I-Love-Q relations: from compact stars to black holes. Class Quantum Grav 33:095005. https://doi.org/10.1088/0264-9381/33/9/095005. arXiv:1601.02171

Yang H, Nichols DA, Zhang F, Zimmerman A, Zhang Z, Chen Y (2012) Quasinormal-mode spectrum of Kerr black holes and its geometric interpretation. Phys Rev D 86:104006. https://doi.org/10.1103/PhysRevD.86.104006. arXiv:1207.4253

York JW Jr (1983) Dynamical origin of black hole radiance. Phys Rev D 28:2929. https://doi.org/10.1103/PhysRevD.28.2929

Yoshida S, Eriguchi Y (1996) Ergoregion instability revisited: a new and general method for numerical analysis of stability. Mon Not R Astron Soc 282:580–586

Yoshino H, Izumi K, Shiromizu T, Tomikawa Y (2017) Extension of photon surfaces and its area: static and stationary spacetimes. Prog Theor Exp Phys 2017:063E01. https://doi.org/10.1093/ptep/ptx072. arXiv:1704.04637

Yue XJ, Han WB (2018) Gravitational waves with dark matter minispikes: the combined effect. Phys Rev D 97:064003. https://doi.org/10.1103/PhysRevD.97.064003. arXiv:1711.09706

Yunes N, Siemens X (2013) Gravitational-wave tests of general relativity with ground-based detectors and pulsar timing-arrays. Living Rev Relativ 16:9. https://doi.org/10.12942/lrr-2013-9. arXiv:1304.3473

Yunes N, Yagi K, Pretorius F (2016) Theoretical physics implications of the binary black-hole mergers GW150914 and GW151226. Phys Rev D 94:084002. https://doi.org/10.1103/PhysRevD.94.084002. arXiv:1603.08955

Zackay B, Venumadhav T, Dai L, Roulet J, Zaldarriaga M (2019) A highly spinning and aligned binary black hole merger in the advanced LIGO first observing run. ArXiv e-prints arXiv:1902.10331

Zeng D (2017) Resolving the Schwarzschild singularity in both classic and quantum gravity. Nucl Phys B 917:178–192. https://doi.org/10.1016/j.nuclphysb.2017.02.005. arXiv:1606.06178

Zerilli F (1970) Gravitational field of a particle falling in a Schwarzschild geometry analyzed in tensor harmonics. Phys Rev D 2:2141–2160. https://doi.org/10.1103/PhysRevD.2.2141

Zhang J, Zhou SY (2018) Can the graviton have a large mass near black holes? Phys Rev D 97:081501. https://doi.org/10.1103/PhysRevD.97.081501. arXiv:1709.07503

Zhang SN, Liu Y, Yi S, Dai Z, Huang C (2016) Do we expect to detect electromagnetic radiation from merging stellar mass black binaries like GW150914? No. ArXiv e-prints arXiv:1604.02537

Zhou M, Cardenas-Avendano A, Bambi C, Kleihaus B, Kunz J (2016) Search for astrophysical rotating Ellis wormholes with X-ray reflection spectroscopy. Phys Rev D 94:024036. https://doi.org/10.1103/PhysRevD.94.024036. arXiv:1603.07448